



## This is to certify that the thesis entitled

# LARGE DEFLECTION RESPONSE OF AN ELLIPTICAL SECTION RING TO DISTRIBUTED AXIAL LOAD presented by

Lawrence A. Nattrass

has been accepted towards fulfillment of the requirements for

<u>Doctoral</u> degree in <u>Engineering</u>

Rolland T. Hunkle

Major professor

0-7639





OVERDUE FINES: 25¢ per day per item

RETURNING LIBRARY MATERIALS:
Place in book return to remove charge from circulation records

DEC 0 3 1997

## LARGE DEFLECTION RESPONSE OF AN ELLIPTICAL SECTION RING TO DISTRIBUTED AXIAL LOAD

by

Lawrence A. Nattrass

## A DISSERTATION

Submitted to

Michigan State University

in partial fulfillment of the requirements

for the degree of

DOCTOR OF PHILOSOPHY

Department of Mechanical Engineering

College of Engineering

### **ABSTRACT**

## LARGE DEFLECTION RESPONSE OF AN ELLIPTICAL SECTION RING TO DISTRIBUTED AXIAL LOAD

By

### Lawrence A. Nattrass

The behavior of a circular ring with an elliptical crosssection was studied to determine its suitability as a spring. The
design parameters for a spring system to support an axial load
included an annular configuration of fixed diameter and minimum
volume. The load and deflection range were specified. Since the
spring supported a mass, the natural frequency of the system was
also a consideration. Considering the need to store a fixed
amount of energy in a minimum volume, the optimum spring appeared
to be one which had a flat or nearly flat load-deflection curve.
The load-deflection characteristics of the ring proved to meet
most of the system parameters. The uniqueness and originality of
the concept necessitated the development of an analytical model,
prediction of performance and failure parameters, and experimental
verification of the design.

An analytical model was developed to predict the force-deflection and stress-deflection characteristics of a given ring.

The effects of friction were considered and the useful range of the ring was described in terms of critical angles for self-locking.

The model agreed with the experimental results.

## **ACKNOWLEDGEMENTS**

This work was performed under the auspices of the U. S. Department of Energy by the University of California Lawrence Livermore Laboratory under Contract W-7405-ENG-48. The support of the Nuclear Explosives Engineering Division is acknowledged.

I would like to thank Professor T. Hinkle for his efforts as my major professor. In addition to his help on this project, Dr. Hinkle provided the support and guidance which made my doctoral program a valuable experience. I would also like to thank Dr. George Mase, Dr. William Bradley, and Dr. Norman Hills for their help as members of the guidance committee.

The dissertation was prepared by Alpha Mammen and Mildred Rundquist. The extra effort and long hours that went into their work are greatly appreciated.

I would also like to express my thanks to Jesse West for his support and assistance in making this thesis possible. Without his help and understanding, my dissertation project would have been forgotten long ago due to the pressure of higher priority projects.

Finally, I wish to thank my wife, Karen, for many years of patience and perseverance, and my son, Owen, who has been involved with various dissertation projects for his entire life.

## TABLE OF CONTENTS

		Page
List of Tables		iii
List of Figures		iv
Chapter I:	Introduction	1
Chapter II:	Problem Description	11
Chapter III:	Evaluation of Alternate Designs	15
Chapter IV:	Preliminary Calculations of	
	a Twisted Ring	46
Chapter V:	Deformation and Stress in an	
	Elliptical Section Ring	56
Chapter VI:	Specimen Fabrication	94
Chapter VII:	Experimental Program	102
Chapter VIII:	Comparison of Calculated and	
	Experimental Values	114
Chapter IX:	Conclusions and Recommendations	143
References		144

## LIST OF TABLES

Γab	le	Page
1	Sample printout from PLATE I	35
2	Belleville spring constants from Formulas	
	for Stress and Strain (2)	37
3	Sample calculation - output from RING	118
4	Sample calculation - output from RING	119
5	Estimate of the coefficient of friction from	
	the hysteresis loop	142

## LIST OF ILLUSTRATIONS

Figu	<sup>-</sup> igure	
1	Typical load-deflection curves for	
	various spring types	3
2	Ring with radial fingers $(M_t = pe)$	6
3	Ring with a continuous load	
	platform (M <sub>t</sub> = pe)	7
4	Schematic representation of a circular	
	ring having an elliptical cross-section	8
5	Design envelope for a spring system	13
6	Design parameters for a helical coil spring	16
7	Load deflection curve for a system of n	
	linear springs	19
8	Buckling of a pinned-end column	22
9	Plate with inner end fixed	28
10	Plate with outer edge fixed	29
11	Conical disk or Belleville Spring	30
12	Plate parameters of use in equations	
	from Formulas for Stress and Strain	31
13	Parameters for flat plate calculation	33
14	Modified Belleville spring	39
15	Deflection model for a Belleville spring	40
16	Belleville spring: Deflection from $\phi_0 = 0$	42
17	Modified Belleville spring: Deflection	
	from $\phi_0 = 0$	45

18	Circular ring loaded by a uniformly	
	distributed twisting moment	17
19	Free-body diagram of a circular ring	
	loaded by a distributed couple	18
20	Displacement of a point, P, due to a	
	rotation $\Delta\theta = \theta_1 - \theta_2$	50
21	Circular section ring for trial	
	calculations	52
22	Ellipse parameters in body coordinates	58
23	Load distribution on an elliptical	
	section ring 5	59
24	Free body diagram of an elliptical section	
	ring 6	50
25	Loading on a section of an elliptical	
	section ring	52
26	Location of the contact point between an	
	ellipse and a flat plate	59
27	Load eccentricity of an elliptical section	
	ring as a function of rotation	72
28	Change in contact point position between	
	an elliptical section ring and a flat	
	plate $(\phi_0 = 0^0)$	73
29	Comparison of load eccentricity for an	
	elliptical section ring, a Belleville	
	spring, and a modified Belleville spring	74

30	Comparison of contact point deflection for	
	an elliptical section ring, a Belleville	
	spring, and a modified Belleville spring	75
31	Force curves from a sample calculation	
	with RING	77
32	Force and stress for a sample calculation	
	with $\phi_0 = 20^0$	78
33	Loci of the positions of the major and minor	
	axes, contact point, neutral axis, and point	
	of maximum strain as measured from the radial	
	axis of the ring	82
34	Friction force direction during (a) loading	
	and (b) unloading	87
35	Sample calculation showing the effect of a	
	friction coefficient, $\mu$ = 0.10, between an	
	elliptical section ring and a flat plate	89
36	Critical angle for self-locking as a function	
	of a/b ratio	93
37	Engineering drawing for Test Specimen 1	97
38	Engineering drawing for Test Specimen 2	98
39	APT4 program listing	99
40	Vendor certification of the titanium	
	purchased for specimen fabrication	100
41	Instrumentation schematic for ring tests	103
42	Test apparatus for load-deflection tests	
	of elliptical section rings	104

43	Elliptical section ring installed in the	
	test machine	105
44	Test data for a titanium ring (a = 0.040,	
	b = 0.010, R = 2.44 inch, $\phi_0 = 30^{\circ}$	107
45	Test data for a titanium ring (a = 0.080,	
	b = 0.020, R = 2.217 inch, $\phi_0 = 20^{\circ}$	108
46	Sample of digitized test data plotted	
	with DPLOT	109
47	Photograph of an elliptical section ring	
	(a = 0.080, b = 0.020, R = 2.217, $\phi_0 = 20^{\circ}$	112
48	Force-deflection curves - sample calculation	116
49	Force and stress curves for $\phi_0 = 20^{\circ}$	
	sample calculation	117
50	Force curves for Test Specimen No. 1 (nominal	
	dimensions)	121
51	Force and stress for Test Specimen No. 1	
	(nominal dimensions)	122
52	Test data for Specimen 1	124
53	Specimen 1 test data corrected for zero shift	125
54	Force and stress for measured cross section	
	of Specimen 1 ( $\phi_0 = 30^\circ$ )	126
55	Photomicrograph of the cross section of	
	Specimen No. 1 (post-test)	127
56	Photomicrograph of the cross section of	
	Test Specimen No. 1 (the section has	
	been etched to indicate grain size)	128

57	Plot of digitized cross section of Specimen	
	No. 1 compared with a true ellipse	129
58	Force curves for measured cross section of	
	Specimen No. 1	131
59	Force and stress for measured cross section	
	of Specimen No. 1 ( $\phi_0 = 40^\circ$ )	132
60	Force curves for Test Specimen No. 2	
	(nominal dimensions)	133
61	Force and stress for Test Specimen No. 2	
	(nominal dimensions)	134
62	Test data for Specimen No. 2	136
63	Specimen 2 test data corrected for	
	zero shift	137
64	Force curves for measured cross section	
	of Specimen No. 2	138
65	Force and stress for measured cross section	
	of Specimen No. 2	139
66	Effect of friction ( $\mu$ = 0.10) on the	
	calculated response for Specimen No. 2	140

#### CHAPTER I

#### INTRODUCTION

A weapon assembly in the nuclear stockpile is expected to function properly after many years of handling and storage under a variety of conditions. The anticipated environment varies from system to system but generally involves a range of operating temperatures and a vibration spectrum. One such assembly designed at Lawrence Livermore Laboratory (LLL) required maintaining the relative positions of components over a specified temperature range. The fact that the components were of dissimilar materials resulted in growth and contraction due to differential thermal expansion. A decision was made to employ a spring subjected to an initial deflection to maintain contact between components.

Springs are commonly used in mechanical design to perform such functions as energy absorption, frequency response regulation, vibration isolation, and force generation. The use of springs to maintain contact between components or to maintain the relative position of components in assembly is common practice. In the application described in this work, the intent was to preload the spring during assembly at ambient temperature. The amount of preload was determined by the deflection required to compensate for the maximum thermally induced contraction. The spring was also required to deflect an additional amount equal to the thermal expansion from ambient to the temperature extreme. In order to allow for cyclic thermal loading, the total deflection

range had to be within the elastic range of the spring material. Several other constraints were also imposed and are discussed in Chapter II.

In general, any elastic medium can be used as a spring.

Springs are characterized according to the nature of the relationship between the applied force and the resultant deflection. The fundamental class of springs are elements having a linear force-deflection curve characterized by a relationship of the form

$$F = kx (I-1)$$

where F is the applied load, x is the deflection, and k is a constant. In actuality, the linearity of the element may exist over only a portion of the deflection range.

Non-linear springs are those characterized by equations of the form

$$F = f(x) \tag{I-2}$$

where f (x) is a particular function. Hardening springs and softening springs are two classes of non-linear springs which are frequently employed in mechanical design. The terms hardening and softening describe the deviation of the force-deflection curve from linear. Figure 1 shows load curves for several classes of springs. The constant force element is a particular class of non-linear spring and is shown for later reference.

Although any elastic medium will function to some degree as a spring, it is generally faster in design practice to select a commonly used and adequately characterized spring form. Several common spring types are widely used in engineering applications and have been thoroughly investigated. Design equations giving

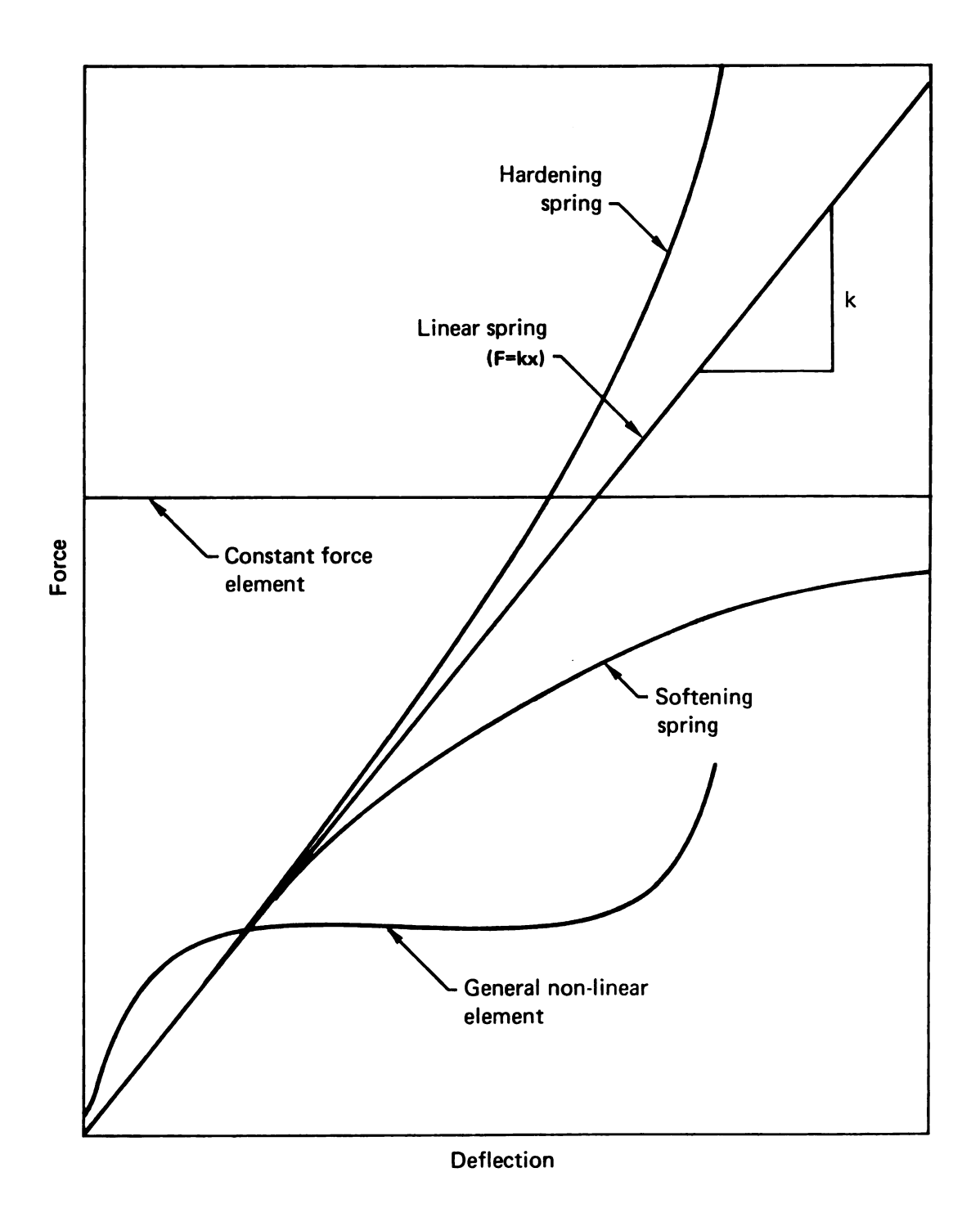


Figure 1. Typical load-deflection curves for various spring types.

force, deflection, and stress for coil springs, leaf springs, Belleville springs, and other types can be found in most engineering handbooks. The typical design cycle for a spring for use in a particular application might proceed as follows:

- Select the critical design parameter
   (force, deflection, or spring rate)
- Define the geometric constraints imposed on the spring design
- 3) Select a spring type which will fit the geometric limitations
- Design the spring using existing design equations, charts, or graphs
- 5) Select a spring material which will not fail at the calculated stress levels

In general, this is an iterative process with the number of cycles dependent upon the experience of the engineer and the nature of the constraints.

The work to design a spring system for use in an assembly at Lawrence Livermore Laboratory was begun in September, 1977 and completed in February 1978. During this period a large number of spring designs, many of them unique and original, were analyzed to determine the degree to which each met the various performance criteria. Most designs were eliminated on the basis of hand calculations using textbook equations or approximations. Several designs were shown to be potential solutions to the problem and were analyzed in depth. In the final selection process, two designs were

fabricated and tested. The test results were then correlated to the analytical work to establish a verified predictive capability.

The purpose of this research was to analyze the response of a circular ring having an elliptical cross-section to a distributed axial load. In particular, the goal was to develop a model which described the large-deformation load-deflection curve and the stresses in the ring. The predictive capability was necessary for the design of a compact non-linear spring which had programmatic use at Lawrence Livermore Laboratory.

The elliptical section ring was invented to provide a constant force element which fit the available space. The concept evolved from a study of a circular section ring loaded by a distributed couple. A ring offered the optimum use of the available space (see Chapter II) but a means of resolving an axial load into a couple was required. Several studies were made of rings with radial fingers as shown in Figure 2 and a ring with a continuous load platform (Figure 3) was considered conceptually.

The author formulated the hypothesis that a ring having a non-circular cross-section could be designed to respond as a constant force spring. An elliptical cross-section was chosen for this study because the curve is defined by a single equation of relative simplicity. This reduced the complexity of the analytical work which necessarily preceded the experimental study of the ring response.

The concept of an elliptical-section ring is shown schematically in Figure 4. Applying the load at the radial tangents of the ellipse produces a distributed twisting couple

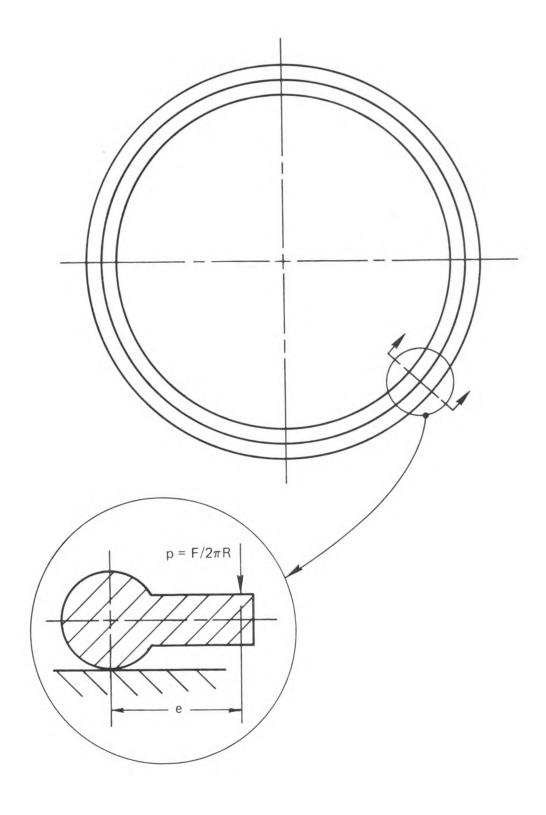


Figure 3. Ring with a continuous load platform ( $M_t$  = pe).

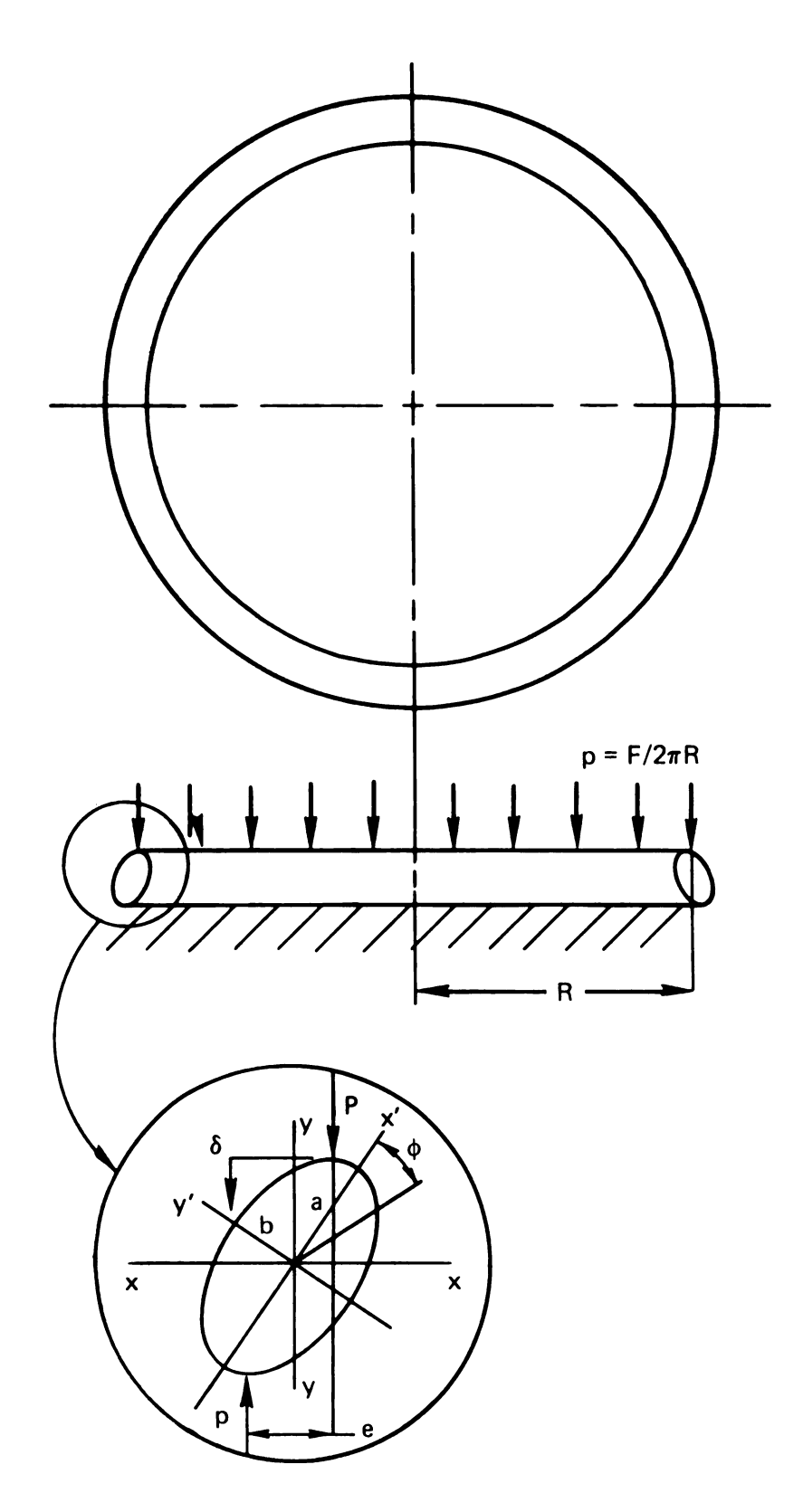


Figure 4. Schematic representation of a circular ring having an elliptical cross-section.

$$M_{+} = Pe \tag{I-3}$$

per unit of circumference. By analogy to a circular-section ring as described by Timoshenko (1) and Roark (2), the ring undergoes a rotation,  $\phi$ , which is of the form

$$\phi = \frac{M_T R^2}{EI_{xx}} = \frac{PeR^2}{EI_{xx}}$$
 (I-4)

where

 $I_{xx} = I_{xx}$ , the moment of inertia of the crosssection about the radial mid-plane

R = mean ring radius

 $\phi$  = angle of twist

 $e = e(\phi)$ , the eccentricity of the loading.

The above relation is approximate for small  $\phi$ . The particular form of  $I_{\chi\chi}(\phi)$  is given by the transformation equation for the moment of inertia tensor

$$I_{xx}(\phi) = I_{x'x'} \cos^2 \phi + I_{y'y'} \sin^2 \phi$$
 (I-5)

The deflection under the load, P, is

$$\delta = \delta(\phi) \tag{I-6}$$

The significance of these approximate descriptions is the clear implication that a non-linear relationship exists between force and deflection. The initial hypothesis of the research was that a region exists in which the force is nearly constant regardless of the deflection.

This report describes the research required to determine

the response of a particular ring section (elliptical) and to verify

the accuracy of the analytical model. The constraints imposed by the assembly for which the spring was designed were the impetus for the invention and are described in Chapter II. Alternate designs are presented in Chapter III as a means of assessing the unusual nature of the problem and the effects of various constraints on the solution. A feasibility study employing the small angle relationships is presented in Chapter IV. The various analytical models developed for the elliptical-section ring are presented in Chapter V.

The fabrication of a large diameter ring with a small, non-circular cross-section presented several challenges. The techniques considered are presented in Chapter VII. Chapter VIII presents a discussion of the computer program used to predict the response of a given ring and discusses correlation between the model and experimental data. Chapter IX presents conclusions and recommendations for future research.

#### CHAPTER II

## PROBLEM DESCRIPTION

The functional requirement imposed on the spring system was that it maintain the relative position of components over a range of temperatures. The spring was required to compensate for differential expansion and contraction of dissimilar materials. The spring system was subject to a variety of design constraints imposed by requirements external to the system. These constraints were both geometric and physical.

The severity of these limitations eliminated ordinary springs and forced the development of a variety of unique and original types of springs. Limitations on time and resources mandated that the development of a spring type procede in a logical and efficient manner. The sequence was

- 1) Discussion of the proposed spring by members of the engineering team to verify that the concept met the criteria and to identify any obvious inadequacies such as material problems or fabrication difficulties.
- 2) Initial design calculations were performed using approximations from appropriate engineering theory or practice. If the design looked feasible and if no insurmountable obstacles, such as stresses exceeding the ultimate strength by several orders of magnitude, were encountered, the development continued.

- 3) A calculational model was developed either from existing equations or derived from theoretical precepts. The resulting equations were programmed and computer solutions were generated.
- 4) Test specimens were fabricated and tested in the laboratory.

This process served to optimize the use of time and resources by directing the engineering effort toward the most viable solutions and by focusing the fabrication and test efforts (which were typically long lead-time items outside the control of the engineer) on the best candidates.

The constraints which drove the design of the spring system imposed a geometric envelope along with several functional requirements. Restrictions were also placed on the types of materials which could be considered. The constraints on the design are illustrated in Figure 5 and are listed below.

- The spring (or system of springs) had to be in an annular configuration of fixed radius.
- 2. The cross-section area occupied by the spring system was to be minimized (an area of  $0.040 \times 0.100$  inch was the initial goal).
- 3. The force exerted at -0.015 inch deflection was to be 300 pounds (deflection was defined from the initial preloaded state).
- 4. The spring was required to deflect ± 0.015 inch elastically.

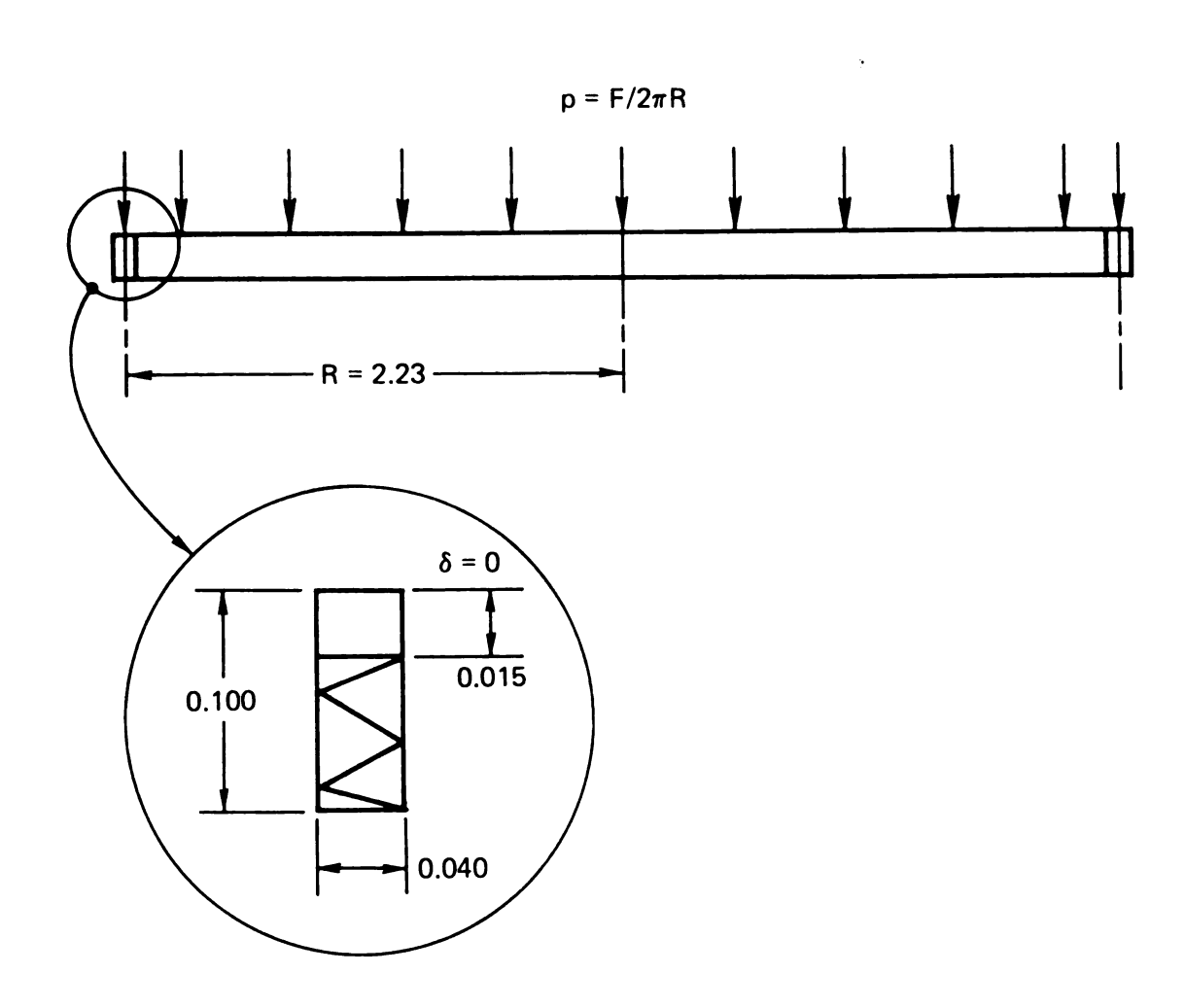


Figure 5. Design envelope for a spring system (300 lbs  $\leq$  F  $\leq$  600 lbs).

- 5. Organic materials such as rubber or plastics were not acceptable.
- 6. Materials selection parameters included formability, machinability, high strength, and ability to withstand elevated temperatures.
- 7. The spring was to be fabricated with state-of-the-art techniques.
- 8. Since the system supported a mass under dynamic conditions, the spring rate affected the resonant frequency.
- Stress considerations in the assembly indicated the desirability of minimizing the maximum force by use of a non-linear spring.

It can be seen that the most stringent constraints were the result of geometric limitations and deflection requirements. The effects of these limits are considered in the next chapter where various design alternatives are explored.

## CHAPTER III

## EVALUATION OF ALTERNATE DESIGNS

The consideration of spring systems other than the elliptical section ring is significant because it illustrates the nature of the problem and the evolution of the solution. As previously mentioned, the effort to design a spring system for the specific application discussed in Chapter II occurred over a five month period. The level of effort devoted to the solution was necessarily a fraction of full time for the members of the design team. Perhaps as many as twenty spring concepts received other than cursory examination and, of these, three have been selected for discussion: coil springs, buckling columns, and flat circular plates (which include Belleville springs).

The coil spring is perhaps the most widely employed spring configuration in engineering design. Coil springs range in size from a half ton coil used to cushion missile silos to a spring measuring 0.032 inch outside diameter and 0.050 inch overall length used in a miniature ball bearing assembly (3). The design of such springs is defined in most machine design tests and mechanical engineering handbooks (3, 4, 5). The pertinent equations are listed below and the parameters are illustrated in Figure 6. The equations are developed from the equilibrium condition

$$T = \frac{PD}{2} \tag{III-1}$$

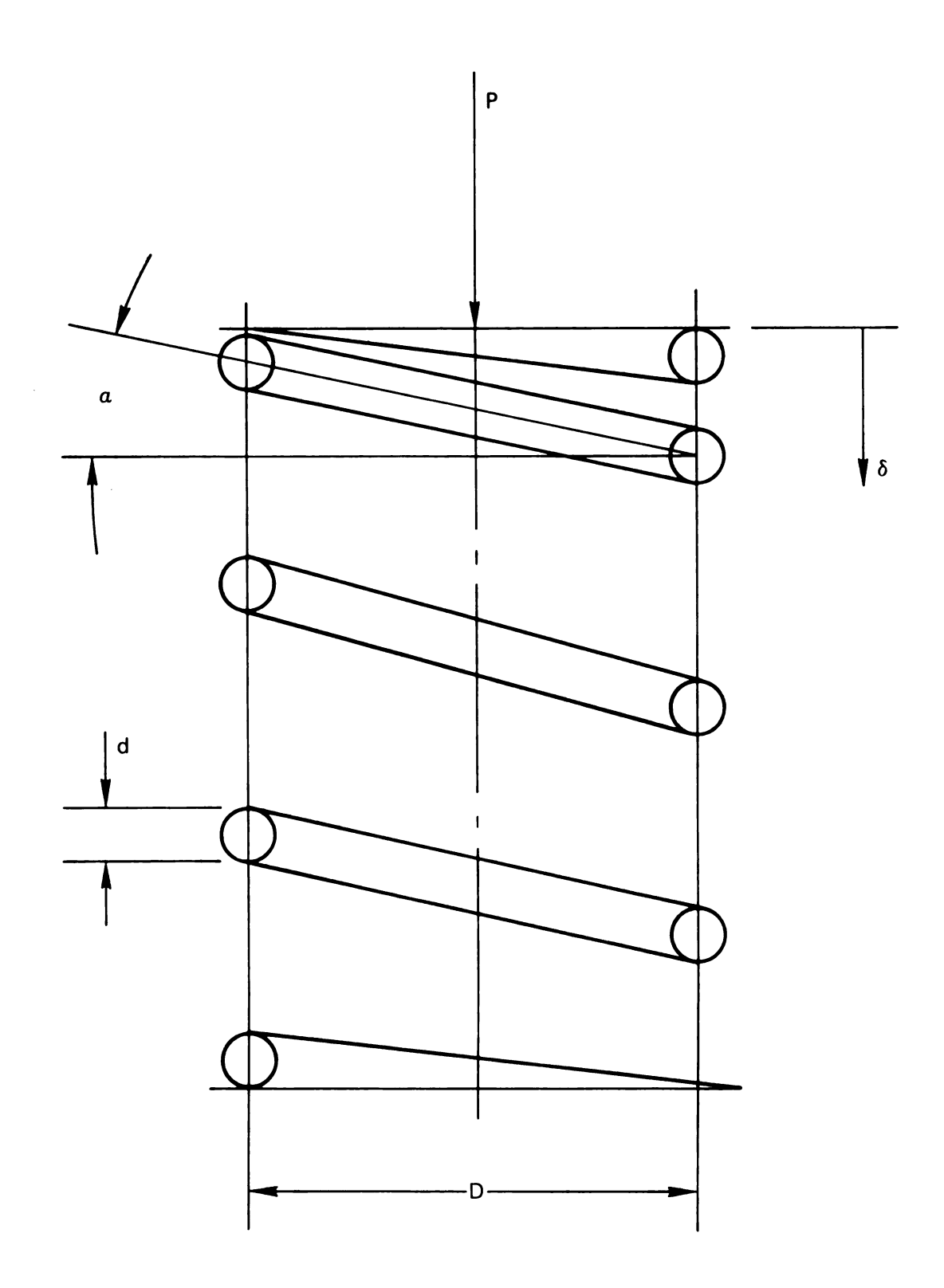


Figure 6. Design parameters for a helical coil spring.

and equality between the work done on the spring and the strain energy in the wire

$$W = \frac{P\delta}{2} = \frac{T\theta}{2} \tag{III-2}$$

where it is assumed that the force increases linearly from zero.

It can be shown that the angle of twist of a bar of circular crosssection is given by

$$\theta = \frac{TL}{GJ} \tag{III-3}$$

where

$$L = \frac{\pi Dn}{\cos \alpha}$$
 the total active length of the spring wire

$$J = \frac{\pi d^4}{32}$$
 the polar moment of inertia of the cross-section

G = shear modulus

Substitution in Equation (III-2) gives

$$\frac{P\delta}{2} = \frac{P^2D^3}{8GJ} \frac{\pi n}{\cos \alpha}$$

Solving for the deflection

$$\delta = \frac{PD^3 \pi n}{4GJ \cos \alpha}$$

or

$$\delta = \frac{8PD^3n}{d^4G \cos \alpha} = \frac{8PC^3n}{Gd} \qquad (C = D/d) \qquad (III-4)$$

for small values of  $\alpha$  such as those encountered in closely coiled springs. The discrepancy between the strain energy in the helical coil and that in a straight bar is neglected in this discussion.

The stress in the wire is due to direct shearing and to the torsional stress. The Wahl equation (4) is an experimentally verified relation which includes the direct shear, the torsional stress, and the effects of curvature. The maximum shear stress in the wire is

$$s_s = K \frac{8PD}{\pi d^3} = K \frac{8PC}{\pi d^2}$$
 (III-5)

where

$$K = \frac{.4C - 1}{4C - 4} + \frac{0.615}{C}$$

The problem specifications outlined in Chapter II require

 $\delta = \pm 0.015$  inch from nominal

$$P = 300$$
 pounds at  $\delta = -0.015$ 

Thus, for any linear spring, a load-deflection curve as shown in Figure 7 is required. Although any preload could be used, the minimum stress in the spring will result if the preload is minimized. Assuming a maximum diameter of 0.040 inch and a height at  $\delta$  = 0.015 of 0.100 inch, the number of springs, N, around the annulus is

$$N = \frac{2\pi R}{D_0} = \frac{2\pi (2.25)}{0.040} = 353$$

where

R = radius of the annulus

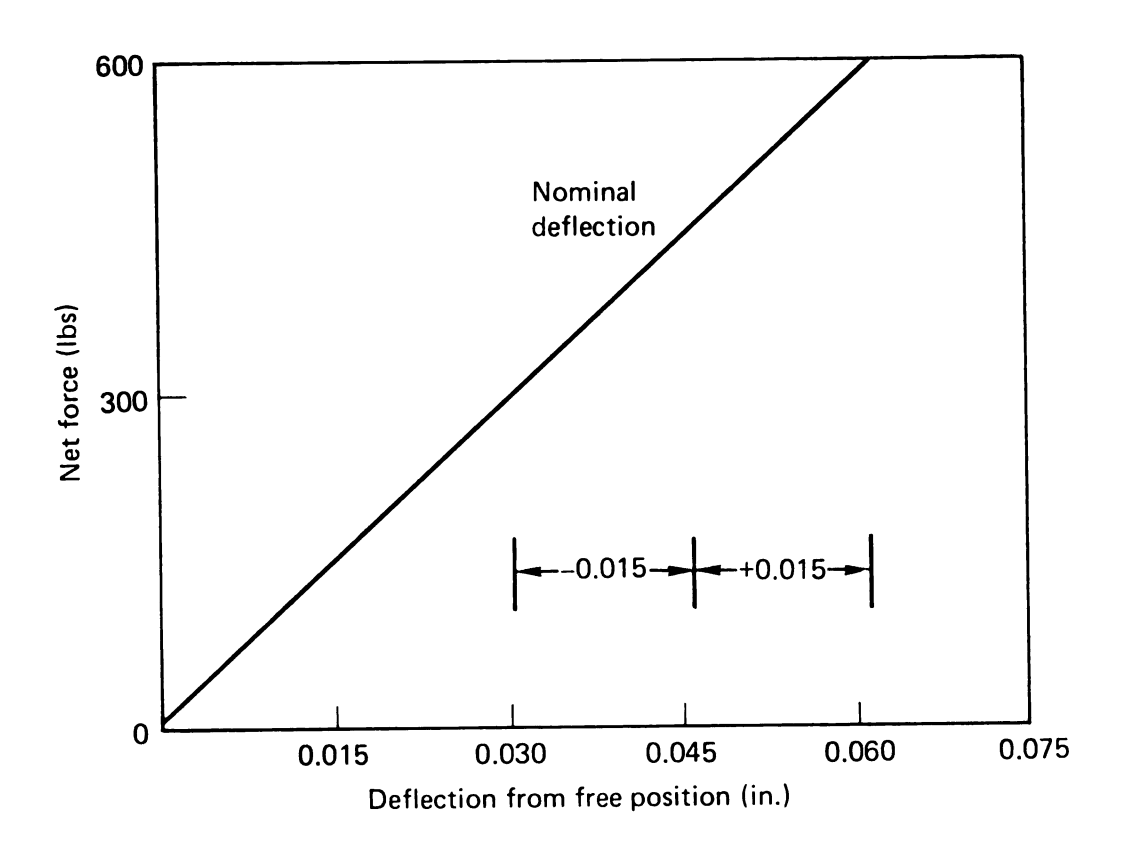


Figure 7. Load deflection curve for a system of n linear springs

use 
$$N = 350$$

Black and Adams (4) give an allowable stress of 75,000 psi for a spring in average service where the wire diameter is less than 0.085 inch. Rearranging Equation (III-4), the number of active coils, n, can be established as

$$n = \frac{\delta Gd}{8PC^3} \tag{III-6}$$

Now, assume a wire diameter of 0.005 inch which implies

$$D = D_0 - d = 0.040 - .005 = 0.035$$
  
 $C = D/d = 7$   
 $K = 1.2$ 

Then, using  $G = 12 \times 10^6$  psi for steel,

n = 
$$\frac{(0.045)(12 \times 10^6)(0.005)}{(8)(\frac{600}{350})(7)^3}$$
 = 113.9

use 
$$n = 114$$

The solid height of the spring is nd = 0.57 inch and the minimum free height is the sum of the solid height and the deflection required or 0.615 inch. Clearly this exceeds the allowable space.

Obviously, a vast number of other springs will satisfy these conditions but will require that some constraint be violated. In addition, the problems associated with manufacturing and installing 350 tiny coil springs were not considered insignificant. On the basis of these factors, the use of an array of coil springs was eliminated as a possible solution.

In previous research, the author investigated the large deflection buckling of columns as an energy absorption device

(6). This study showed that, in the absence of lateral constraints, the force required to deflect a buckled column elastically remained constant until the material failed. Materials having high strength and low modulus were required to achieve large elastic deformations. The glass fiber/epoxy systems used in the earlier work were not acceptable in this design, therefore, high strength titanium alloys and steel alloys were evaluated.

The governing differential equation for a buckled column such as shown in Figure 8 is

$$EI \frac{d^2y}{dx^2} = -Py \qquad (6, 7) \qquad (III-7)$$
or
$$\frac{d^2y}{dx^2} + k^2y = 0,$$
where
$$k^2 = \frac{P}{FT}$$

The solution of this equation is

$$y = A \sin kx$$
 (III-8)

where

$$k\ell = \sqrt{\frac{p\ell^2}{EI}} = n\pi \tag{III-9}$$

or

$$P = \frac{n^2 \pi^2 EI}{\ell^2}$$
 (III-10)

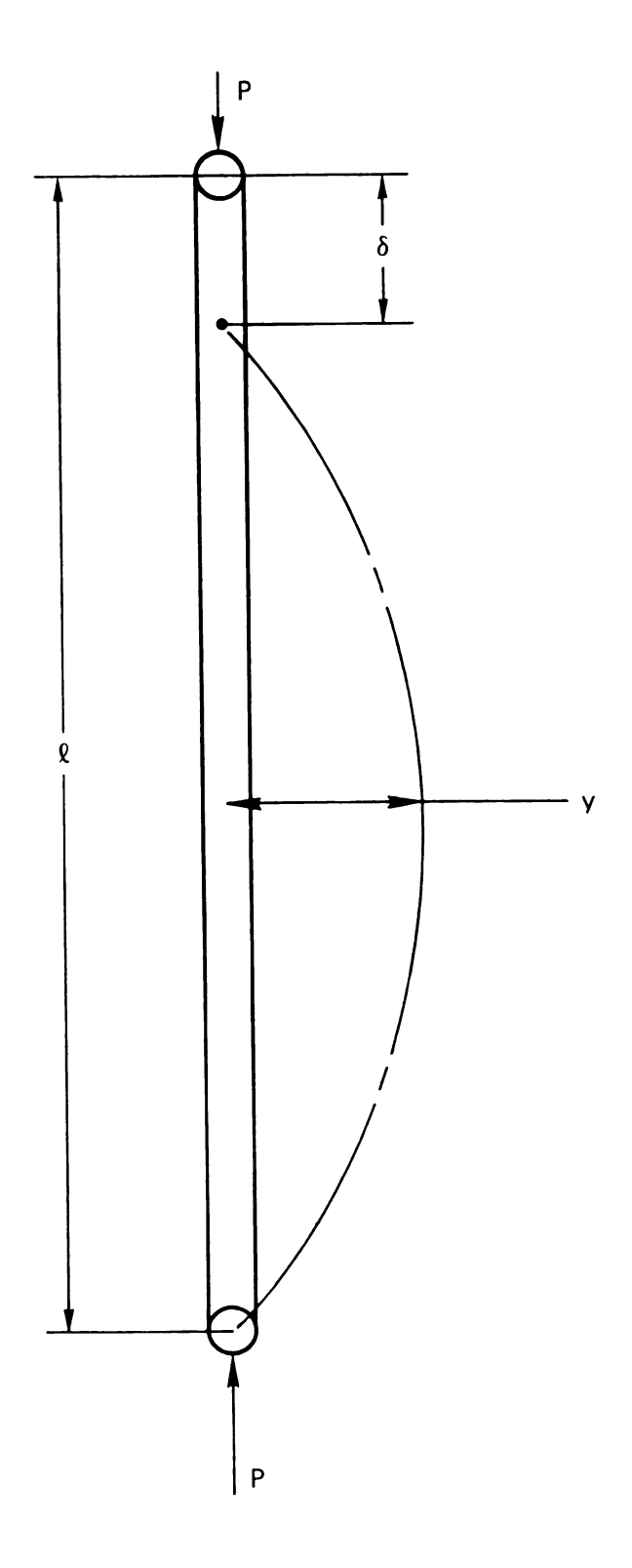


Figure 8. Buckling of a pinned-end column

which is the Euler buckling equation for a pinned-end column. The lowest order solution is n = 1. The amplitude of the deformed shape, A, is indeterminate which implies that the force required is constant with amplitude and therefore with end deflection. This was established experimentally (6).

The end deflection of the column can be determined from the projected length of the sinusoid

$$S = \int_0^{\ell} \left( 1 + \frac{2\pi^2 A^2}{\lambda^2} \cos^2 \frac{2\pi x}{\lambda} \right) dx$$

$$= \ell + \frac{\pi^2 A^2 \ell}{\lambda^2} + \frac{\lambda}{8\pi} \sin \frac{4\pi \ell}{\lambda}$$
(III-11)

where

$$\lambda = \ell/n$$
  
 $n = 1/2, 1, 3/2$ 

For

and, for  $\delta \ll s$ ,  $s \approx \ell$ ,

and

$$\delta = \frac{\pi^2 A^2}{s} \tag{III-13}$$

The bending stress in the column can be established from the curvature of the deformed part and is given by

$$\sigma = \frac{\pi^2 \text{ AcE}}{s^2}$$
 (III-14)

where

c = half of the thickness of the column

E = modulus of elasticity

One of the cases calculated for the problem was based on the following assumptions:

A = 0.040 (the width of the groove)

 $\sigma = 150,000 \text{ psi}$ 

Substituting and solving Equation (III-13) for the free length,

$$s = \frac{\pi^2 A^2}{\delta} = 0.351$$

which exceeds the maximum allowable height. Assuming that this constraint could be relaxed, the stress equation can be solved for the thickness

$$t = 2c = \frac{\sigma s^2}{2\pi^2 AE}$$

t = 0.0015 for titanium

and t = 0.0008 for steel

If a circular section is assumed for the column, the moment of inertia for the cross-section is

$$I = \frac{\pi d^4}{64}$$

and the force equation can be written

$$P = \frac{\pi^3 Ed^4}{64\ell^2}$$

or

$$P = 3.2 \times 10^{-4}$$
 pound for titanium and  $P = 4.5 \times 10^{-5}$  for steel

The number of columns required is

$$n = \frac{600}{P} = 1.33 \times 10^7$$
 for steel

This design was clearly infeasible as were several other column designs.

A different approach to the column problem assumed a rectangular cross-section for which the Euler equation becomes

$$P_{cr} = \frac{P}{m} = \frac{\pi^2 \text{ Ebh}^3}{3\ell^2}$$
 (III-15)

where

P = 300 pounds, the total load

m = the number of columns

$$I = \frac{bh^3}{12}$$
 is the momentum of inertia for a rectangular section.

In this example, the yield strength of steel was taken to be  $5 \times 10^4$  psi which is the approximate value for some stainless steels in the fully annealed condition. This condition would result if the columns were required to survive a furnace braze cycle.

Certain quantities are more accurately estimated then others in a design situation. In this case, the yield strength and modulus of the material are easily obtained, the required deflection is known, and the free height can be estimated. The unknowns are the number of columns, the width of each column, and the thickness. If

the width is assumed to be the width of the groove, then the thickness can be found from the stress equation as follows

$$\sigma = \frac{4\pi^2 \text{ ACE}}{\ell^2}$$

$$\delta = \frac{\pi^2 \text{ A}^2}{\ell} \longrightarrow A = \frac{1}{\pi} \sqrt{\delta \ell}$$

$$t = 2c$$

Substituting

$$\sigma = \frac{2\pi \sqrt{\delta t} E}{\ell^{3/2}}$$

$$t = \frac{\sigma \ell^{3/2}}{2\pi \sqrt{\delta} E}$$
(III-16)

or

The number of columns is computed from the Euler equation as written in Equation (III-15)

$$n = \frac{3P\ell^3}{\pi^2 Ebt^3}$$

The data for the problem are summarized below:

P = 300 pounds

 $E = 28 \times 10^6 \text{ psi}$ 

b = 0.040 inch

 $\delta = 0.035$  inch

 $\ell$  = 0.100 inch

 $\sigma = 5 \times 10^4 \text{ psi}$ 

then

t = .00005 inch

$$n = 6.5 \times 10^5$$

Although this was a marked improvement over the first attempt, it

was decided that buckling columns of a reasonable design would not fall within the problem constraints.

As a final example of the alternate spring systems evaluated, consider the effort to design a flat circular plate with a central hole which would meet the functional constraints. The plate geometry was ideally suited to the application and the advantages offered by the relative simplicity of fabrication and assembly were such that constraints on the diameters could be relaxed slightly to permit use of a plate. Three plate types were considered: a flat plate of constant thickness fixed at the inner edge as shown in Figure 9, a similar plate fixed instead at the outer edge as shown in Figure 10, and a conical disk of constant thickness. The conical disk, or Belleville spring, is shown in Figure 11. It is the design closest in principle to the elliptical section ring. Calculations will be presented for the plate with the inner edge fixed and for the Belleville spring.

Plate equations are available from many references, those used in this study were taken from Roark (2) and are typical of the handbook type equations. The constraint and load conditions considered in this analysis corresponded to Case 1 of the "Formulas for flat circular plates of constant thickness". The general and particular cases are shown in Figure 12 along with the boundary conditions. Parameters of interest are

$$y_a = \frac{-wa^4}{bD} \left( \frac{c_2 c_9}{c_8} - c_3 \right)$$
 (III-17)

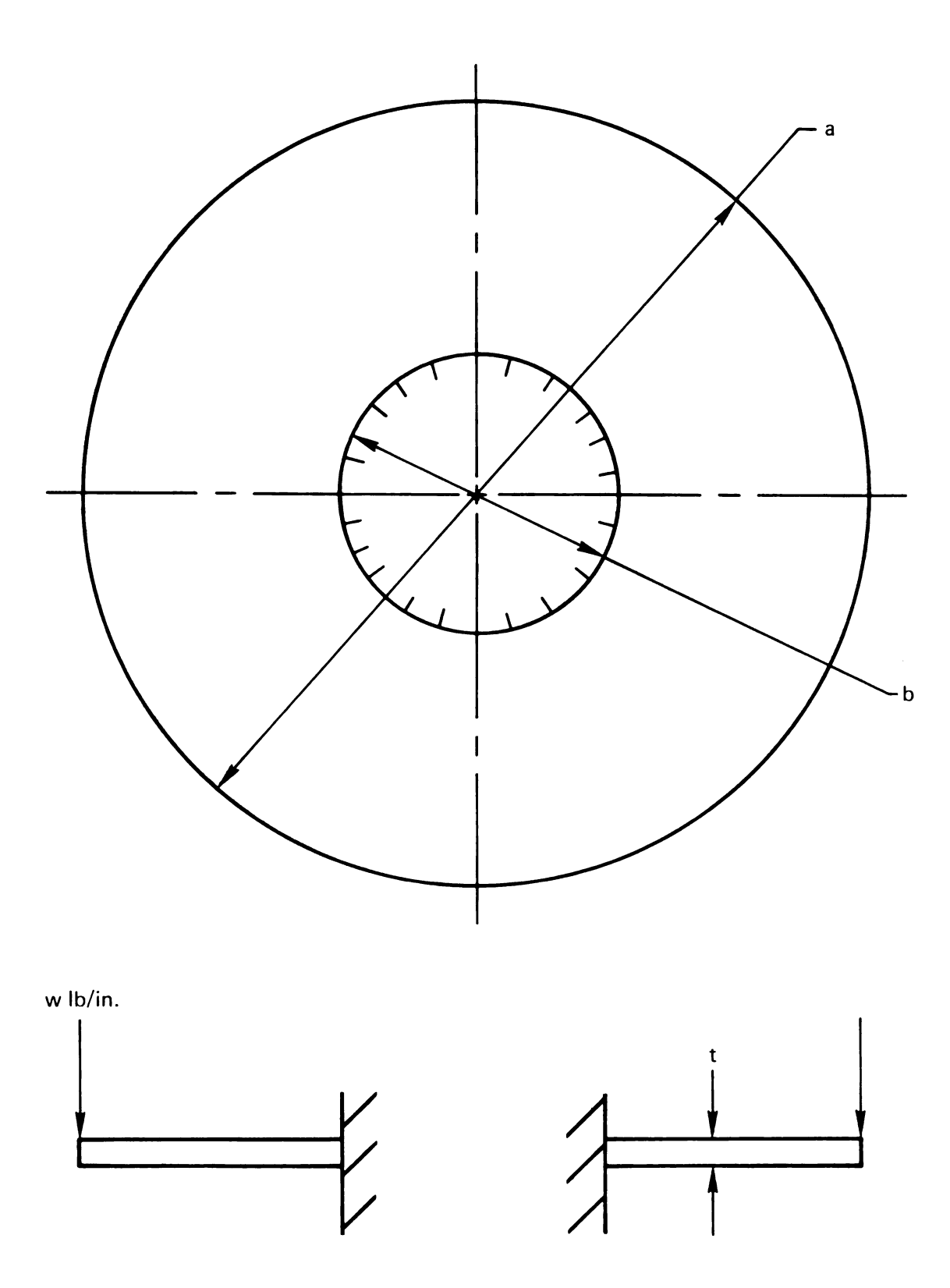


Figure 9. Plate with inner edge fixed.

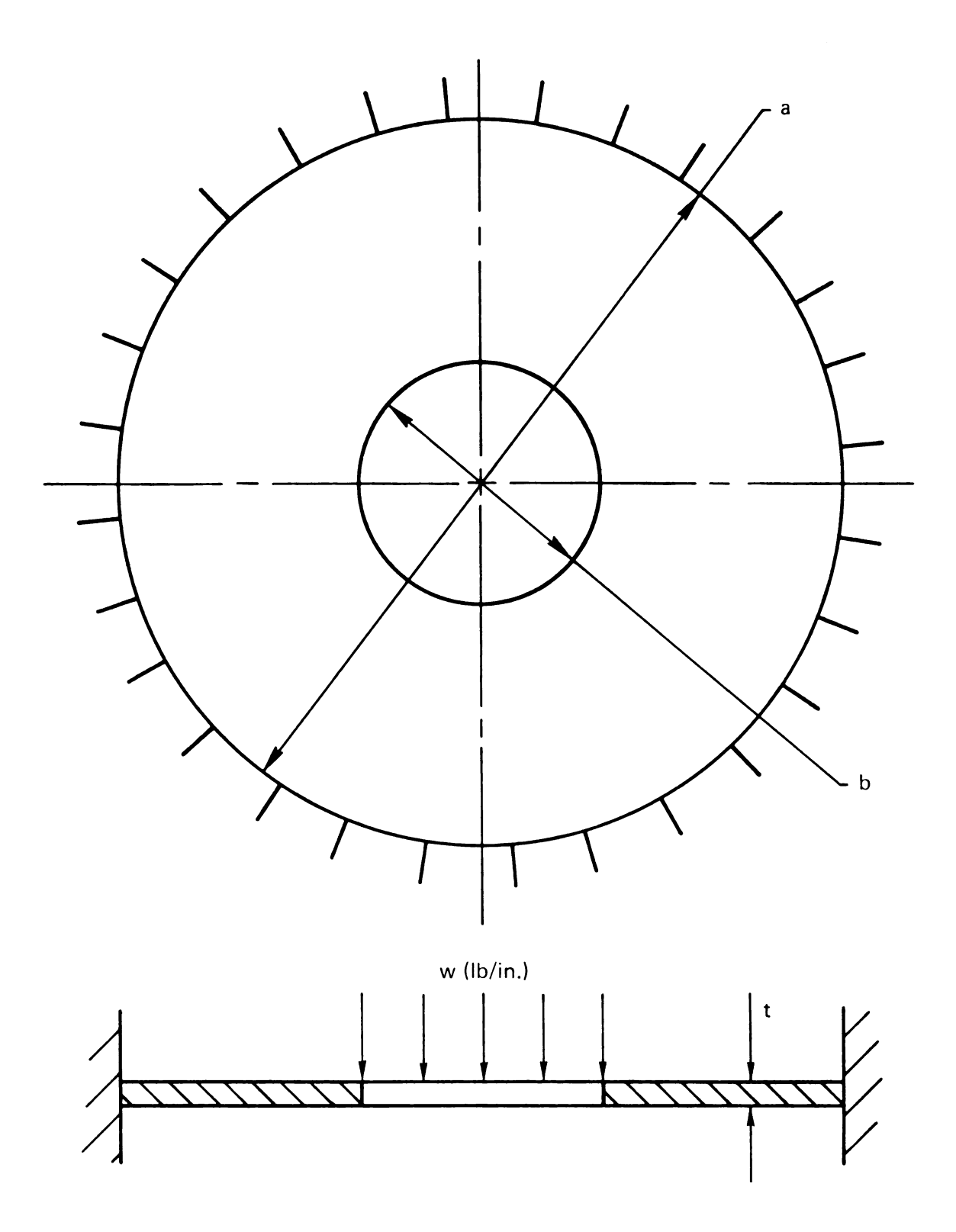


Figure 10. Plate with outer edge fixed.

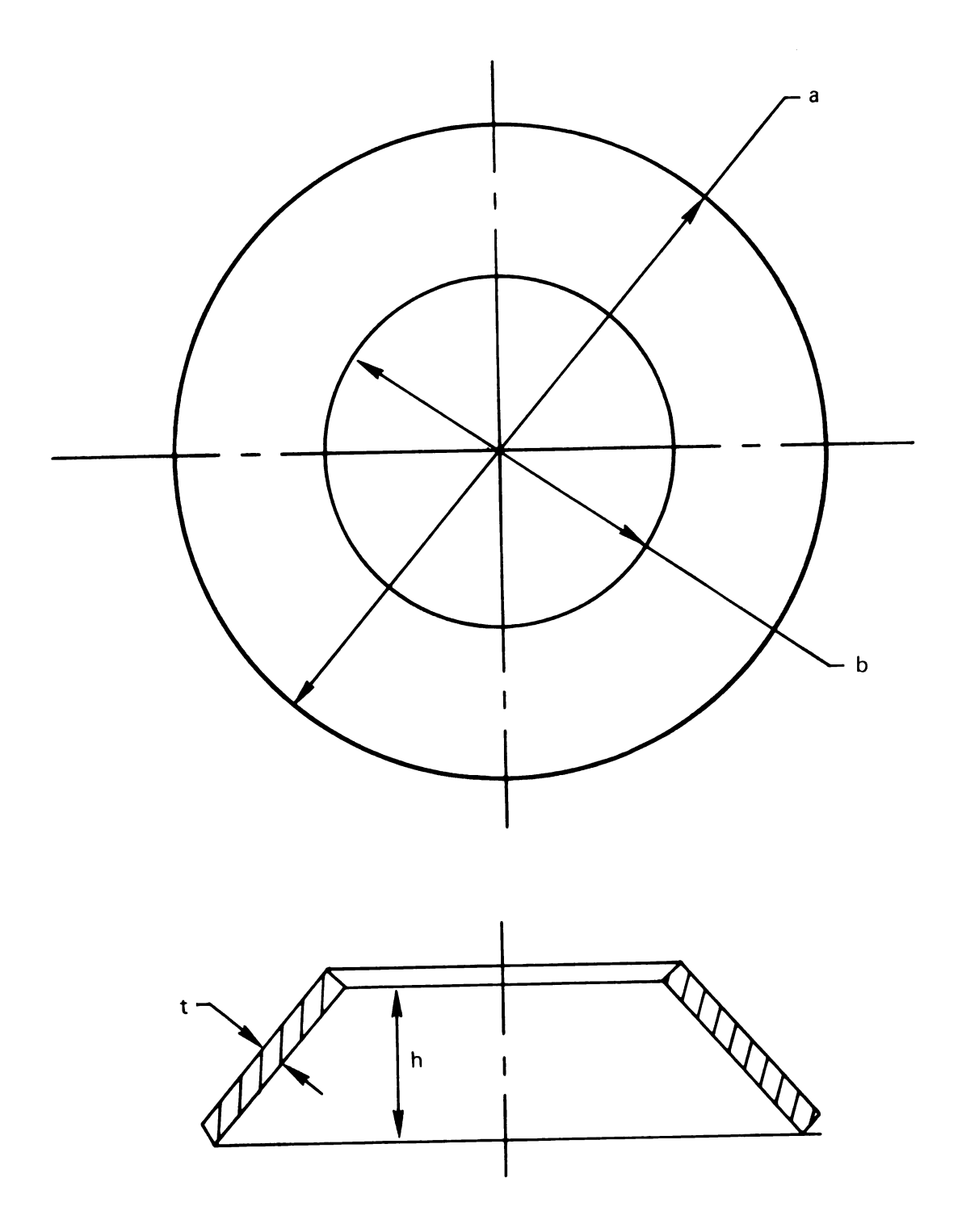


Figure 11. Conical disk or Belleville spring.

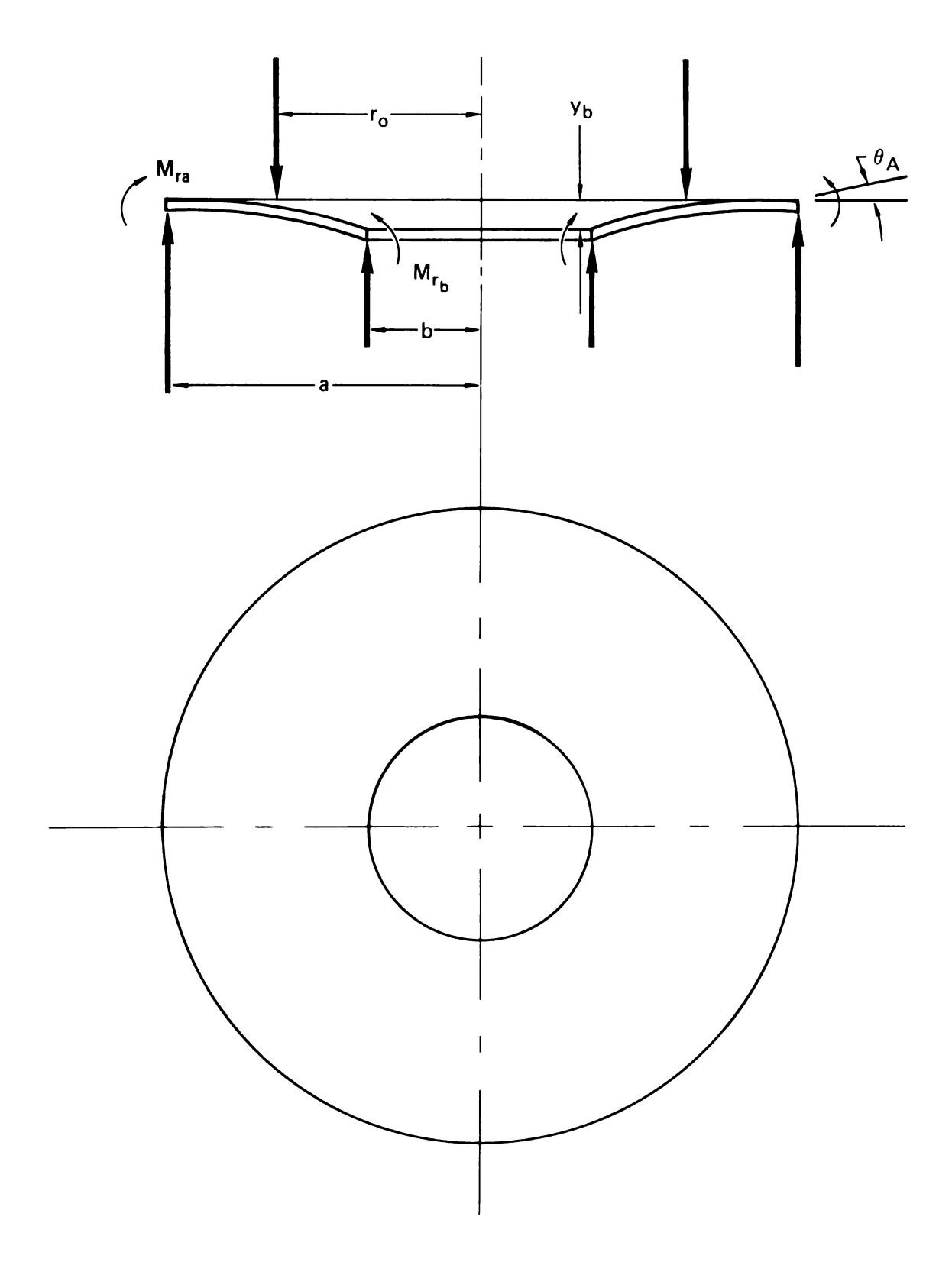


Figure 12. Plate parameters of use in equations from Formulas for Stress and Strain. [2]

$$\sigma = \frac{6M}{t^2} \tag{III-18}$$

where

$$D = \frac{Et^3}{12(1 - v^2)}$$
 (III-19)

$$M = \frac{-wa^2}{b} \frac{C_9}{C_8}$$
 (III-20)

$$c_2 = \frac{1}{4} \left[ 1 - \left( \frac{b}{a} \right)^2 \left( 1 + 2 \ln \frac{a}{b} \right) \right]$$
 (III-21)

$$c_3 = \frac{b}{4a} \left\{ \left[ \left( \frac{b}{a} \right)^2 + 1 \right] \ln \frac{a}{b} + \left( \frac{b}{a} \right)^2 - 1 \right\}$$
 (III-22)

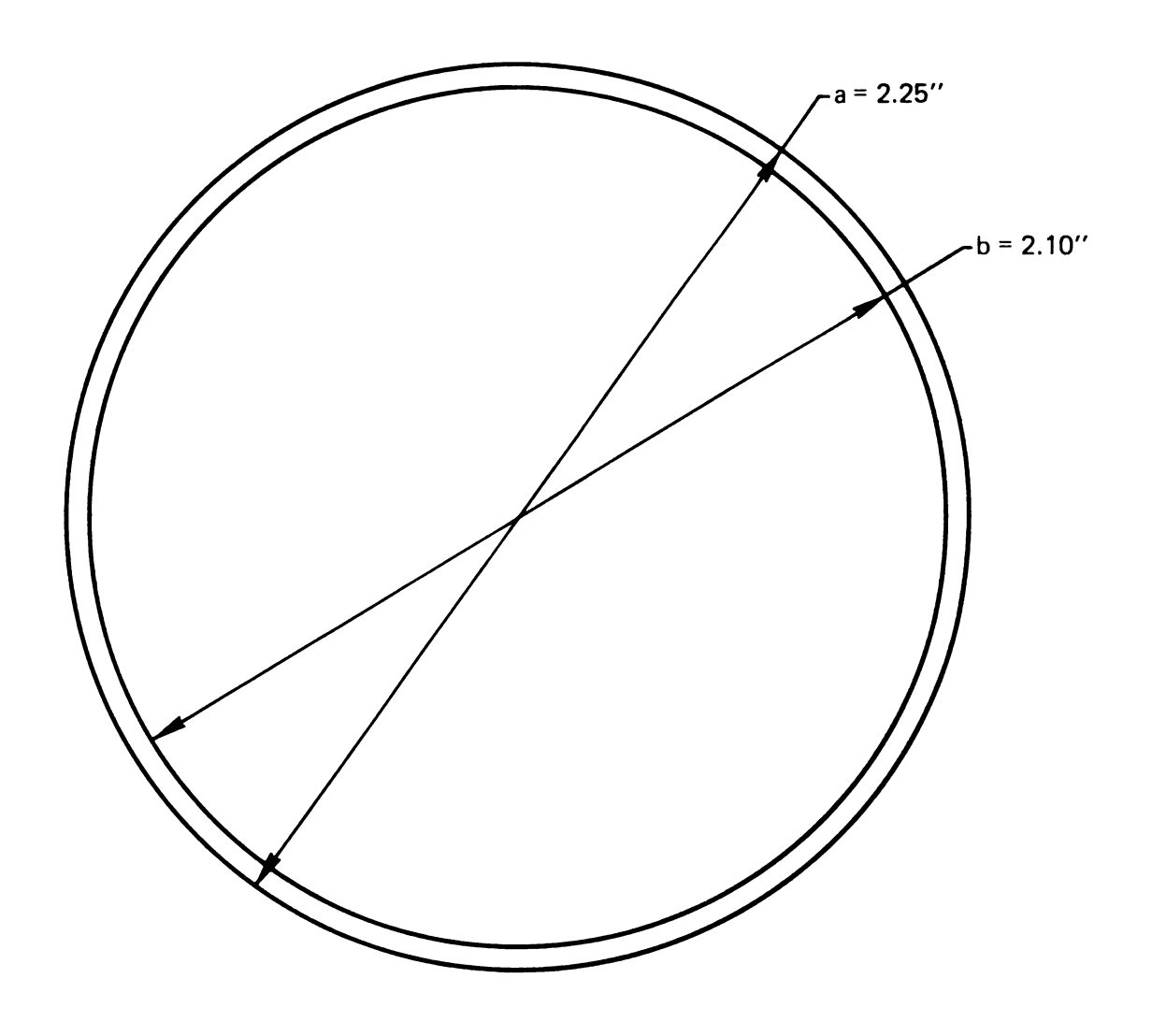
$$c_8 = \frac{1}{2} \left[ 1 + v + (1 - v) \left( \frac{b}{a} \right)^2 \right]$$
 (III-23)

$$C_9 = \frac{b}{a} \left\{ \left[ \frac{1+\nu}{2} \right] \ln \frac{a}{b} + \left[ \frac{1-\nu}{4} \right] \left[ 1 - \left( \frac{b}{a} \right)^2 \right] \right\} \quad (III-24)$$

A trial case was assumed as shown in Figure 13. The material chosen was a titanium alloy, B120VCA, which has the following properties (5)

E = 14.8 x 
$$10^6$$
 psi  
v = 0.21  
 $\sigma_y = 1.90 \times 10^5$  psi  
 $\sigma_u = 2.00 \times 10^5$  psi

The constraints  ${\rm C_2}$ ,  ${\rm C_3}$ ,  ${\rm C_8}$ , and  ${\rm C_9}$  contain material data and radii and do not require thickness. These values were found to be



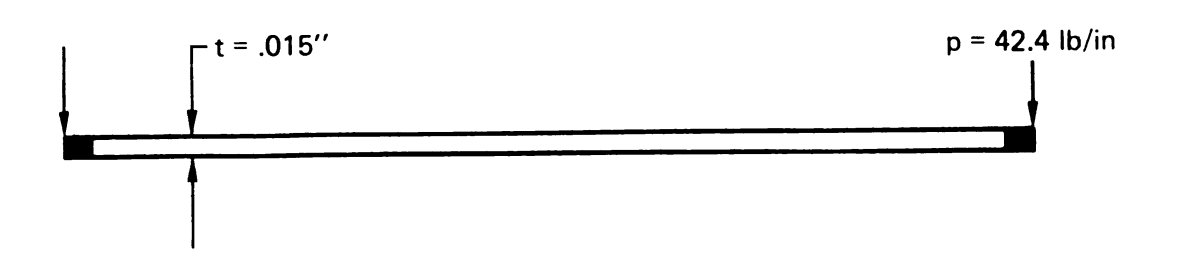


Figure 13. Parameters for flat plate calculation.

$$C_2 = 2.17 \times 10^{-3}$$
 $C_3 = 2.04 \times 10^{-4}$ 
 $C_8 = 0.955$ 
 $C_9 = 0.063$ 

The maximum moment in the plate was

$$M = \frac{-wa^2}{b} \frac{C_9}{C_8} = -6.740$$
 (III-25)

Assuming a maximum working stress of  $1.80 \times 10^5$  psi, the thickness required was

$$t = \sqrt{\frac{6M}{\sigma}} = 0.015$$

The deflection at maximum load was calculated to be

$$y = 0.007$$
 inch

which was not adequate.

The results of the hand calculation above were sufficiently close to meeting the constraints to justify a more detailed study. A computer program, PLATEI, was written to sweep through ranges of thickness for various combinations of inner and outer radius. The results of a typical run are presented in Table 1. Cases which resulted in acceptable stresses and deflections are flagged. The conclusion regarding the use of plates was that the inner radius necessary to achieve the stress and deflection levels specified was outside the acceptable range. The evaluation of plates having fixed outer edges produced a similar conclusion.

## TABLE 1. SAMPLE PRINTOUT FROM PLATEI.

# CIRCULAR PLATE WITH INNER EDGE FIXED

INNER RADIUS= 1.9000 OUTER RADIUS= 2.2500

MATERIAL DATA: E= 1.680E+07 NU= .300

LOADING: 300.00 POUNDS TOTAL 21.2207POUNDS/INCH

THICKNESS	DEFLECTION	STRESS
. 0050	1.703E+00	2.040E+06
.0100	2.129E-01	5.099E+05
.0150	6.307E-02	2.266E+05
.0200	2.661E-02	1.275E+05
. 0250	1.362E-02	8.158E+04
.0300	7.884E-03	5.665E+04
.0350	4.965E-03	4.162E+04
. 0400	3.326E-03	3.187E+04
. 0450	2.336E-03	2.518E+04
. 0500	1.703E-03	2.040E+04
. 0550	1.279E-03	1.686E+04
.0600	9.855E-04	1.416E+04
. 0650	7.751E-04	1.207E+04
.0700	6.206E-04	1.041E+04
.0750	5.046E-04	9.065E+03
. 0800	4.158E-04	7.967E+03
. 0850	3.466E-04	7.057E+03
.0900	2.920E-04	6.295E+03
. 0950	2.483E-04	5.650E+03
.1000	2.129E-04	5.099E+03

The Belleville spring is a non-linear spring which is widely used in applications requiring a tailored load-deflection curve including those cases in which a considerable range of deflection at constant force is necessary (2). Roark (2) gives equations based on the work of Almen and Lazlo (8). Roark's presentation of two constants in tabular form necessitated the use of interpolation to obtain values for a solution. The equations for load and stress were

$$P = \frac{E\delta}{(1 - v^2) \text{ Ma}^2} \left[ (h - \delta) \left( h - \frac{\delta}{2} \right) t + t^3 \right]$$
 (III-26)

$$\sigma = \frac{-E\delta}{(1 - v^2) \text{ Ma}^2} \left[ C_1 \left( h - \frac{\delta}{2} \right) + C_2 t \right]$$
 (III-27)

where  $C_1$  and  $C_2$  were the tabularized constants based on the ratio a/b. Table 2 includes several entries from Roark.

The test case was solved using a Hewlett Packard HP-67 programmable calculator and some available routines. The problem parameters are listed below:

P = 300 pounds

 $\delta = 0.035$  inch

a = 2.25 inch

b = 2.21 inch

The ratio a/b = 1.02 was not a tabulated case, therefore, a linear regression analysis of the tabular data was used to obtain a value of M = 0.1312. It was decided to assume values for the free height, h, and to solve for the thickness. Rearranging the

TABLE 2: BELLEVILLE SPRING CONSTANTS FROM

FORMULAS FOR STRESS AND STRAIN [2]

a/b	$c_1$	$c_2$
1.0		
1.2	1.02	1.05
1.4	1.07	1.14
1.6	1.14	1.23
1.8	1.18	1.30
2.0	1.27	1.46
3.0	1.43	1.74
5.0	1.77	2.38

equations resulted in a cubic function in t:

$$t^3 + (h - \delta) \left(h - \frac{\delta}{2}\right) t + \frac{P(1 - v^2) Ma^2}{E\delta} = 0$$

which became, for a steel spring,

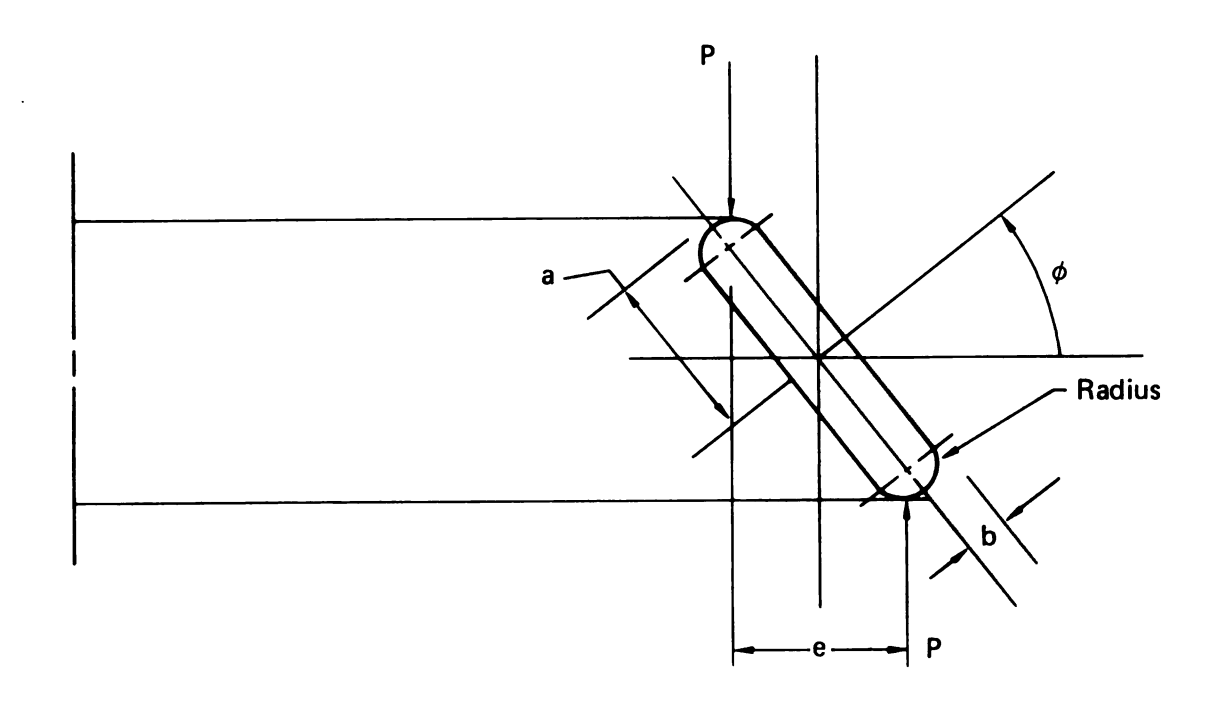
$$t^3 + (h - \delta) \left(h - \frac{\delta}{2}\right) t + (2.17 \times 10^{-4}) = 0$$
 (III-28)

This equation was solved for a series of reasonable heights and yielded negative and complex thicknesses. The assumption was that the spring parameters and the load requirements were incompatible. Further analysis was deferred because of time constraints.

The Belleville spring was of additional interest because of the similarities between the elliptical section ring and the conical washer. The load in both cases is applied through the tangent points of a rotated, non-circular section resulting in a variable moment arm. The deflection of each is a non-linear function of rotation. Since the Belleville spring is a standard engineering design, it is of interest to characterize its response and compare it to that of the elliptical section ring. A modified Belleville spring with circular ends as shown in Figure 14 was also studied.

A cross-section of a Belleville spring is showm in Figure 15. The eccentricity of load application, e, can be seen to be

$$e = 2r \sin (\phi - \Theta_t)$$
 (III-29)



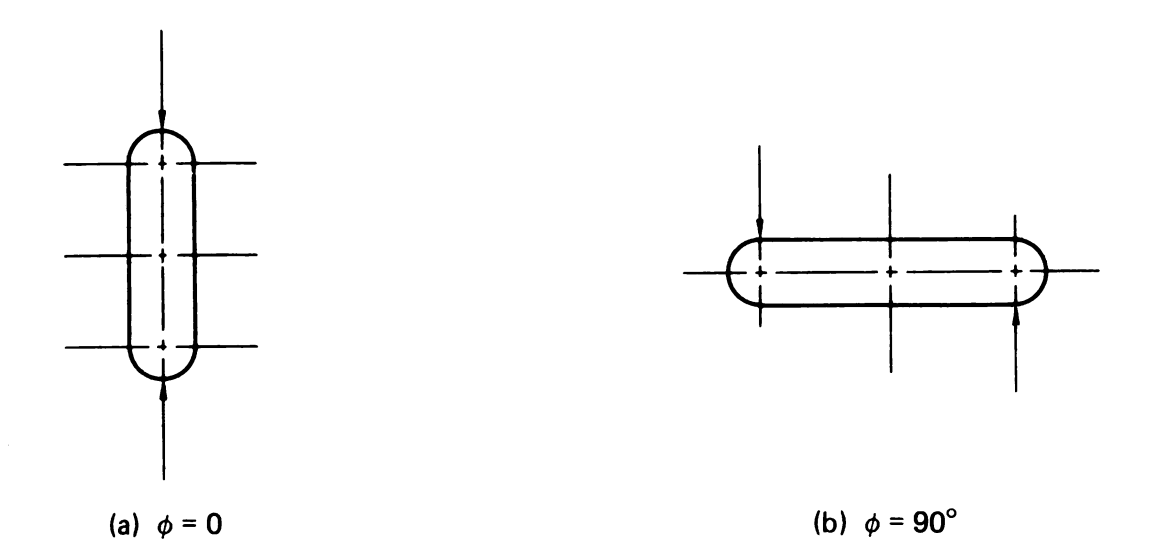


Figure 14. Modified Belleville spring.

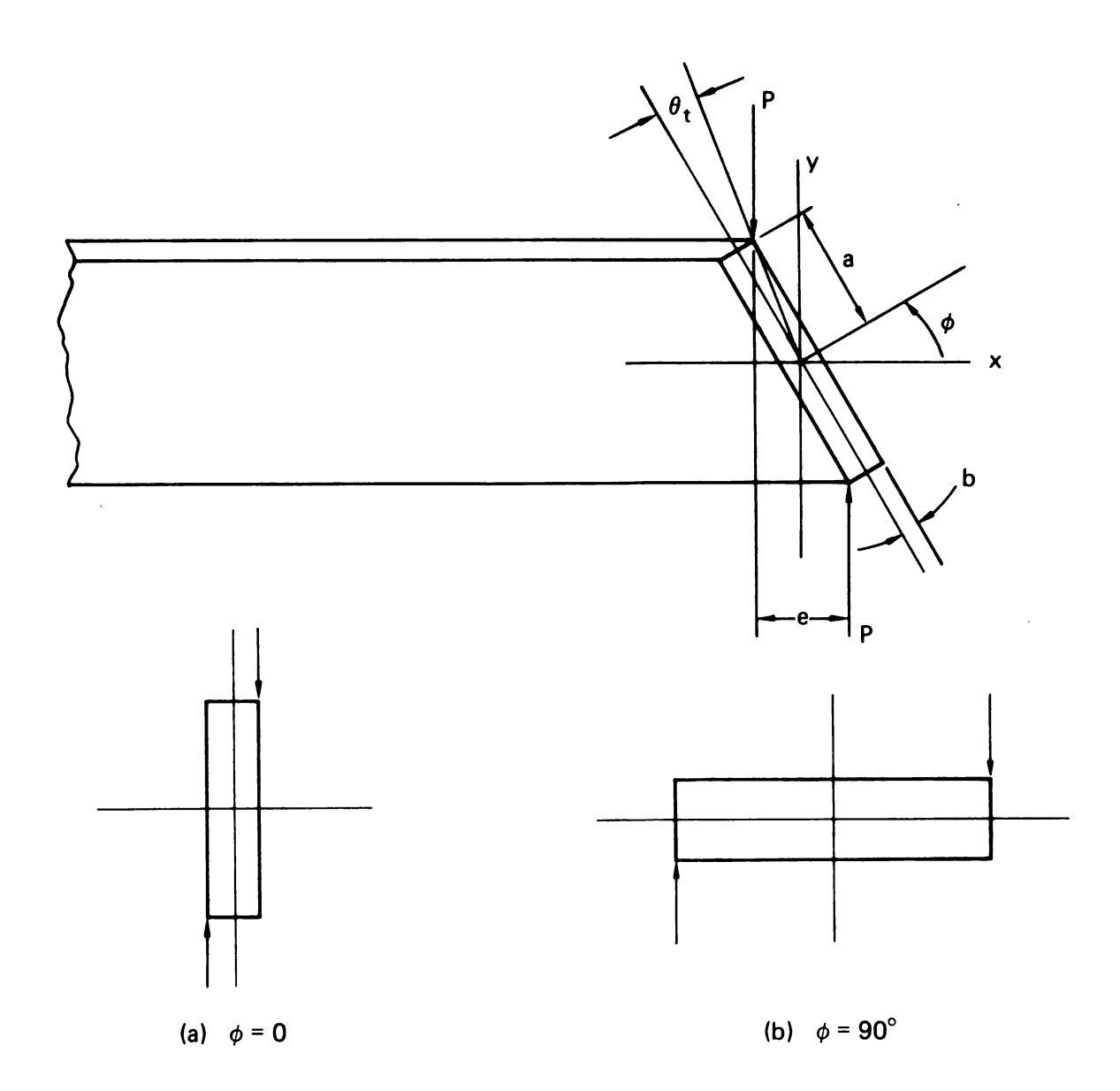


Figure 15. Deflection model for a Belleville spring.

where

$$r = \sqrt{a^2 + b^2} \tag{III-30}$$

$$\Theta_{t} = \tan^{-1} (b/a)$$
 (III-31)

The deflection resulting from a rotation from  $\varphi=\varphi_O$  to  $\varphi$  = 0 is given by

$$\delta = 2r \left(\cos \left(\phi - \Theta_{t}\right) - \cos \left(\phi_{0} - \Theta_{t}\right)\right)$$
 (III-32)

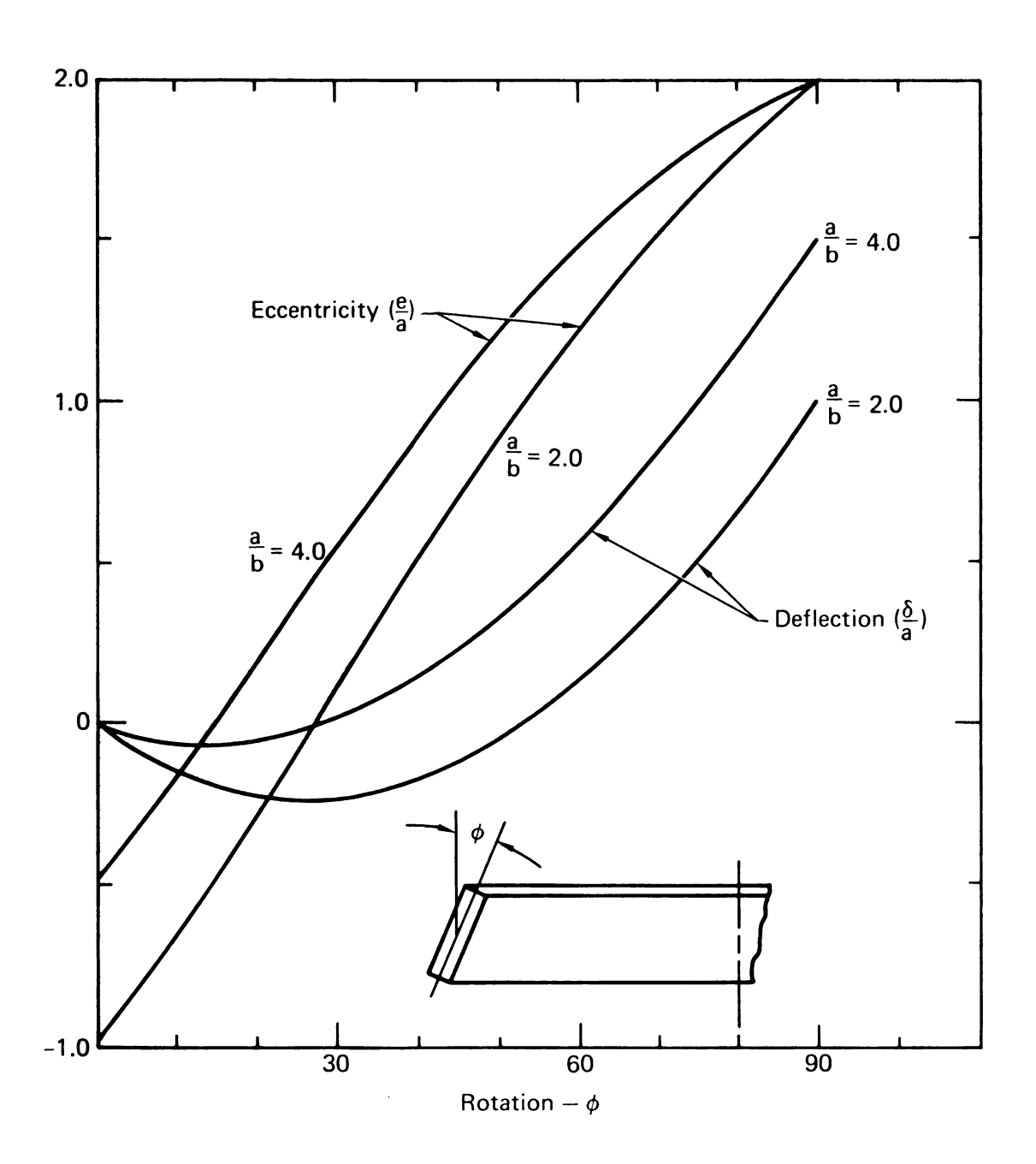
Equations III-29 and III-32 may be normalized to the parameter  $\frac{a}{b}$  in order to consider generalized response. The eccentricity becomes

$$\frac{e}{a} = 2 \left( \frac{\left(\frac{a}{b}\right)^2 + 1}{\left(\frac{a}{b}\right)^2} \right)^{1/2} \left( \sin \phi - \Theta_t \right)$$
 (III-33)

and the deflection becomes

$$\frac{\delta}{a} = 2 \left( \frac{\left(\frac{a}{b}\right)^2 + 1}{\left(\frac{a}{b}\right)^2} \right)^{1/2} \left( \cos \left(\phi - \Theta_t\right) - \cos \left(\phi_0 - \Theta_t\right) \right) \quad (III-34)$$

Note that these equations are based on the assumption of neglibile distortion of the cross-section. Figure 16 illustrates the change in load eccentricity with position for a fixed value of  $\frac{a}{b}$ . At  $\phi$  = 0, the moment arm of the applied load is equal to



16. Belleville spring: Deflection from  $\phi_{_{\mathbf{O}}}$  = 0.

the plate thickness and the moment is negative according to the convention established. The curve passes through zero at  $\phi = \theta_t$  and reaches a maximum value equivalent to the length of the section (e = 2a) at  $\phi = 90^\circ$ .

The negative portion of the curve indicates that the moment of the applied force opposes positive rotations. This condition exists until the corner has rotated past the vertical ( $\phi = \theta_t$ ). Figure 16 also contains a plot of normalized displacement as a function of rotation (Equation III-34). In this case, the negative portion of the curve results from the fact that the height of the section increases as the corner moves upward in the range of rotations

In the case of the modified Belleville spring (see Figure 14), the line of action of the applied force must always pass through the center of curvature of the radiused end. The equations for eccentricity and deflection can be seen to be

$$e = 2r \sin \phi$$
 (III-35)

and

$$\delta = 2r (\cos \phi \cos \phi_0)$$
 (III-36)

where

$$r = a - b (III-37)$$

The general response of the modified Belleville spring may be characterized by the equations when normalized to ratio

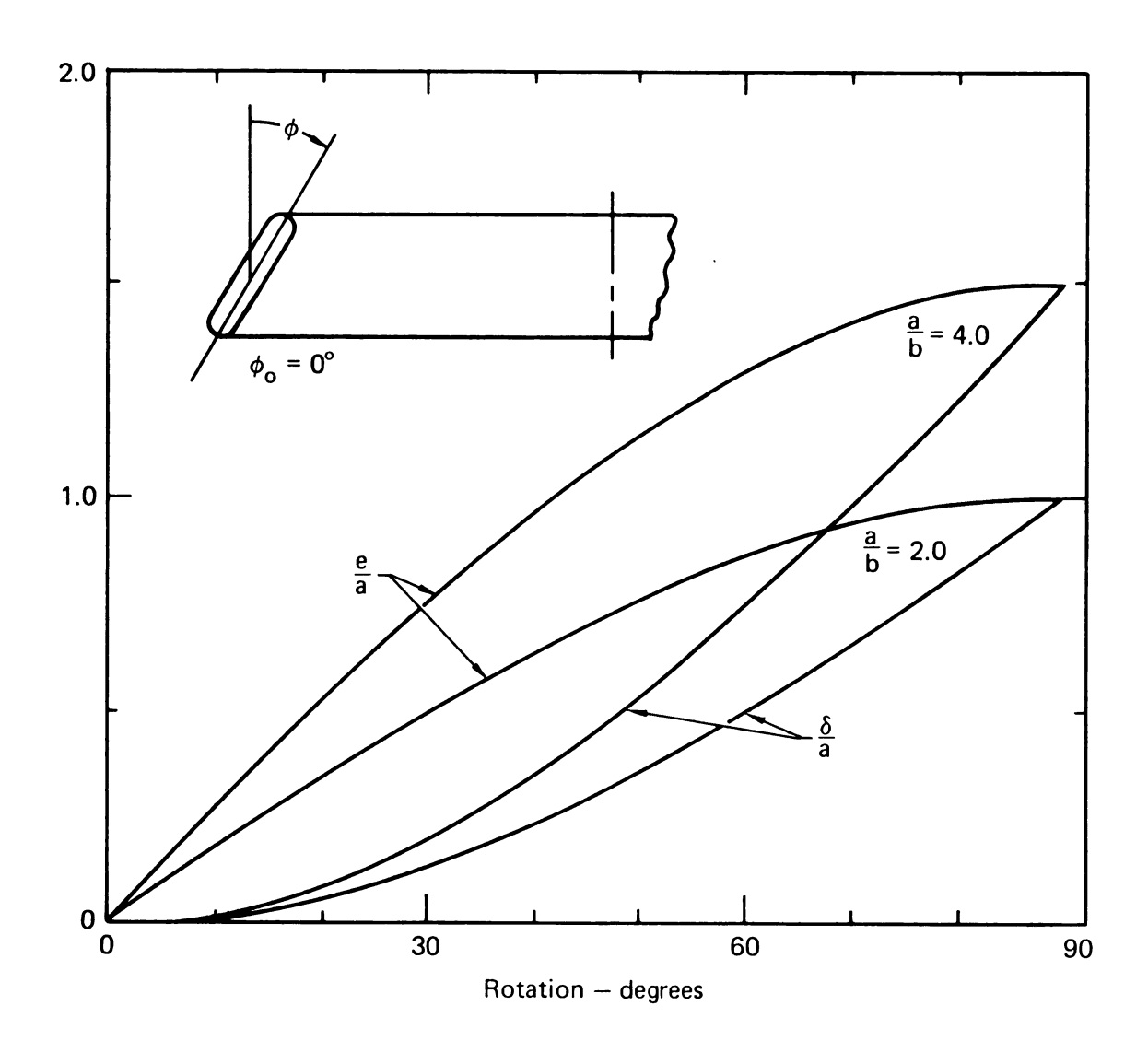
$$\frac{e}{2a} = (1 - \frac{b}{a}) \sin \phi \qquad (III-38)$$

$$\frac{\delta}{2a} = (1 - \frac{b}{a}) (\cos \phi - \cos \phi_0)$$
 (III-39)

which are plotted in Figure 17. In this case, the eccentricity of loading is initially zero and increases to a maximum given by e = 2(a-b) at  $\delta = 90^{\circ}$ . The deflection ranges from zero to  $\delta = 2(a-b)$  at  $\phi = 90^{\circ}$ .

These general response characteristics will be discussed relative to the characteristics of the elliptical section ring in Chapter V.

The results of these and many other studies were negative in the sense that no solutions were found to the design problem. The conclusion drawn from these efforts was that a continuous elastic medium would offer the greatest probability for success. The flat plate calculations and a study of a ring in torsion (see Chapter IV) led the author to postulate the response of a non-circular section ring and to assume that stresses could be held to reasonable levels.



17. Modified Belleville spring: Deflection from  $\phi_{\mathbf{o}}$  = 0.

### CHAPTER IV

## PRELIMINARY CALCULATIONS OF A TWISTED RING

The analysis of alternate spring systems showed that any system meeting the constraints of the problem would be highly stressed. The critical element of effective design was felt to be the development of an accurate predictive capability for deflections and stresses. In order to justify pursuing this endeavor, some preliminary estimates of force, deflection, and stresses were required. A review of the literature showed the most applicable work to be that of Timoshenko describing the twisting of a circular ring of uniform section by distributed couples as shown in Figure 18 (1). Timoshenko refers to a development by R. Grammel (9) for the case when the angle of twist is not small, but the author was unable to obtain a copy of this paper. Additional relevant work was done by Rodriguez (10) discussing the three dimensional bending of a ring on an elastic foundation. Although Timoshenko's derivation was based on the assumption of small angle rotation, it was felt to be of sufficient accuracy to establish the viability of the concept as a potential solution. The procedure is similar to that employed in developing the actual model. The free body diagram of one half of the ring is shown in Figure 19. A summation of the moments about diameter AB may be written

$$dM_{AB} = (M_t R d\alpha) \sin \alpha,$$
 (IV-1)

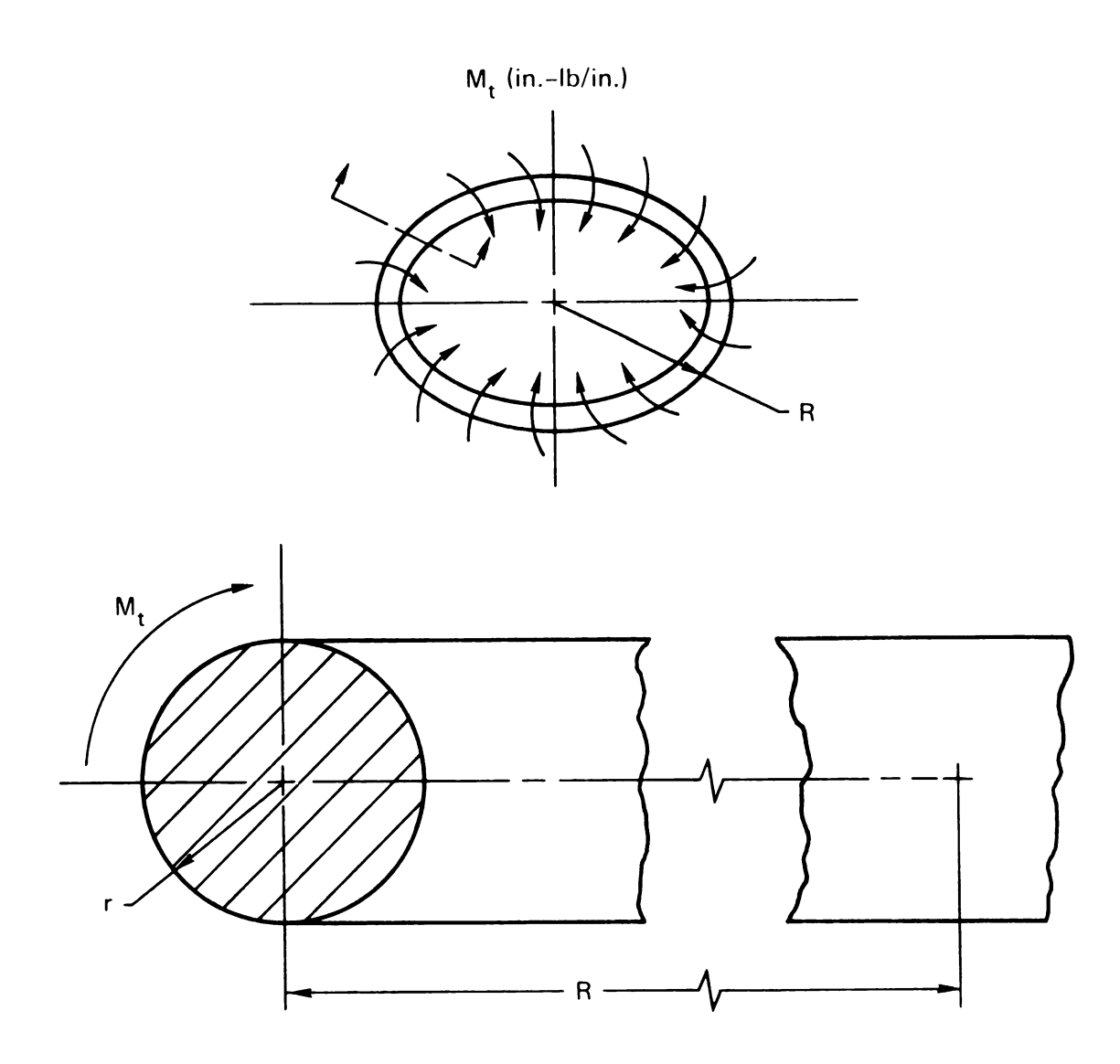


Figure 18. Circular ring loaded by a uniformly distributed twisting moment.

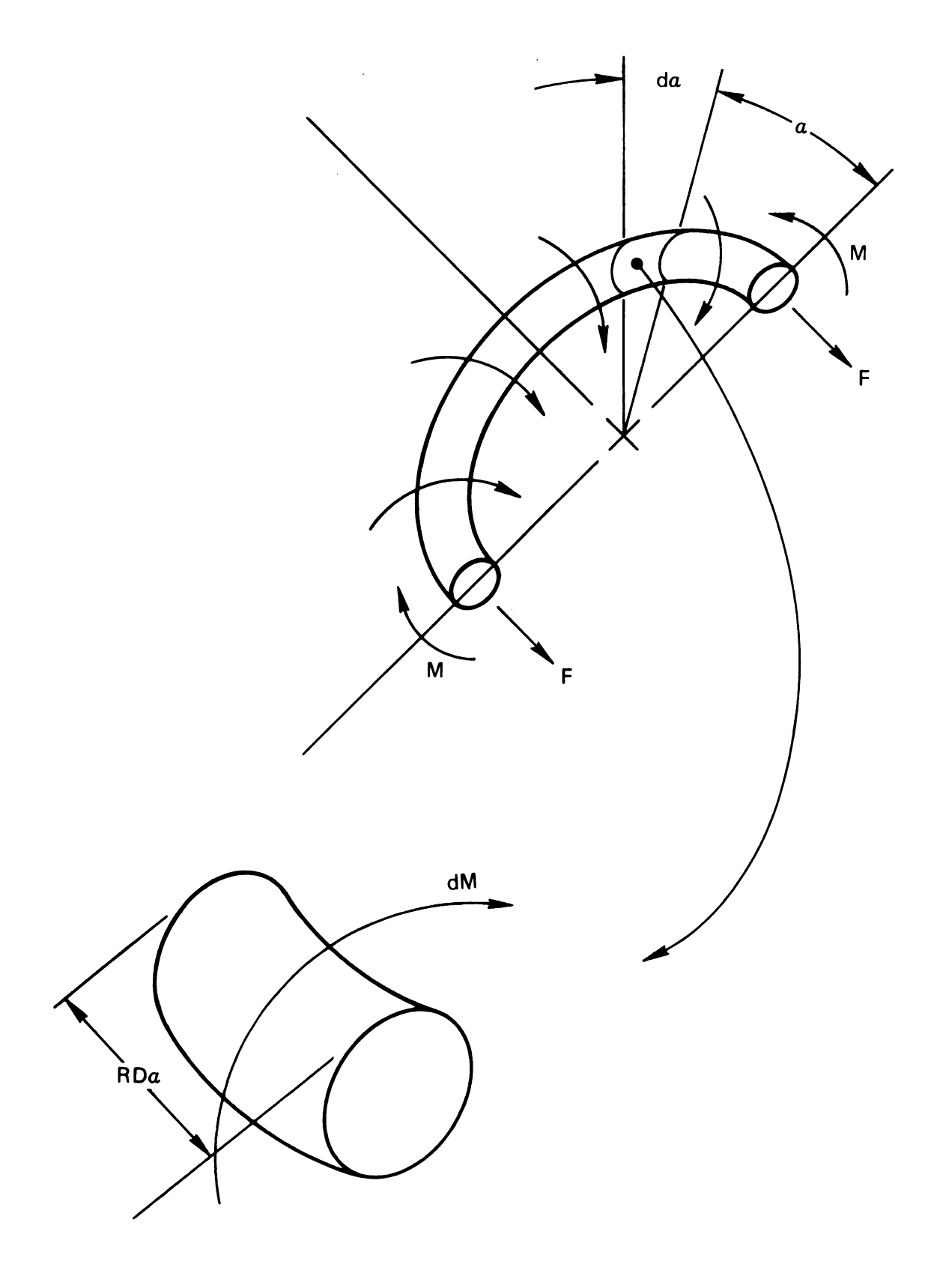


Figure 19. Free-body diagram of a circular ring loaded by a distributed couple.

thus

$$M_{AB} = 2 \int_{0}^{\pi/2} M_{t}R \sin \alpha \, d\alpha = -2M_{t}R, \qquad (IV-2)$$

which results in a bending moment, M, on each cross-section equal to half of the moment,  $M_{AB}$ , or

$$M = \frac{M_{AB}}{2} = -M_{t}R. \tag{IV-3}$$

Symmetry conditions require that the motion results from the rotation of each cross-section in its own plane.

The displacement of any point P results in a change in radius and in a corresponding change in the length of the annular fiber passing through P. The displacement of P is

$$\overline{PP'} = \rho\theta \qquad (IV-4)$$

as indicated in Figure 20. In this analysis, the angle of rotation,  $\theta$ , is assumed to be small and the cross-section is taken to be small relative to the diameter. The change in the radius of P is

$$\Delta R = (\rho \theta) \left(\frac{y}{\rho}\right) = \theta y$$
 (IV-5)

Since the cross-section is small relative to the radius, the radius of any fiber is approximately equal to R and the strain in a fiber is given by

$$\varepsilon = \frac{\Delta \ell}{\ell} = \frac{2\pi (R + \Delta R) - 2\pi R}{2\pi R}$$

or

$$\varepsilon = \frac{\Delta R}{R} = \frac{\theta y}{R} \tag{IV-6}$$

The fiber stress resulting from the strain is

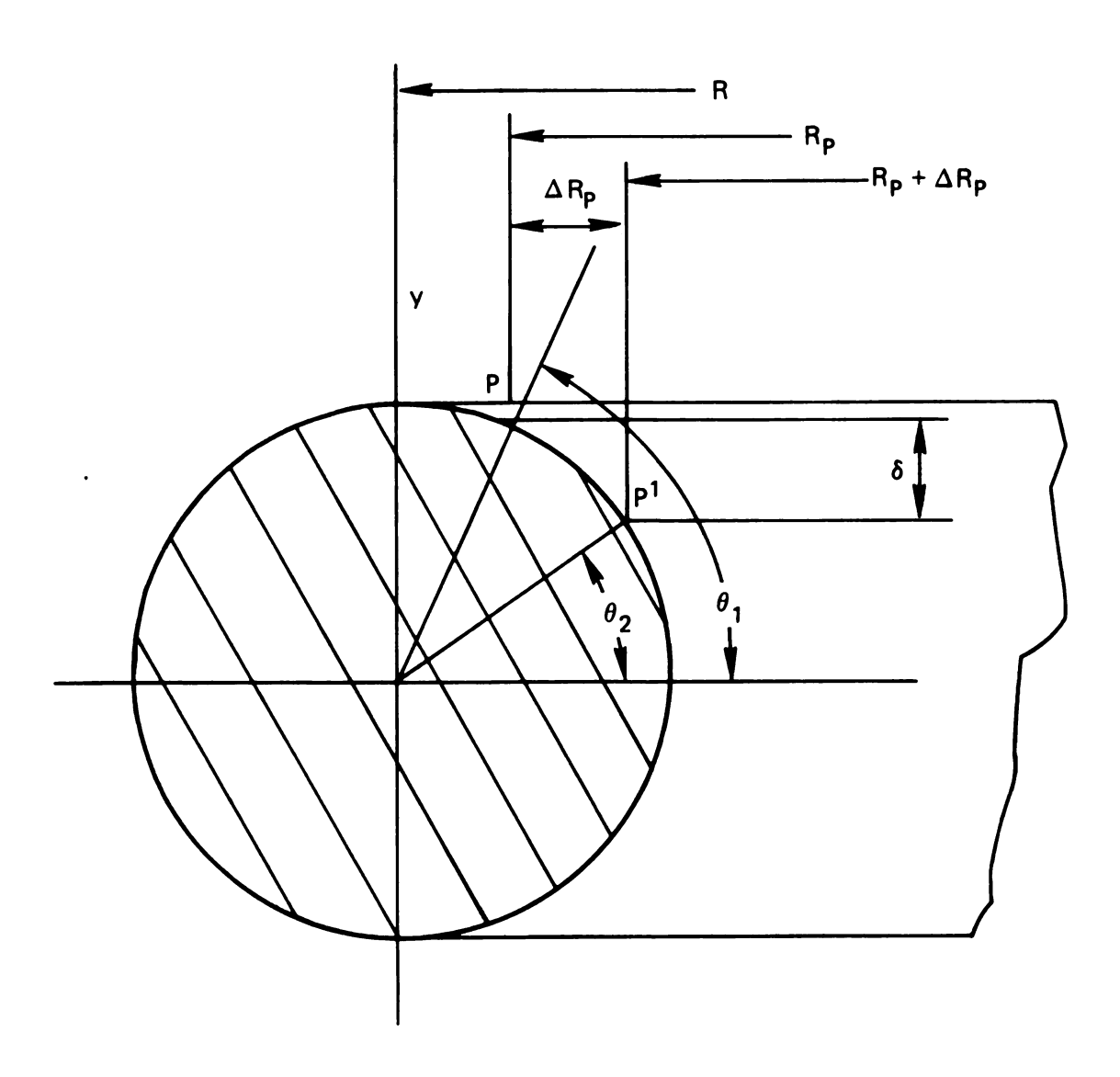


Figure 20. Displacement of a point, P, due to a rotation  $\Delta\theta$  =  $\theta_1$  –  $\theta_2$ .

$$\sigma = E\varepsilon = \frac{E\theta y}{R} \tag{IV-7}$$

Equilibrium conditions for the half ring may be written in the form

$$\int_{A} \sigma dA = \int_{A} \frac{E\theta y}{R} dA = 0$$
 (IV-8)

and

$$\int_{A} \sigma y dA = \int_{A} \frac{E\theta y^{2}}{R} dA = M$$
 (IV-9)

Equation (IV-8) shows that the centroid lies on the x-axis.

Equation (IV-9) may be rewritten as follows:

but

$$\int_{A} \frac{E\theta}{R} y^{2} dA = \frac{E\theta}{R} \int_{A} y^{2} dA = M,$$

$$\int_{A} y^2 dA \equiv I_{xx}$$

and so

$$\frac{\text{EI}_{XX}}{\text{p}} \theta = M \tag{IV-10}$$

The angle of rotation due to a distributed couple,  $M_{\mbox{\scriptsize t}}$ , can be shown to be

$$\theta = \frac{M_t R^2}{EI_{xx}}$$
 (IV-11)

In order to assess the viability of the concept of a ring under twist as a solution to the specific problem, consider the example shown in Figure 21. The assumptions made in this calculation were

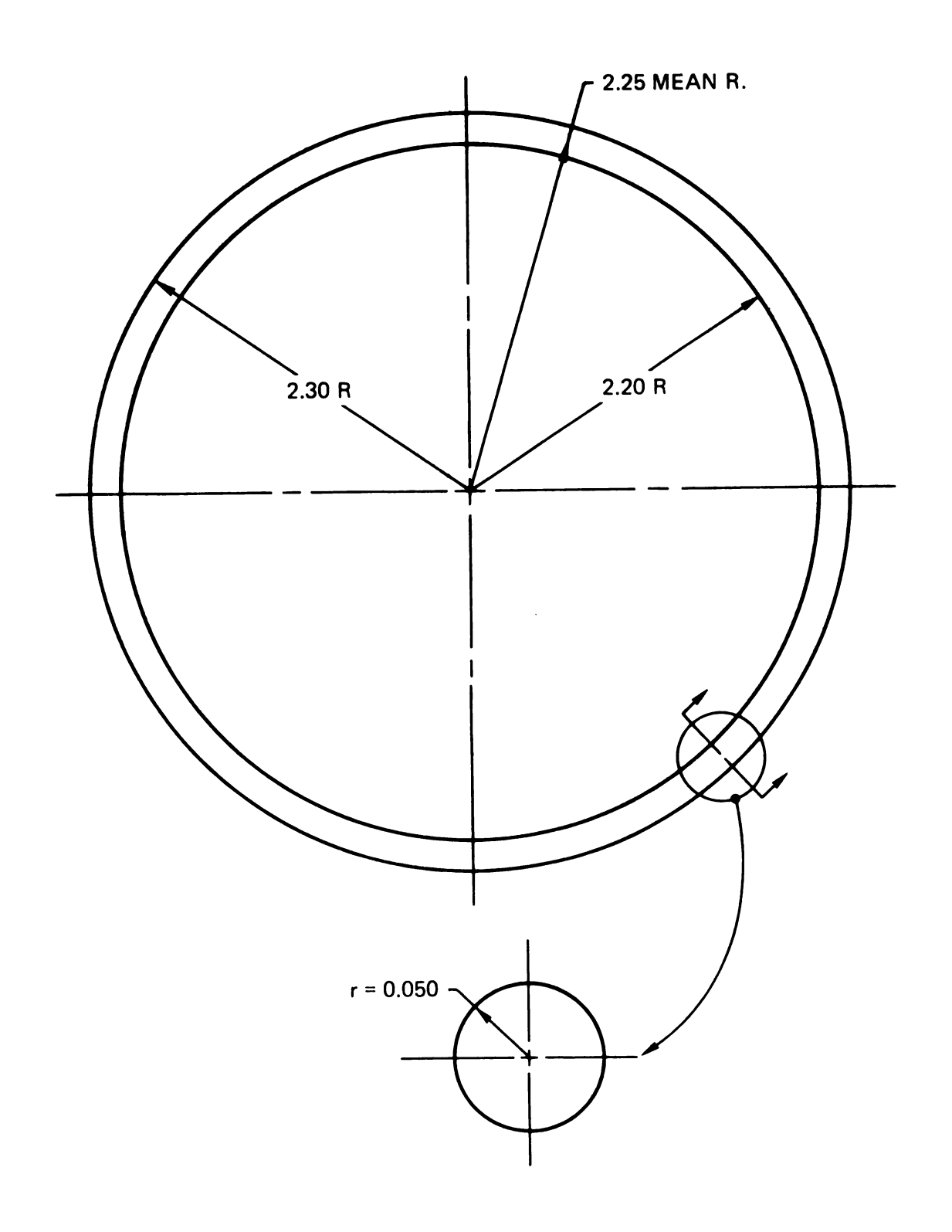


Figure 21. Circular section ring for trial calculations.

- the envelope could be expanded to 0.100 inch square, thus the radius, r, of the cross-section has a maximum value of 0.050 inch
- the axial load was to be applied at an eccentricity,e = 2r.
- 3) the deflection required was  $\delta = 0.060$  inch (assuming a linear force-deflection curve).

Clearly, the small angle assumptions were violated in this example but it was felt that the results would be indicative of the magnitude of the force, deflection, and stress. This knowledge justified the decision to continue the analysis.

The deflection resulting from a rotation through an angle,  $\boldsymbol{\theta}$ , is

$$\delta = 2r(\sin \theta_1 - \sin \theta_2) \tag{IV-12}$$

where  $\theta_1$ , and  $\theta_2$  are the initial and final angles of the lever arm. It was assumed for purposes of this example that  $\theta_1$  =  $90^{\circ}$  and thus

$$\delta = 2r(1 - \sin \theta_2)$$

or

$$\theta_2 = \sin^{-1}\left(1 - \frac{\delta}{2r}\right) \tag{IV-13}$$

Substitution of the example data in Equation (IV-13) gave a final angle

$$\theta_2 = \sin^{-1}\left(1 - \frac{0.060}{2(0.050)}\right) = 23.6^{\circ}$$

or

$$\theta_2 = 0.41$$
 radian

The force required to maintain this rotation can be established from Equation (IV-11)

$$M_t = \frac{EI_{xx}\theta}{R^2}$$

and

$$M_{t} = \frac{Pe}{2\pi R} = \frac{Pr}{\pi R} \tag{IV-14}$$

as shown in Figure 19. Note also that

$$I_{xx} = \frac{\pi r^4}{4} \tag{IV-15}$$

for a circular cross-section. The net load on the spring is

$$P = \frac{\pi^2 \theta Er^3}{AR} , \qquad (IV-16)$$

and substitution of the problem parameters gave

$$P = \frac{\pi^2(0.41)(14.8 \times 10^6)(0.050)^3}{(4)(2.25)} = 835 \text{ pounds}$$

The stress was determined from Equation (IV-7) and was found to be

$$\sigma = 1.35 \times 10^5 \text{ psi}$$

The material assumed in the example was titanium.

The force calculated was acceptably close to the design range and the stress levels were acceptable for the application of

high strength engineering materials. The conclusion of this study was that a more rigorous analysis of the ring response was required and justified.

#### CHAPTER V

### DEFORMATION AND STRESS IN AN ELLIPTICAL SECTION RING

The example in Chapter IV demonstrated that twisting of a ring represented a feasible solution to the spring design problem as specified in Chapter II. The indication was that a ring could be designed for large deformations in the elastic range. It was hypothesized that a suitable choice of cross-section would result in a load-deflection curve with a constant force region over a sufficient range of deflections. The study also showed the deficiencies of the available models in approximating ring response. The design of a ring of non-circular section for use as a large-deformation spring definitely required a more precise calculational model. The purpose of this chapter is to present the derivation of equations describing the ring response to distributed axial load.

As previously discussed, the original concept was that of a circular ring having an arbitrary non-circular cross-section. Initially, it was assumed that the boundary curve of the section could be optimized to provide the optimum load-deflection behavior for a specific spring requirement. The enormity of that undertaking was quickly recognized, however, and the more modest goal of analyzing the response with a particular boundary curve was established. An elliptical section was chosen because the shape is easily described for fabrication and because it can be widely varied by appropriate selection of the major and minor axes. The

parameters of the elliptical section ring are shown in Figure 22 and the load application is depicted in Figure 23. Following common practice, the semi-major axis is designated as a, and the semi-minor axis as b. The equation of the ellipse may be written as

$$\frac{x^2}{b^2} + \frac{y^2}{a^2} = 1 \tag{V-1}$$

where x and y are principal axes.

The distributed load is applied and reacted through the radial tangents as shown in Figure 23 and may be replaced by a distributed couple.

e = moment arm

The net force carried by the spring is

$$F = 2\pi Rp$$

As in Chapter IV, the equilibrium conditions for the half ring are

$$\Sigma F_{\mathbf{x}} = 0 \qquad (V-3a)$$

$$\Sigma F_{\mathbf{y}} = 0 \qquad (V-3b)$$

$$\Sigma F_{z} = 0 \qquad (V-3c)$$

$$\Sigma F_{z} = 0 (V-3d)$$

which are satisfied identically as shown in the free-body diagram (Figure 24). An element of the ring defined by  $d\psi$  and located an an angle  $\psi$  from the x-axis is subjected to external moments

$$dM_{\chi} = dM \sin \psi$$
 (V-4)

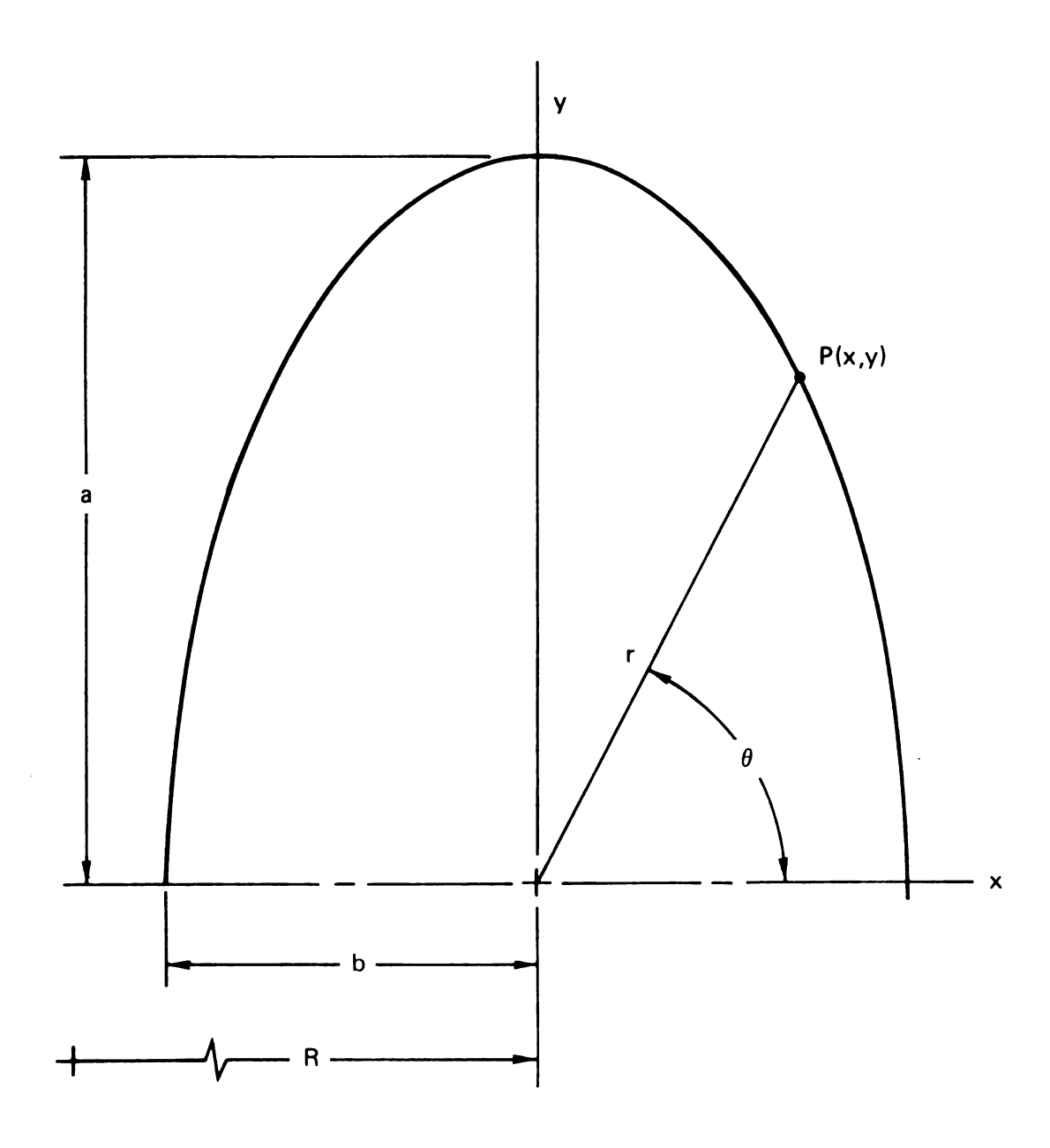


Figure 22. Ellipse parameters in body coordinates.

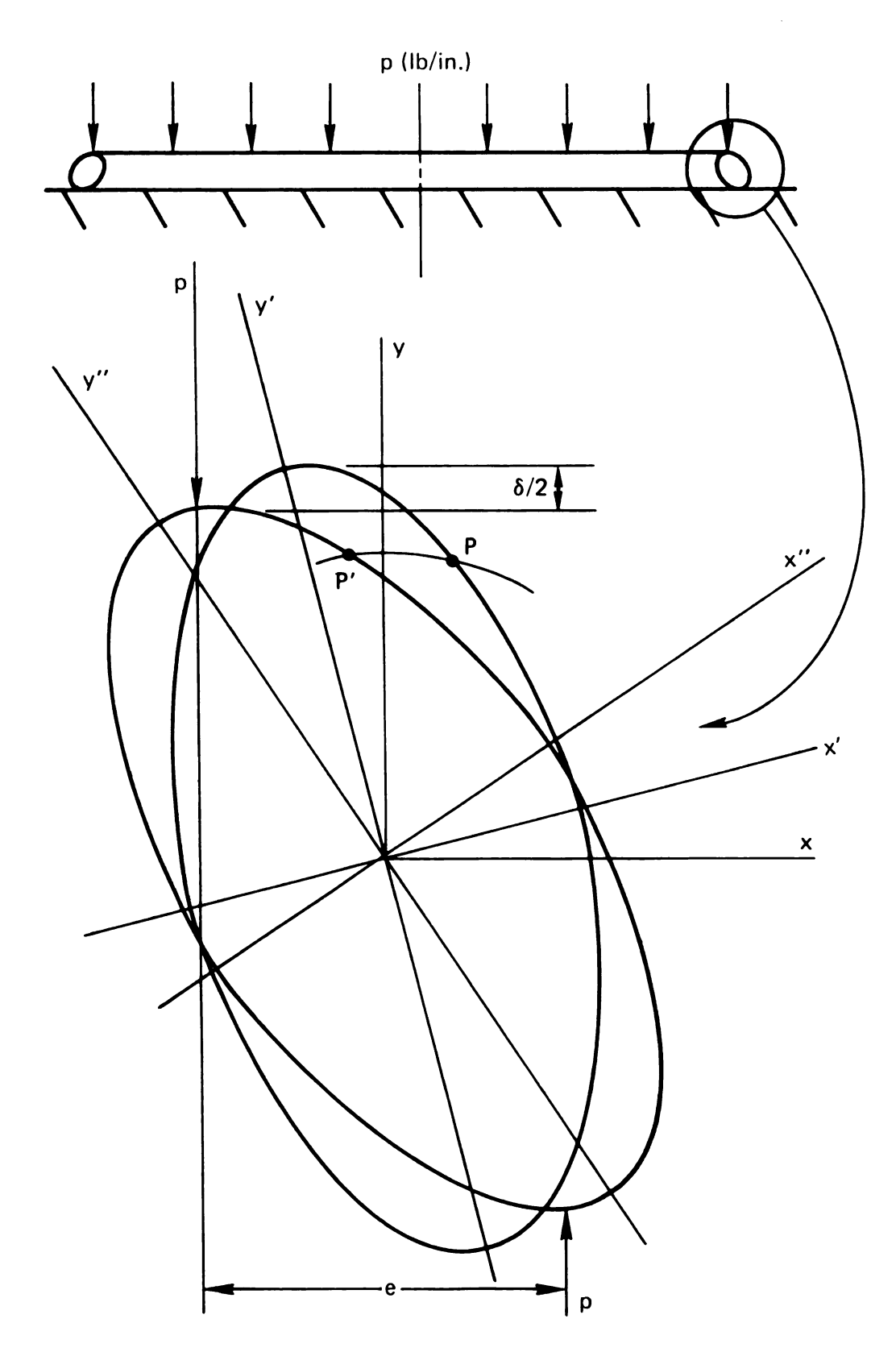


Figure 23. Load distribution on an elliptical section ring

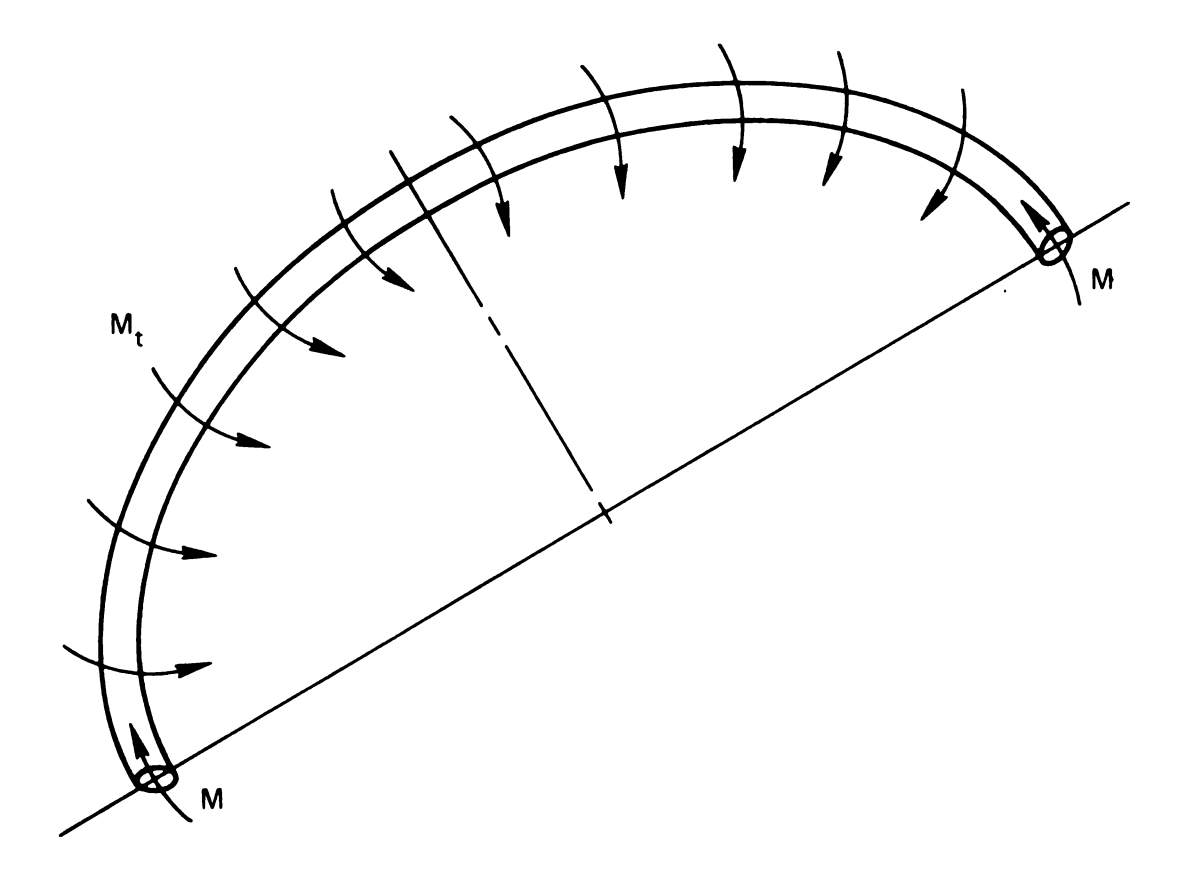


Figure 24. Free body diagram of an elliptical section ring.

$$dM_{y} = -dM \cos \psi \qquad (V-5)$$

where

$$dM = M_{t}R d\psi \qquad (V-6)$$

as shown in Figure 24. Equilibrium of moments about the x-axis and y-axis for the half ring is defined by

$$\Sigma M_{x} = 2M_{x} = \int_{0}^{\pi} M_{t}R \sin \psi \, d\psi$$

$$M_{x} = M_{t}R$$
(V-7)

and

$$\Sigma M_{y} = 2M_{y} = -\int_{0}^{\pi} M_{t}R \cos \psi d\psi = 0$$

$$M_{v} = 0$$
(V-8)

where  $M_x$  and  $M_y$  are the resultant bending moments due to the distribution of stresses over the cross-section in the x-y plane.

The strain and therefore the stress at a point, P, in the cross-section may be defined in terms of the change in length of the circumferential fiber through P in a manner analogous to the procedure employed in Chapter IV. Consider a point P(x, y) on an ellipse as shown in Figure 25.

The distance  $\overline{OP}$  as a function of the angular position of P is found from the coordinates

$$x_p = r(\theta) \cos \theta$$
 (V-9)

$$y_D = r(\theta) \sin \theta$$
 (V-10)

and from Equation (V-1). The length of  $\overline{OP}$  is

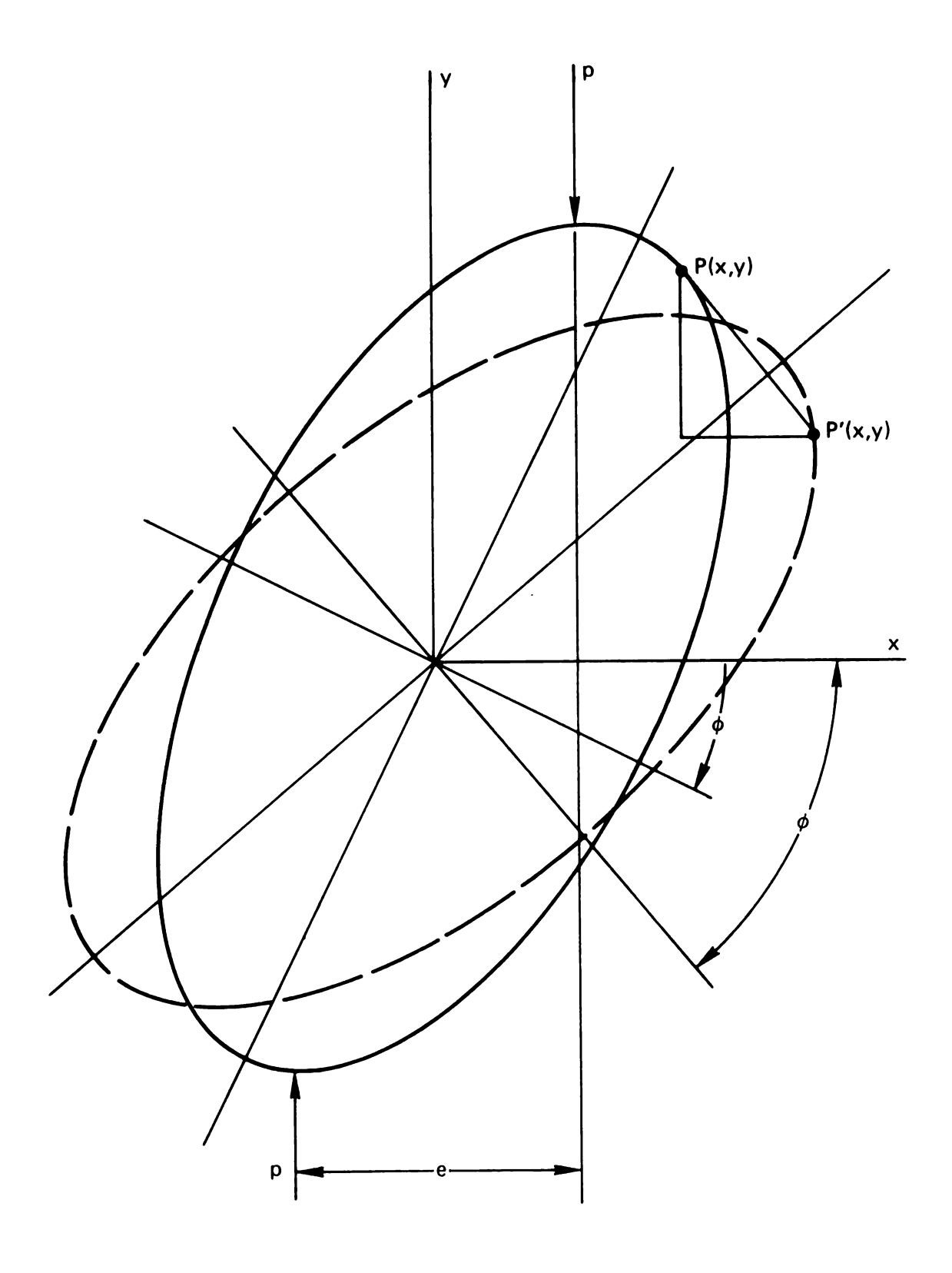


Figure 25. Loading on a section of an elliptical section ring.

$$r(\theta) = \frac{ab}{\sqrt{a^2 \cos^2 \theta + b^2 \sin^2 \theta}}$$
 (V-11)

If, as shown in Figure 24, the ellipse is rotated about the local z-axis, the point, P(x, y), is transformed to P'(x, y). Assuming no distortion of the cross-section, the coordinates of P in the body axes, x'-y' are

$$x' = r(\theta) \cos \theta \tag{V-12}$$

$$y' = r(\theta) \sin \theta$$
 (V-13)

Note that x'-y' are principal axes of the inertia tensor. The transform of P(x, y) to P'(x, y) is defined by

$$\begin{cases} x \\ y \\ y \\ \text{sin } \phi \end{cases} = \begin{bmatrix} \cos \phi & -\sin \phi \\ \sin \phi & \cos \phi \end{bmatrix} \quad \begin{cases} x \\ y \\ p \end{cases} \quad (V-14)$$

or

$$\left\{x\right\}_{p'} = \left[a(\phi)\right] \left\{x\right\}_{p}$$
 (V-15)

It is obvious from Figure 23 that the moment arm, e, is zero for  $\varphi=0$  and  $\varphi=\pi/2$ . In these positions, no torque is exerted upon the ring and the only deformation will be the result of compressive strain through the section. In order to avoid this condition in applications, it is necessary to fabricate the ring with the axes of the ellipse oriented at some initial angle,  $\varphi_0$ , to the x-y axes. The position of P at  $\varphi=\varphi_0$  is

$$\{x\}_{p'} = [a(\phi_0)] \{x\}_{p}$$
 (V-16)

and, following a successive transform to P" at

$$\{x\}_{p^{H}} = [a(\phi_{0})] \{x\}_{p}$$
 (V-17)

The strain,  $\epsilon$ , in the circumferential fiber through P is defined by

$$\varepsilon_{\mathbf{p}^{\dagger}\mathbf{p}^{\dagger\prime}} = \left(\frac{\Delta \mathbf{l}}{\mathbf{l}}\right)_{\mathbf{p}^{\dagger}\mathbf{p}^{\prime\prime}} = \frac{2\pi(\mathbf{R} + \mathbf{x}_{\mathbf{p}^{\prime\prime}}) - 2\pi(\mathbf{R} + \mathbf{x}_{\mathbf{p}^{\prime\prime}})}{2\pi \overline{\mathbf{R}}_{\mathbf{p}}}$$
(V-18)

and, assuming the cross-section to be small relative to the radius,

$$\overline{R}_{p} \approx R$$
 (V-19)

thus

$$\varepsilon_{\mathbf{p}^{\dagger}\mathbf{p}^{\parallel}} = \frac{\mathbf{x}_{\mathbf{p}^{\parallel}} - \mathbf{x}_{\mathbf{p}^{\dagger}}}{R} \tag{V-20}$$

Substituting the relationships for  $x_p$ ' and  $x_p$ " from Equations (V-17) and (V-16), respectively,

$$\varepsilon_{p'p''} = \frac{1}{R} \left[ (\cos \phi - \cos \phi_0) x_p - (\sin \phi - \sin \phi_0) y_p \right]$$
 (V-21)

As in classical beam theory, the transverse stress is assumed negligible and the effects of shear are ignored so that the stress at the point is given by

$$\sigma_{\mathbf{p'p''}} = \mathbf{E} \varepsilon_{\mathbf{p'p''}} \tag{V-22}$$

The equilibrium conditions for the cross-section are

$$\int_{A} \sigma dA = \Sigma F_{z} = 0 \qquad (V-23)$$

$$\int_{A} \sigma x dA = \Sigma M_{y} = 0 \qquad (V-24)$$

$$\int_{A} \sigma y dA = \sum M_{x} = 2M_{x} \qquad (V-25)$$

Equation (V-23) becomes

$$\int_{A}^{\sigma dA} = \frac{E}{R} \int_{A} \left\{ (\cos \phi - \cos \phi_0) \cos \theta - (\sin \phi - \sin \phi_0) \right\}$$

$$\sin \theta r(\theta) dA$$

from the symmetry of the cross-section. The equilibrium of moments about the y-axis (Equation (V-24)) becomes

$$\int_{A} \sigma x dA = \frac{E}{R} \int_{A} \epsilon x dA + \frac{E}{R} \int_{A} \epsilon (-x) dA = 0$$

which results from the antisymmetric positions of the crosssections at opposite ends of a ring diameter. Finally, the moments about the x-axis are seen from Equation (V-25) to be

$$\int_{A} \sigma y dA = 2 \frac{E}{R} \int_{A} \left\{ (\cos \phi - \cos \phi_0) x - (\sin \phi - \sin \phi_0) y \right\} y dA$$

$$= 2 \frac{E}{R} (\cos \phi - \cos \phi_0) \int_{A} xy dA - 2 \frac{E}{R} (\sin \phi - \sin \phi_0) \int_{A} y^2 dA$$

$$- \sin \phi_0) \int_{A} y^2 dA$$

Recall that

$$\int_{A} y^2 dA \equiv I_{xx}$$
 (V-26)

$$\int_{A} xydA \equiv I_{xy} \tag{V-27}$$

where  $I_{xy}$  is non-vanishing since the x-y axes are not principal. Therefore,

$$\int_{A} \sigma y dA = 2 \frac{E}{R} \left[ I_{xy}(\cos \phi - \cos \phi_0) - I_{xx}(\sin \phi - \sin \phi_0) \right]$$

$$= \Sigma M_{X} = 2M_{X} = 2M_{L}R$$

from Equation (V-7). The moment-rotation relationship may be seen to be

$$M_{t} = \frac{E}{R^{2}} \left[ I_{xy}(\cos \phi - \cos \phi_{0}) - I_{xx}(\sin \phi - \sin \phi_{0}) \right] \qquad (V-28)$$

The values of  $I_{xx}$  and  $I_{xy}$  are determined from the transform of the moment of inertia tensor

$$[I(x,y)] = [a(\phi)][I(x',y')][a(\phi)]$$
 (V-29)

or

$$I_{xx} = I_x \cos^2 \phi + I_y \sin^2 \phi \qquad (V-30)$$

$$I_{xy} = (I_y - I_x) \sin \phi \cos \phi \qquad (V-31)$$

and the principal moments of inertia (2)

$$I_{x} = \frac{\pi a^{3}b}{4} \tag{V-32}$$

$$I_{y} = \frac{\pi a b^{3}}{4} \tag{V-33}$$

Again referring to Figure 25, the load is applied through the horizontal tangents. Designating the point of tangency as Q(x, y), the following observations are made

$$\mathbf{e} = 2|\mathbf{x}_0| \tag{V-34}$$

and

$$\delta = 2|y_{0"} - y_{0'}| \tag{V-35}$$

The condition of tangency with the x-axis is

$$\left(\frac{dy}{dx}\right)_{Q} = 0 = \frac{\left(\frac{dy}{d\theta}\right)_{Q}}{\left(\frac{dx}{d\theta}\right)_{Q}}$$
 (V-36)

where

$$x(\theta) = r(\theta) \cos (\theta + \phi) \tag{V-37}$$

$$y(\theta) = r(\theta) \sin (\theta + \phi)$$
 (V-38)

from Equations (V-12), (V-13), and (V-14). Differentiating with respect to  $\theta$ ,

$$\frac{dx(\theta)}{d\theta} = -r(\theta) \sin (\theta + \phi) + \frac{dr(\theta)}{d\theta} \cos (\theta + \phi)$$
 (V-39)

$$\frac{dr(\theta)}{d\theta} = \frac{d}{d\theta} \left( \frac{ab}{\sqrt{a^2 \cos^2 \theta + b^2 \sin^2 \theta}} \right)$$

$$= \frac{r(\theta)}{2D^2} (a^2 - b^2) \sin 2\theta$$
(V-40)

where

$$D = (a^2 \cos^2\theta + b^2 \sin^2\theta)$$
 (V-41)

Thus

$$\frac{dx(\theta)}{d\theta} = -r(\theta) \sin (\theta + \phi) + \frac{r(\theta)}{2D^2} (a^2 - b^2) \sin 2\theta \cos (\theta + \phi)$$

$$\frac{dx(\theta)}{d\theta} = -\frac{r(\theta)}{D^2} (a^2 \cos \theta \sin \phi + b^2 \sin \theta \cos \phi) \qquad (V-42)$$

Similarly

$$\frac{dy(\theta)}{d\theta} = r(\theta) \cos (\theta + \phi) + \frac{r(\theta)}{2D^2} (a^2 - b^2) \sin 2\theta \sin (\theta + \phi)$$

$$\frac{dy(\theta)}{d\theta} = \frac{r(\theta)}{D^2} (a^2 \cos \theta \cos \phi - b^2 \sin \theta \sin \phi) \qquad (V-43)$$

Then

$$\frac{dy}{dx} = \frac{dy}{d\theta} \cdot \frac{d\theta}{dx} = -\left(\frac{a^2 \cos \theta \cos \phi - b^2 \sin \theta \sin \phi}{a^2 \cos \theta \sin \phi + b^2 \sin \theta \cos \phi}\right) \tag{V-44}$$

Equating Equation (V-44) to zero gives

$$\frac{dy}{dx}_{Q} = -\left(\frac{a^{2} \cos \theta_{t} \cos \phi - b^{2} \sin \theta_{t} \sin \phi}{a^{2} \cos \theta_{t} \sin \phi - b^{2} \sin \theta_{t} \cos \phi}\right) = 0$$

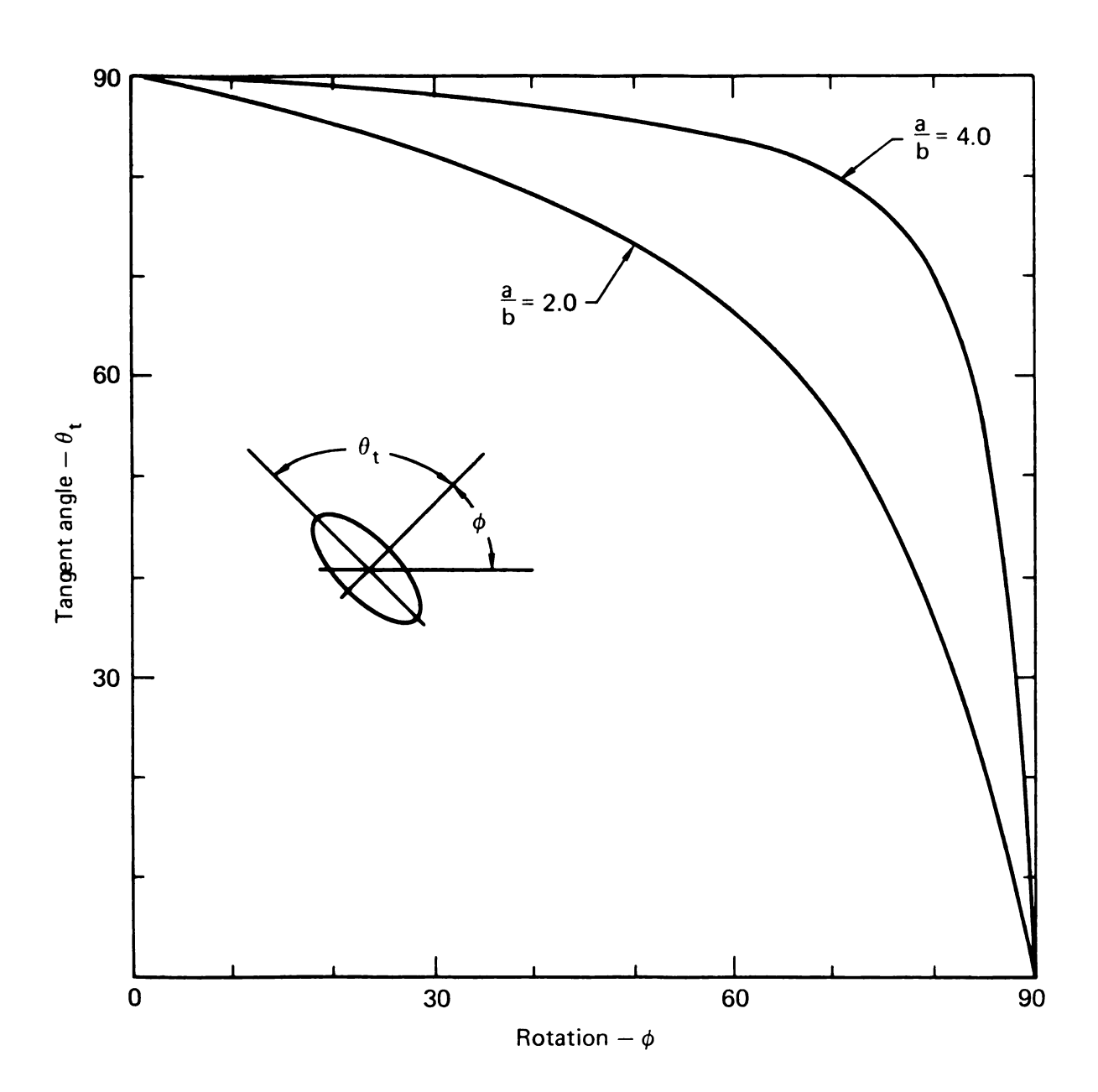
or

$$a^{2} \cos \theta_{t} \cos \phi = b^{2} \sin \theta_{t} \sin \phi$$

$$\tan \theta_{t} = \frac{a^{2}}{b^{2}} \cot \phi$$
(V-45)

at the point of horizontal tangency. The orientation of the contact point relative to the minor axis of the ellipse is shown in Figure 26 for the case a/b = 2.0 and a/b = 4.0. The contact point is on the major axis when  $\phi = 0^{\circ}$  and on the minor axis when  $\phi = 90^{\circ}$ . At other positions, the contact point lies between the axes of the ellipse. The coordinates of Q are given by

$$r_{t} = \frac{ab}{\sqrt{a^{2} \cos^{2} \theta_{t} + b^{2} \sin^{2} \theta_{t}}}$$
 (V-46)



26. Location of the contact point between an ellipse and a flat plate.

$$x_{t}' = r_{t} \cos \theta_{t} \tag{V-47}$$

$$y_t' = r_t \sin \theta_t$$
 (V-48)

The moment arm of the applied load is

$$e = 2r_t \cos (\phi + \theta_t)$$
 (V-49)

as seen from Equation (V-34).

The deflection under the applied load from  $\varphi_{0}$  to  $\varphi$  is defined as

$$\delta = 2|y_{0"} - y_{0'}| \tag{V-35}$$

or

$$\delta = 2 \left| r(\theta_{t''}) \sin(\phi + \theta_{t''}) - r(\theta_{t'}) \sin(\phi_0 + \theta_{t'}) \right| \qquad (V-50)$$

where Q' and Q" are the points of tangency in the initial and deformed states, respectively.

Equations (V-49) and (V-50) may be normalized to the ratio  $\frac{a}{b}$  and the angle of rotation,  $\phi$ , in order to study the generalized response of an elliptical section ring. The resultant relationships are

$$\frac{e}{a} = 2 \left[ \frac{\cos (\phi + \theta_t)}{\sqrt{\left(\frac{a}{b}\right)^2 \cos^2 \theta_t + \sin^2 \theta_t}} \right]$$
 (V-51)

and

$$\frac{\delta}{a} = 2 \left| \frac{\sin (\phi + \theta_{t''})}{\sqrt{\left(\frac{a}{b}\right)^2 \cos^2 \theta_{t''} + \sin^2 \theta_{t''}}} - \frac{\sin (\phi + \theta_{t'})}{\sqrt{\left(\frac{a}{b}\right)^2 \cos^2 \theta_{t'} + \sin^2 \theta_{t'}}} \right| \qquad (V-52)$$

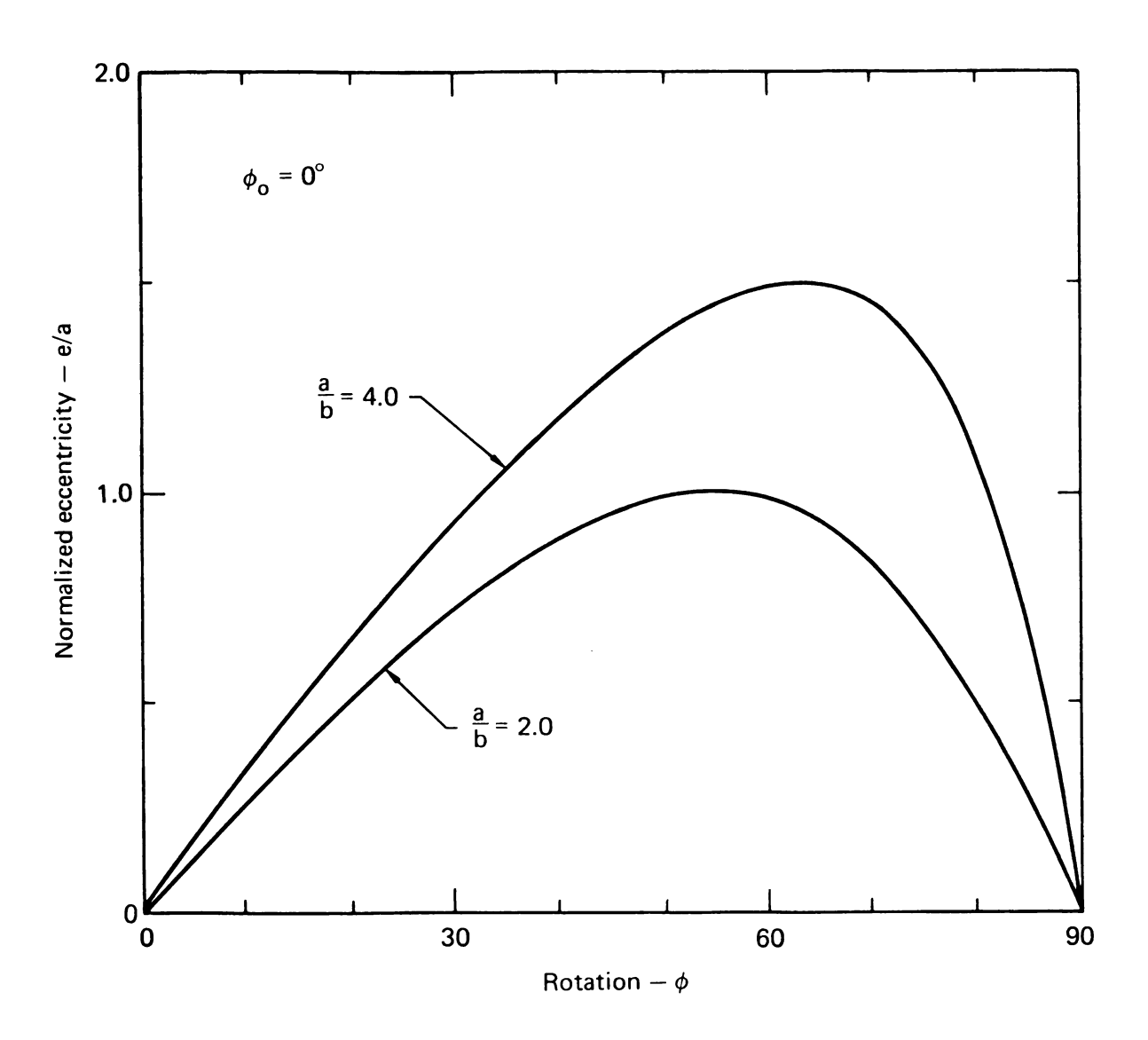
where

$$\tan \theta_t = \left(\frac{a}{b}\right)^2 \cot \phi \tag{V-45}$$

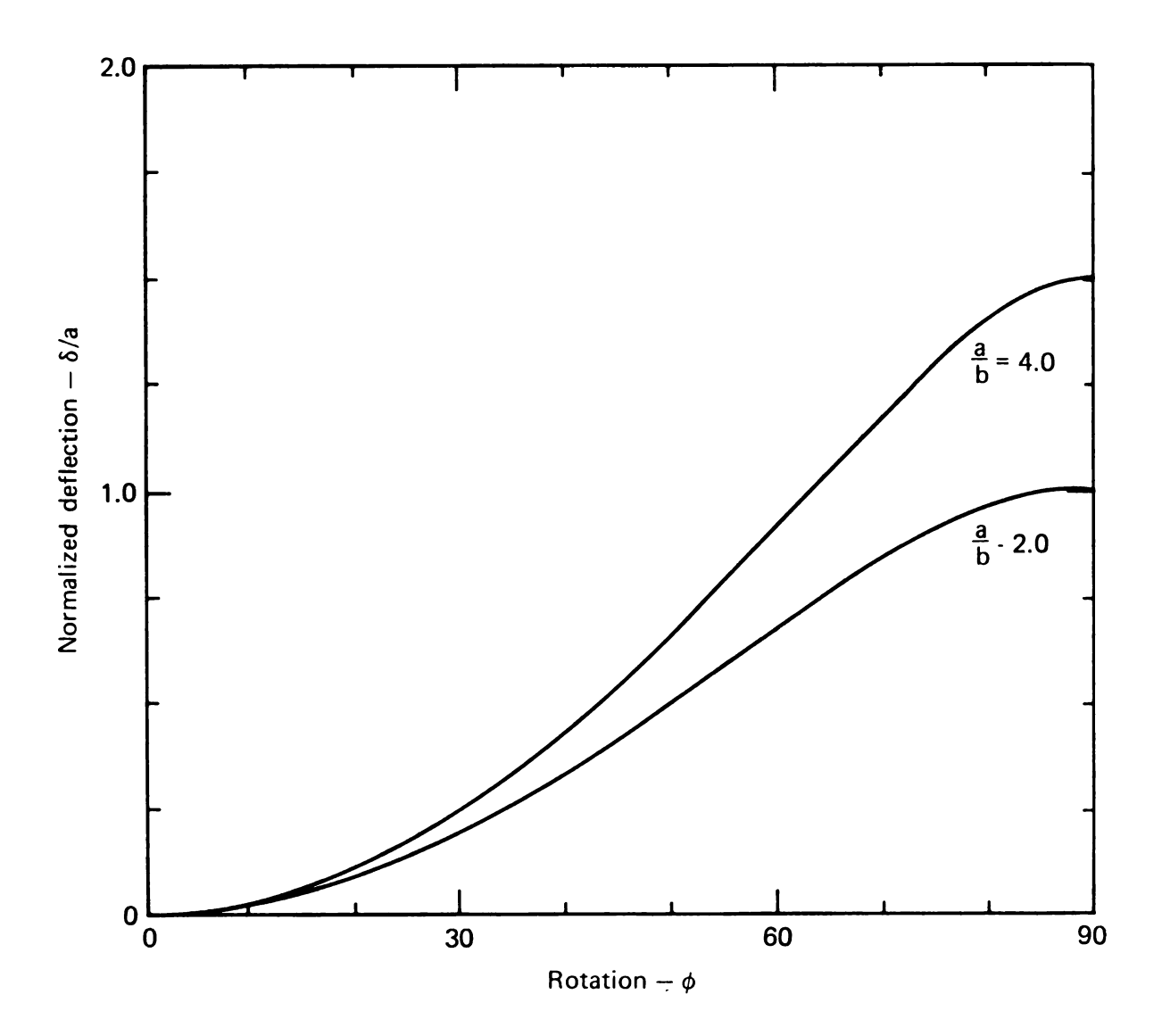
and the primed and double primed cases in Equation (V-52) refer to the initial and final values of  $\phi$ , respectively.

Figure 27 is a plot of Equation (V-51) and shows the variation in the moment arm over the range  $0 \le \phi \le 90^{\circ}$  for a/b = 2.0 and a/b = 4.0. Since the twisting moment required to deform the spring also varies with angle, the force will vary in a non-linear fashion as hypothesized. The curves for deflection as a function of angle are plotted in Figure 28 using the relationship given in Equation (V-52) for the case  $\phi_0 = 0$ .

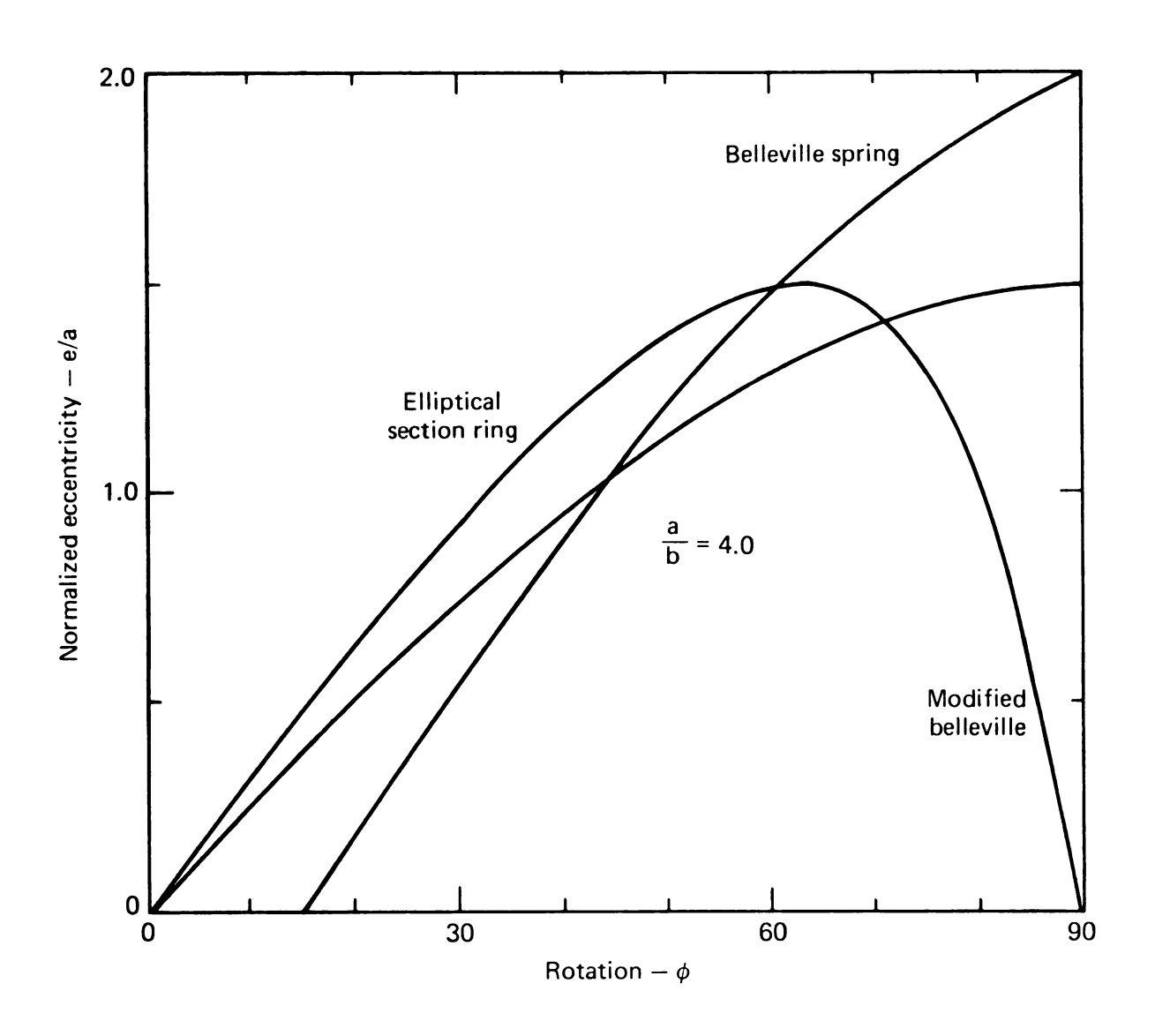
Figures 29 and 30 show the above curves with data for the Belleville and modified Belleville springs discussed in Chapter III. The negative eccentricity shown for the standard Belleville spring occurs until the corner of the rectangular section is vertical. Similarly, the negative deflections in Figure 29 indicate that the point of load application moved further from the origin. Obviously, these conditions are incompatible with the actual response



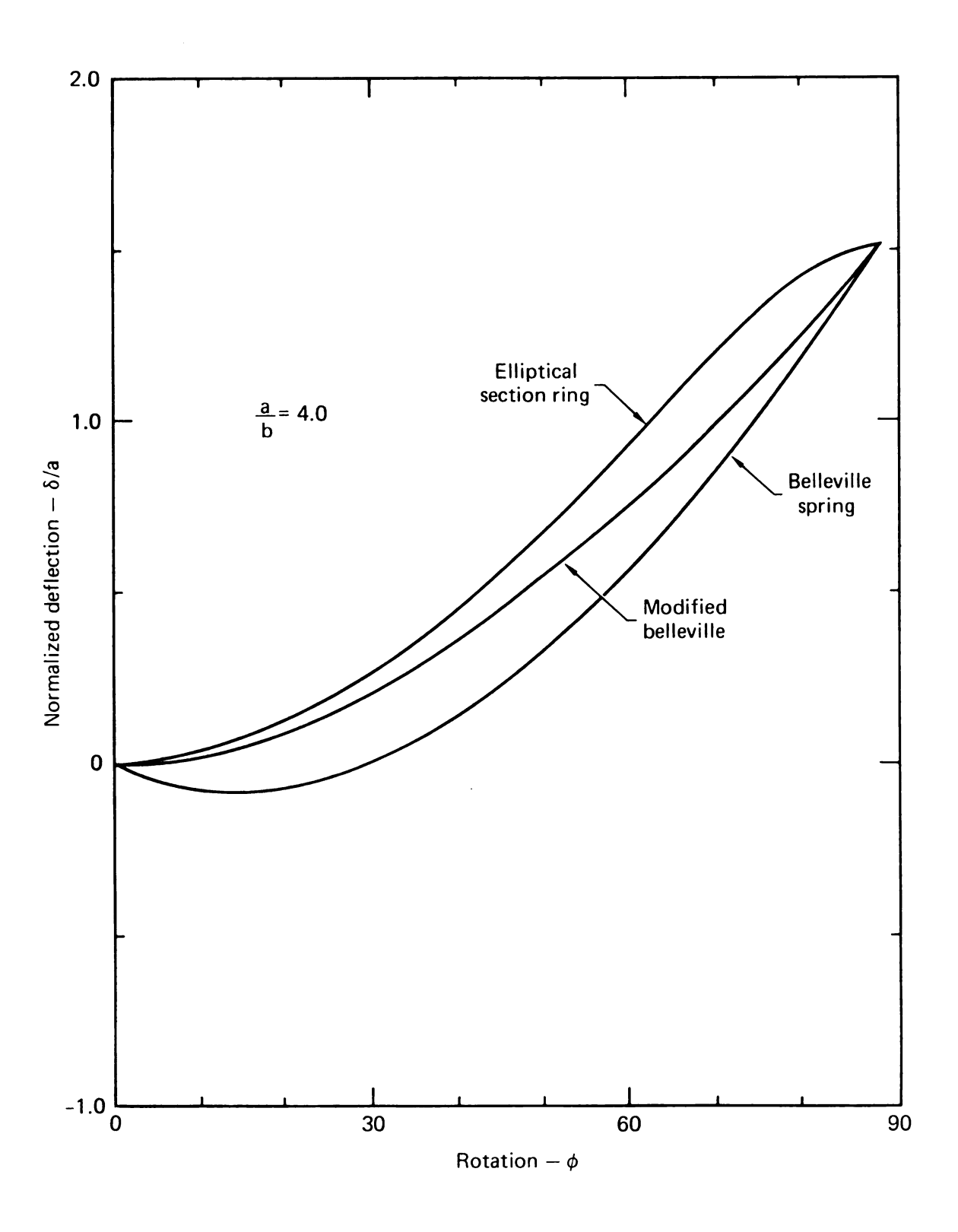
27. Load eccentricity of an elliptical section ring as a function of rotation.



28. Change in contact point position between an elliptical section ring and a flat plate ( $\phi_{o}$  = 0°).



29. Comparison of load eccentricity for an elliptical section ring, a Belleville spring, and a modified Belleville spring.



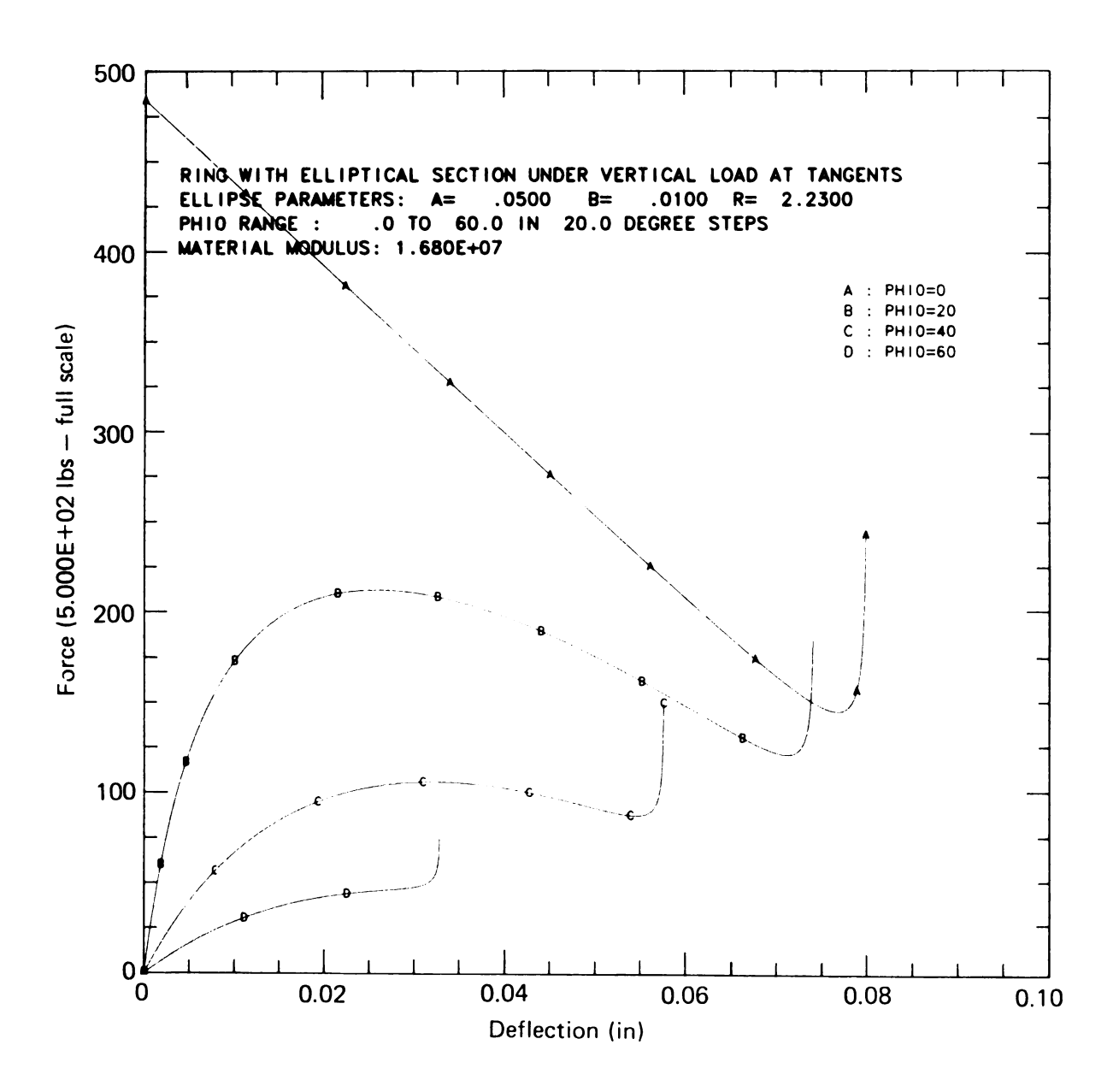
30. Comparison of contact point deflection for an elliptical section ring, a Belleville spring, and a modified Belleville spring.

and should be disregarded. (It would be possible to reformulate the equations to start with the corners vertical but that option has not been pursued in this study.) The significant point of comparison between these three designs is that only in the case of the elliptical section ring does the eccentricity decrease. This allows the designer greater flexibility.

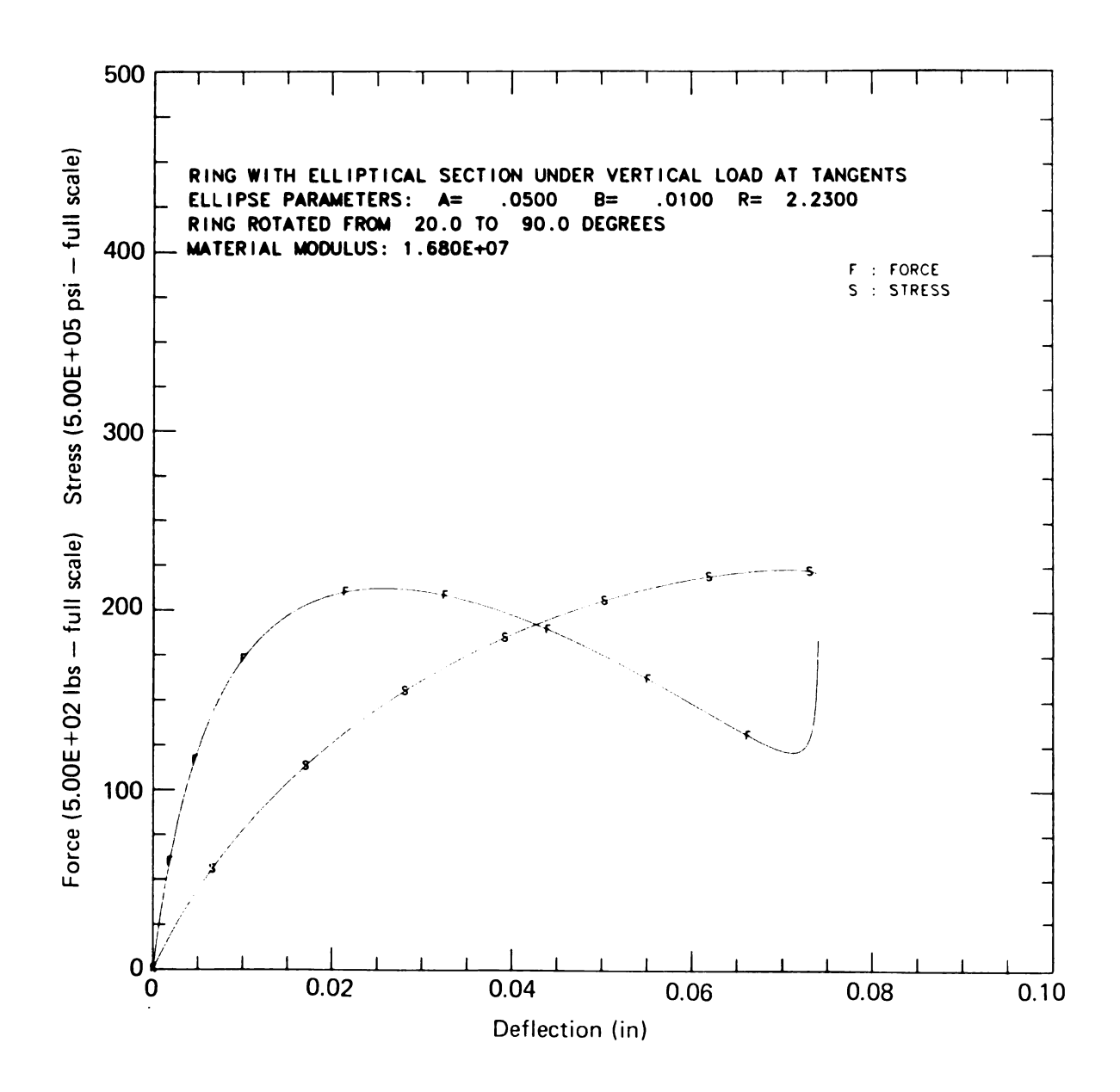
The force-deflection characteristics for a test case are presented in Figure 31. The test case shows the calculated response of a titanium ring (a = 0.050, b = 0.010, R = 2.23) for  $\phi_0$  =  $0^{\circ}$ ,  $20^{\circ}$ ,  $40^{\circ}$ , and  $60^{\circ}$ . The stresses resulting from rotation of the ring over the range  $20^{\circ} \leq \phi \leq 90^{\circ}$  are shown in Figure 32. The expected non-linearities are evident in the data. Considering the test case relative to the problem specifications in Chapter II, the force level for curve B ( $\phi_0$  =  $20^{\circ}$ ) is lower than required (200 lb instead of 300 lb). The usable deflection range (0.070 inch) is marginal since some preload would be required. Stresses encountered in this design exceed the levels attainable with common materials but are reasonable for a first attempt. These calculations indicate that an elliptical section ring which meets the specifications very probably exists.

Since the spring is to be designed to function in the elastic range of the material, the value of the maximum stress in the ring is of interest to the designer. The maximum stress will be defined in terms of the maximum strain.

$$\varphi_{\text{max}} = E_{\varepsilon_{\text{max}}}$$



31. Force curves from a sample calculation with RING.



32. Force and stress for a sample calculation with  $\phi_{\rm o}$  = 20°.

which in turn is defined in terms of the displacement of a point from  $\phi_{\Omega}$  to  $\phi\colon$ 

$$\varepsilon_{\text{max}} = \frac{1}{R} \left( x_{\text{p"}} - x_{\text{p}} \right)_{\text{max}} \tag{V-53}$$

where

$$\varepsilon(\theta) = \frac{r(\theta)}{R} \left[ \left( \cos \phi - \cos \phi_0 \right) \cos \theta - \left( \sin \phi - \sin \phi_0 \right) \sin \theta \right]$$
Differentiation with respect to  $\theta$ 

Differentiating with respect to  $\theta$ ,

$$\frac{d\varepsilon}{d\theta} = \frac{1}{R} \frac{d}{d\theta} \left( x_{p''} - x_{p'} \right) = \frac{1}{R} \left[ \frac{dx}{d\theta} \Big|_{x=x_{p''}} - \frac{dx}{d\theta} \Big|_{x=x_{p'}} \right]$$

where

$$\frac{dx}{d\theta} = \frac{d}{d\theta} \left( r(\theta) \cos (\theta + \phi) \right)$$

$$= -\frac{r(\theta)}{D^2} \left[ a^2 \cos \theta \sin \phi + b^2 \sin \theta \cos \phi \right]$$
(V-42)

SO

$$\frac{d\varepsilon}{d\theta} = -\frac{r(\theta)}{RD^2} \left[ a^2 \cos \theta \left( \sin \phi - \sin \phi_0 \right) + b^2 \sin \theta \left( \cos \phi - \cos \phi_0 \right) \right] \tag{V-54}$$

where 
$$D = a^2 \cos^2 \theta + b^2 \sin^2 \theta$$

The location of the point of maximum strain is defined by the angle,  $\theta_{\varsigma}$  , where

$$\frac{d\varepsilon}{d\theta} = 0 = \frac{r(\theta_s)}{RD^2} \left[ a^2 \cos \theta_s \left( \sin \phi - \sin \phi_0 \right) + b^2 \sin \theta_s \left( \cos \phi - \cos \phi_0 \right) \right]$$

or

$$\tan \theta_{s} = -\frac{a^{2}}{b^{2}} \left( \frac{\sin \phi - \sin \phi_{0}}{\cos \phi - \cos \phi_{0}} \right)$$

which further simplifies to

$$\tan \theta_{S} = \frac{a^{2}}{b^{2}} \cot \left( \frac{\phi + \phi_{0}}{2} \right)$$
 (V-55)

The coordinates of the point of maximum strain may be determined from Equations (V-11) (V-9), (V-10), and (V-14). The values of the maximum strain and maximum stress are specified by Equations (V-21) and (V-22).

The neutral axis of the cross-section is defined as the locus of points of zero strain and is described by equating Equation V-21) to zero:

$$\varepsilon = \frac{1}{R} \left[ (\cos \phi - \cos \phi_0) x_p - (\sin \phi - \sin \phi_0) y_p \right] = 0$$
 (V-21)

$$y_{p} = \left(\frac{\cos \phi - \cos \phi_{0}}{\sin \phi - \sin \phi_{0}}\right) x_{p} \tag{V-56}$$

which reduces to

$$y_p = \left(-\tan\frac{1}{2} (\phi + \phi_0)\right) x_p \qquad (V-56a)$$

The location of the neutral axis relative to the principal axes of moment of inertia is

$$\theta_{NA} = \tan^{-1} \left( \frac{y_p}{x_p} \right) = -\frac{1}{2} \left( \phi + \phi_0 \right) \tag{V-57}$$

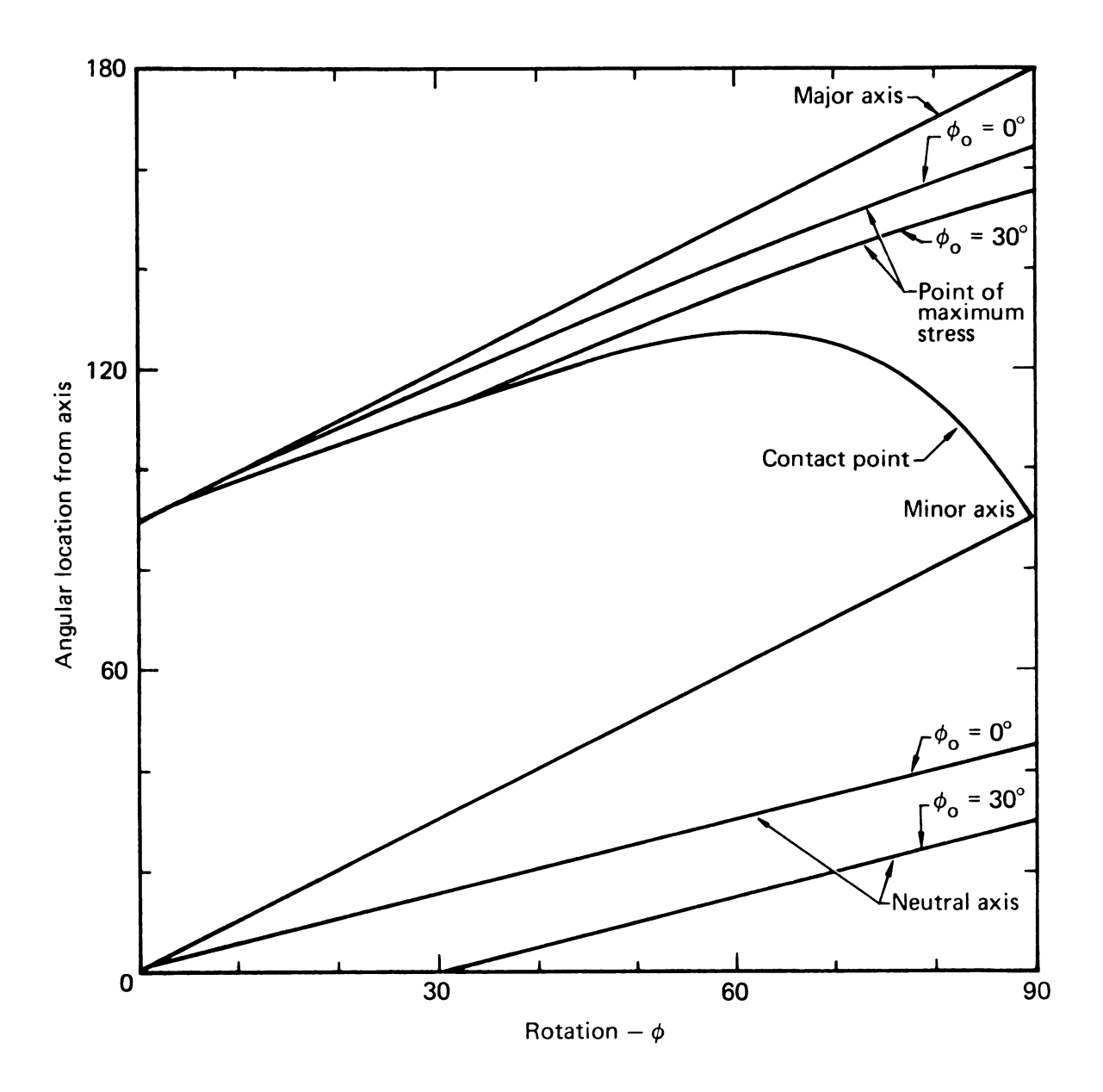
Note that the neutral axis is not along the x-axis as would be expected from the simple theory of beams. Oden (11), however, indicates that the orientation of the neutral axis is not, in general, perpendicular to the plane of the resultant moment.

The data plotted in Figure 26 showed the position of the contact point relative to the axes of the ellipse. The location of the contact point relative to the radial axis of the ring is given by

$$\phi_t = \phi + \theta_t$$

which is plotted in Figure 33 along with the angular locations of the major and minor axes. The case shown is  $\frac{a}{b}=2.0$ . Superposed on this plot are the loci of the points of maximum strain and the neutral axis locations for various values of  $\phi_0$ . Note that the neutral axis is coincident with radial axis only at  $\phi=\phi_0$ . Note also that the point of maximum stress occurs at the contact point only when  $\phi=\phi_0$ . Figure 33 illustrates that the point of maximum stress is not necessarily on the perpendicular to the neutral axis of the section.

It is of interest to compare the above development with that based on the assumption of small angles of rotation (see Chapter IV). Consider first the strain as defined by Equation (V-21)



33. Loci of the positions of the major and minor axes, contact point, neutral axis, and point of maximum strain as measured from the radial axis of the ring.

$$\varepsilon = \frac{1}{R} \left[ (\cos \phi - \cos \phi_0) \times + (\sin \phi - \sin \phi_0) y \right]$$

$$= \frac{2}{R} \sin \frac{1}{2} (\phi - \phi_0) \left[ x \sin \frac{1}{2} (\phi + \phi_0) + y \cos \frac{1}{2} (\phi + \phi_0) \right]$$
(V-21)

Then, let

$$\phi = \phi_0 + \Delta \phi \tag{V-58}$$

and assume  $\Delta \phi \ll \phi_0$ , so that

$$\varepsilon = \frac{1}{R} (\Delta \dot{\phi}) (x \sin \phi_0 + y \cos \phi_0) \qquad (V-59)$$

but

$$y_p' = (x \sin \phi_0 + y \cos \phi_0)$$

The strain at a point then becomes

$$\varepsilon = \frac{y_p}{R}(\Delta \phi) \tag{V-59a}$$

which agrees with Equation (V-6).

The stress-moment equilibrium, Equation (V-28), reduces to

$$M_{t} = \frac{E}{R^{2}} \left[ I_{xy} \left( \cos \phi - \cos \phi_{0} \right) - I_{xx} \left( \sin \phi - \sin \phi_{0} \right) \right]$$
 (V-28)

$$\approx \frac{E}{R^2} \left[ - I_{xx}(\Delta \phi) \right] \tag{V-60}$$

which is similar to Equation (IV-10)). The neutral axis for small angle rotations is obviously the x-axis:

$$y = 0$$

from Equation (V-59a).

The correlation with small-angle rotations and simple beam theory shows that the developments are consistent with existing knowledge.

In view of the intended application of the spring and the small size of the elliptical section, the possibility of high bearing stresses was considered. The contact stresses predicted by Hertzian theory were developed in terms of the radius of curvature of the ellipse at the point of contact.

The ring was assumed to behave as a cylinder loaded by a flat plate. The stresses are given by (2)

$$\sigma_{c} = 0.798 \sqrt{(K_{D})(C_{F})}$$
 (V-61)

and the width of the contact zone is

$$w_c = 1.60 \sqrt{p K_D C_E}$$
 (V-62)

where

$$K_{D} = 2r = 2\left(\frac{1}{\rho}\right) \tag{V-63}$$

$$c_{E} = \left(\frac{1 - v_{1}^{2}}{E_{1}}\right) + \left(\frac{1 - v_{2}^{2}}{E_{2}}\right)$$
 (V-64)

where

 $E_1v_1$  = plate material properties

 $E_{2}v_{2}$  = ring material properties

The radius parameter in Equation (V-63) is defined from the equation of the ellipse and the definition of radius of curvature (12):

$$\rho = \frac{\left[1 + \left(\frac{dy}{dx}\right)^{2}\right]^{3/2}}{+ \frac{d^{2}y}{dx^{2}}}$$
 (V-65)

At the point of contact (tangent to the ring)

$$\frac{dy}{dx} = 0$$

and

$$\rho = \frac{1}{\frac{d^2y}{dx^2}}$$
 (V-65a)

Equation (V-1) can be rearranged to give

then

$$y = \frac{a}{b} \left( b^2 - x^2 \right)^{1/2}$$

$$\frac{dy}{dx} = -\frac{ax}{b} \left( b^2 - x^2 \right)^{-1/2} \tag{V-66}$$

$$\frac{d^2y}{dx^2} = \frac{-ab}{\sqrt{b^2 - x^2}}$$
 (V-67)

and

$$\rho = \pm \frac{\sqrt{b^2 - x^2}}{ab} \tag{V-68}$$

In this case, x and y are in the body coordinate system and are the local coordinates of the point of tangency as defined by Equations (V-46), (V-47), and (V-48).

In the analysis of a dynamic system, the friction between components having relative motion can have a significant effect on the response. Since the elliptical section ring incorporates the change of contact point as a key feature, it is necessary to consider the role of friction in the spring response. In any mechanical system, friction acts so as to retard relative motion between the elements of the friction pair (13) as shown in Figure 34 (a) and (b). The friction force reverses direction between the loading cycle and unloading cycle.

The mechanism of friction between two solids is not well understood but the macroscopic effects can be characterized in the simple form:

$$f = \mu F \tag{V-69}$$

where f is the friction force resulting between two bodies bearing a normal force, F, and having a coefficient of friction,  $\mu$ . This relationship is considered valid over a range of boundary conditions and relative velocities (5). The degree of accuracy is highly influenced by the selection of the friction coefficient.

The friction coefficient between two materials is dependent upon a variety of factors such as the degree of lubrication and the relative hardness of the materials. Experimental constants are typically given as a range of values (5) from which the designer must find the most appropriate choice for a particular system.

Neglecting the problems associated with the selection of a coefficient of friction, the effect of a friction force on an

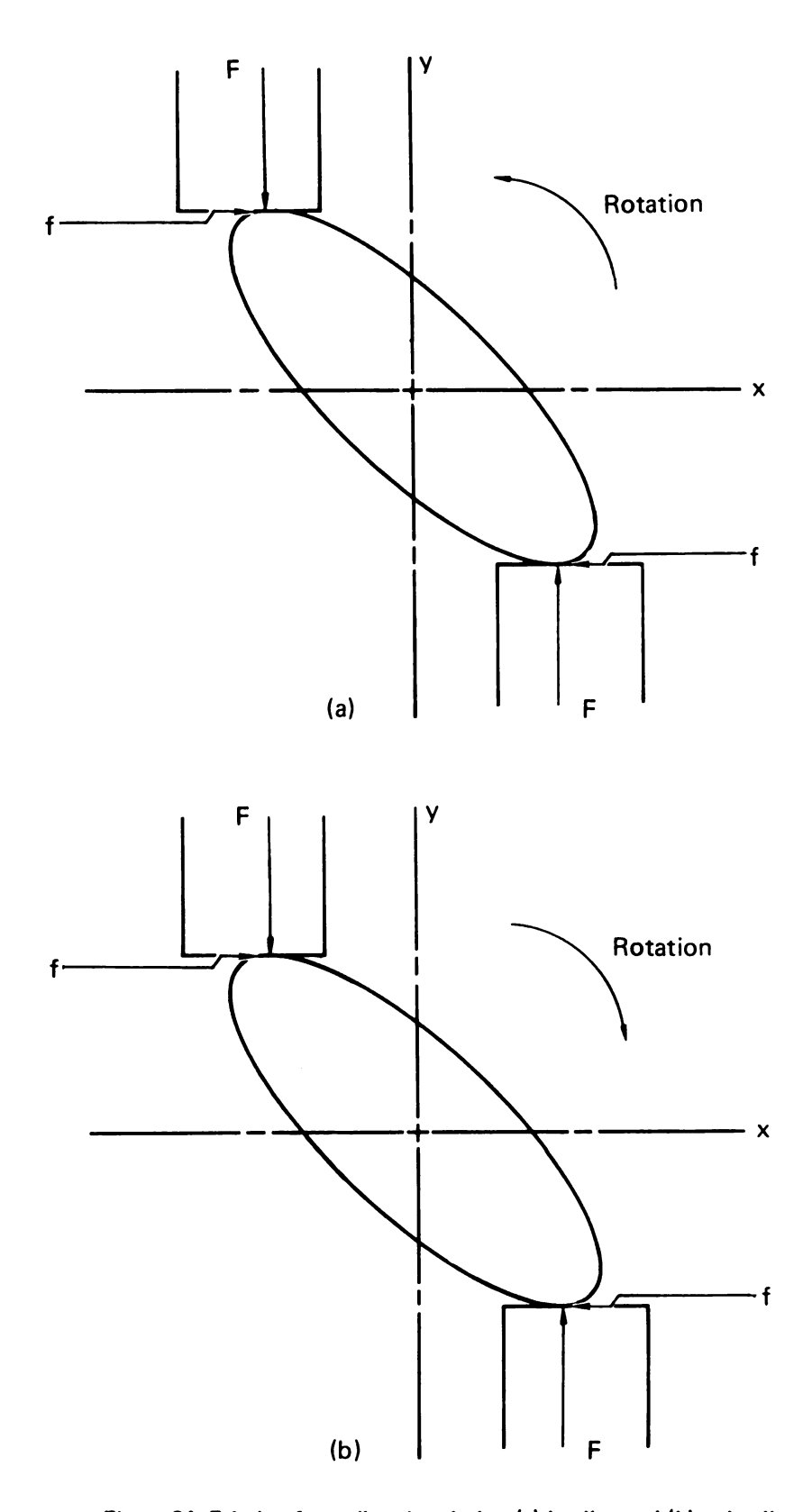


Figure 34. Friction force direction during (a) loading and (b) unloading.

elliptical section ring is to alter the moment-force relationship at any given angle,  $\phi$ . Equation (V-2) describes the relationship between the applied force, p, and the moment required to maintain the deformation, M, as

$$M = pe$$

where e is the eccentricity or distance between the contact points in the radial direction. Equation (V-2) may also be written in terms of the contact point coordinates as

$$M = 2p(-x_+)$$

with the sign change necessary as a result of the convention chosen for forces and moments. The moment required to maintain the deformed state is independent of the applied loads which implies that the presence of friction must change the forces required to exert the moment on the body. The moment required at each value of  $\phi$  is given by Equation (V-28). The moment-force relationship for loading (increasing  $\phi$ ) is given by

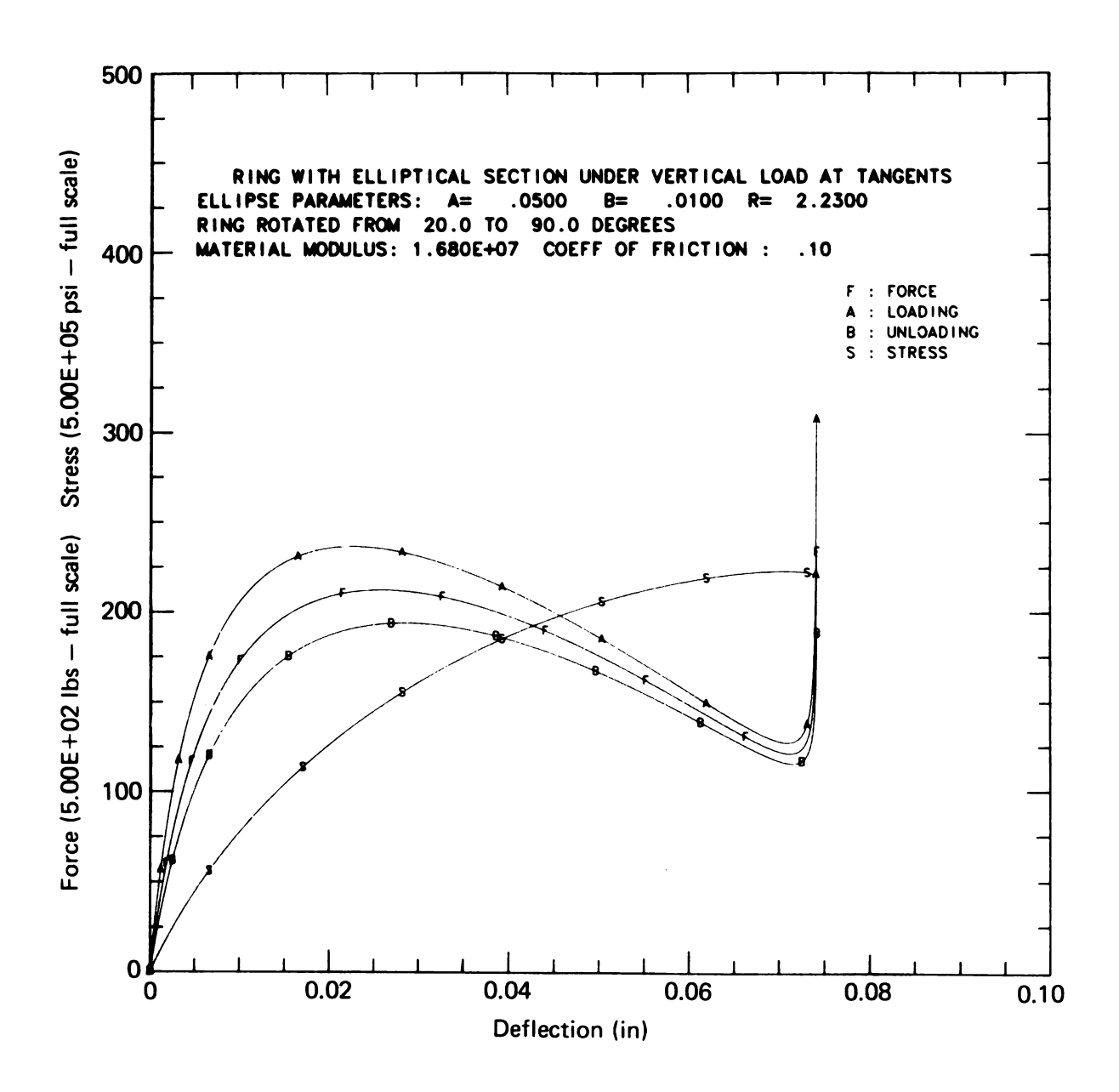
$$M_t = 2p (-x_t - \mu y_t)$$
 (V-70)

and for unloading by

$$M_{+} = 2p (-x_{+} + \mu y_{+})$$
 (V-71)

which can then be solved for the applied load necessary to maintain a deformed condition. Figure 35 shows the effect of friction on a sample calculation.

Since the coefficient of friction is not readily available for many friction pairs, it will be advantageous to extract an estimate of the friction in a given system from the hysteresis in



35. Sample calculation showing the effect of a friction coefficient,  $\mu$  = 0.10, between an elliptical section ring and a flat plate.

the force-deflection data (see Figure 35). This is accomplished by equating Equations (V-70) and (V-71) and solving for the coefficient of friction

$$\mu = -\frac{(p_{\ell} - p_{u}) x_{t}}{(p_{\ell} + p_{u}) y_{t}}$$
 (V-72)

where the subscripts  $\ell$  and u denote loading and unloading, respectively. The coordinates  $x_t$  and  $y_t$  are the locations of the tangent point, so

$$\mu = -\frac{(p_{\ell} - p_{u}) \cot (\phi + \theta_{t})}{(p_{\ell} + p_{u})}$$
 (V-73)

This relationship will allow an estimate of the friction coefficient to be made from experimental data.

A phenomenon frequently associated with friction pairs such as brakes and clutches is the self-locking effect which occurs when the sum of the resistance load and the frictional force exceeds the applied load. Consider Equation (V-70),

$$M_t = 2p(-x_t) - 2\mu py_t$$

Clearly, if

$$2p(-x_t) \le M_t + 2\mu py_t$$
 (V-74)

no motion can occur. This implies that if the ring is twisted to a certain point, no further deflection will be obtained by increasing the normal load. A further implication of Equation (V-74)

is apparent when the free ring  $(\phi=\phi_0)$  is considered. In this case,  $\text{M}_{t}$  = 0 and

$$2p(-x_+) \le 2\mu py_+ \tag{V-75}$$

describes the limiting conditions. The inequality states that it is possible to construct a ring which cannot be moved from its initial position by the application of a normal force. In order to avoid this embarrassing occurrence, define the angle,  $\phi_{\rm C}$ , to be the minimum free angle which allows the ring to deform. Equation (V-74) reduces to

$$x_t = -\mu y_t$$

or

$$\tan (\phi_c + \theta_t) = -\frac{1}{\mu} \tag{V-76}$$

Recognizing that  $\tan \theta_t = \left(\frac{a}{b}\right)^2 \cot \phi_c$ ,

$$-\frac{1}{\mu} = \tan \left(\phi_c + \theta_t\right) = \frac{\left(\frac{a}{b}\right)^2 \cot \phi_c + \tan \phi_c}{1 - \left(\frac{a}{b}\right)^2}$$
 (V-77)

which becomes

$$\mu \tan^2 \phi_c - \left( \left( \frac{a}{b} \right)^2 - 1 \right) \tan \phi_c + \mu \left( \frac{a}{b} \right)^2 = 0$$

The solution to this quadratic is

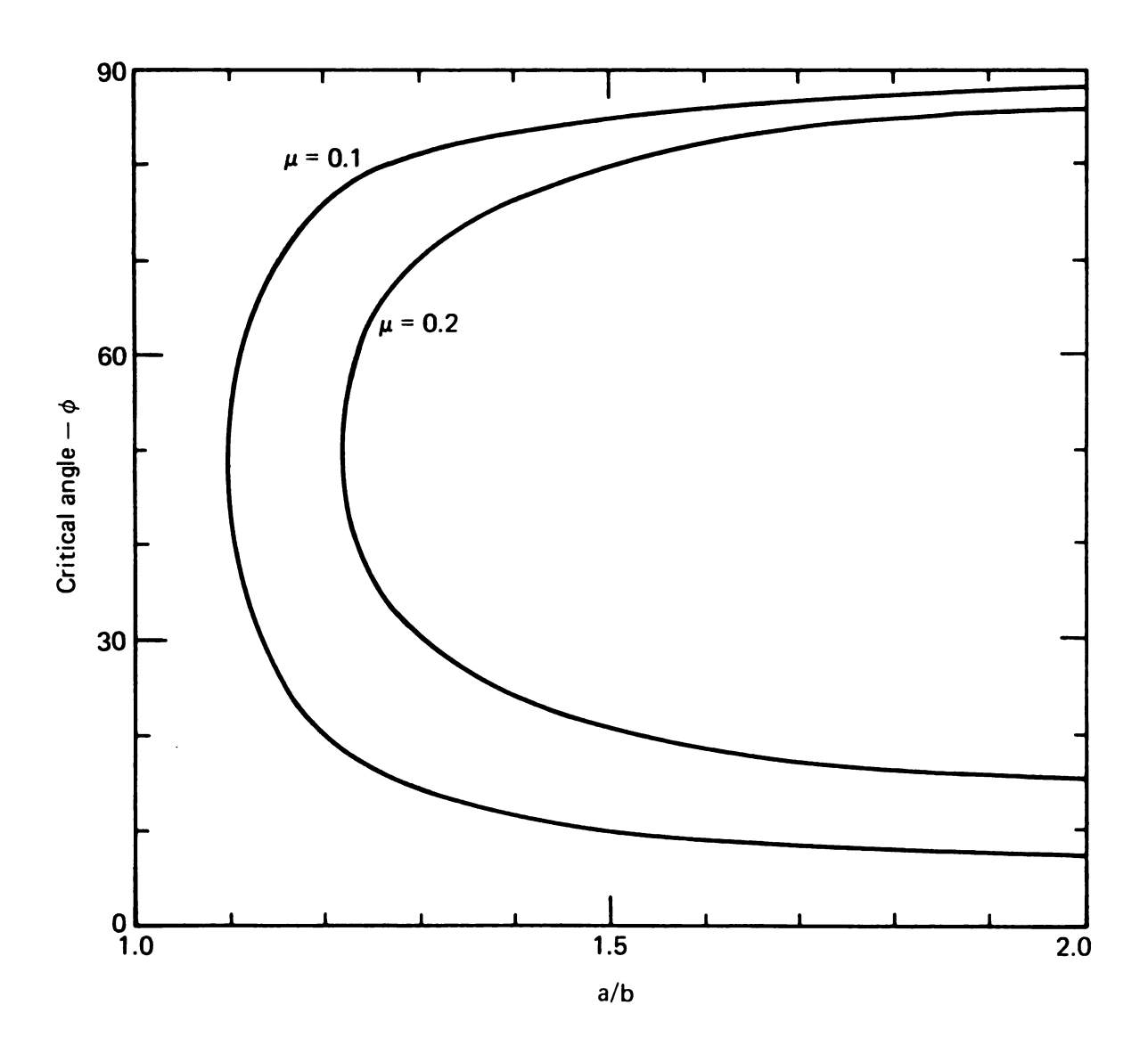
$$\tan \phi_{C} = \frac{\left(\left(\frac{a}{b}\right)^{2} - 1\right) \pm \sqrt{\left(\left(\frac{a}{b}\right)^{2} - 1\right)^{2} - 4\mu^{2}\left(\frac{a}{b}\right)^{2}}}{2\mu} \quad (V-78)$$

which defines the critical angle for a given ring. Equation (V-78) is plotted in Figure 36 for a range of values of  $\mu$ . The space inside the curves represent values of  $\phi_0$  for which motion is possible.

The analysis of a particular ring proceeds as follows:

- (a) The required data are R, a, b,  $\phi_0$ ,  $\phi_{MX}$ , and material properties for the ring and plate.
- (b) The moments of inertia of the cross-section,  $(I_{xx}, I_{yy}, and I_{xy})$  are determined (Equations (V-30) and (V-31)).
- (c) The moment required to maintain the deformed state is calculated from Equation (V-28).
- (d) The location of the horizontal tangent is determined using Equations (V-46), (V-47), and (V-48).
- (e) The deflection from  $\phi_0$  to  $\phi$  is calculated (Equation (V-50)).
- (f) The eccentricity of loading is determined (Equation (V-49)).
- (g) The specific strain and strain in the cross-section are determined from Equations (V-21), (V-55), and (V-52).

This sequence is readily programmed for digital computer solution, permitting the designer to study the effects of variable changes rapidly and quantitatively.



36. Critical angle for self-locking as a function of a/b ratio.

## CHAPTER VI

## SPECIMEN FABRICATION

One of the constraints imposed on the spring system was the requirement that fabrication not require new technology. The Material Fabrication Division at Lawrence Livermore Laboratory provides shop support to the design groups and is equipped with an array of equipment for precision metal working including a variety of numerically controlled (N/C) machines, electro-chemical milling (ECM) equipment, electrical discharge machining (EDM) facilities, and diamond-turning machines. Facilities for welding, pressing, and heat treatment are also available. Specialized capabilities can be obtained from outside firms when required to complete a job.

Selection of the design parameters for the test specimens was done as indicated in Chapter V. Fabrication of a ring with such a small section at a relatively large diameter required careful evaluation of the available techniques. Three methods were considered: numerically controlled machining, electrical discharge machining, and extrusion.

The simplest approach seemed to be the extrusion process in which the material is forced through a die of the required cross-section. The elliptical section wire would then be formed into a ring and welded or brazed to achieve closure. Several problems were inherent in this method. The basic problem was the lack of experience among shop personnel in extruding titanium thus requiring a development program. Hot extrusion would anneal the

material and cause grain growth thereby reducing the strength. An additional drawback was the requirement for a weld which meant that, even if the other problems could be solved, a local heat-affected zone of lower strength would be present. The use of an age-hardening titanium alloy much as Ti-6Al-4V was considered as a means of solving these problems by permitting a post-weld heat treatment. A study of the available literature indicated however that heat treatment of weld zones involves material which is at a different initial state than the parent material and generally results in cracking (13).

Electrical discharge machining is a process in which a shaped electrode is used to remove material. The process can be used to shape complex sections in materials which are difficult to machine conventionally. The process occasionally results in microscopic pitting of the surface. Since the surface of the ring is the most highly stressed region, such pits would act as stress concentrations and degrade the effective strength of the specimen. The EDM and ECM processes would require fixturing similar to that required for conventional machining and would be considerably slower.

The optimum method for fabricating the test specimens was conventional machining on a numerically controlled machine. In this process, the past geometry is described in an N/C computer language which generates a series of tool drive commands on a tape. The tool drive commands define the cutter location from a reference point. Shop facilities at Lawrence Livermore Laboratory

include a Sunstrand 5- axis mill, several Excello N/C lathes, and a Sheffield y-z gage for N/C inspection. Consultations with shop management indicated that, despite problems with fixturing the ring to avoid deformation and out-of-round conditions, the use of conventional N/C techniques was the best approach.

The N/C programming language currently in use at Lawrence Livermore Laboratory is APT4. In addition to its use in the shops, APT4 can be programmed to treat various computer graphics media as output devices and has found widespread application by design draftsmen in generating pictures of complex parts and assemblies. Figure 37 and Figure 38 show drawings generated using the APT4 language. Figure 39 is a listing of the APT4 commands required to generate the geometry.

Commercially pure titanium is described in the literature as easily machined (13) and no special hazards are noted that might be encountered under normal machining practice. Job orders were written for the fabrication of the samples. The cost estimate for the  $0.020 \times 0.080 \times 4.435$  dia. ring was 60 hours. The second ring was larger ( $0.040 \times 0.160 \times 4.435$  dia.) and did not require new fixturing or programming. The estimate was 16 hours. A sheet of 99.98% pure titanium measuring 24 x 48 x 0.5 inches was purchased at a cost of \$ 575.00. The material certification provided by the vendor is shown in Figure 40.

Inspection of the ring to verify the size and orientation of the elliptical cross-section proved to be impossible because the elliptical portion was too small to be measured on available

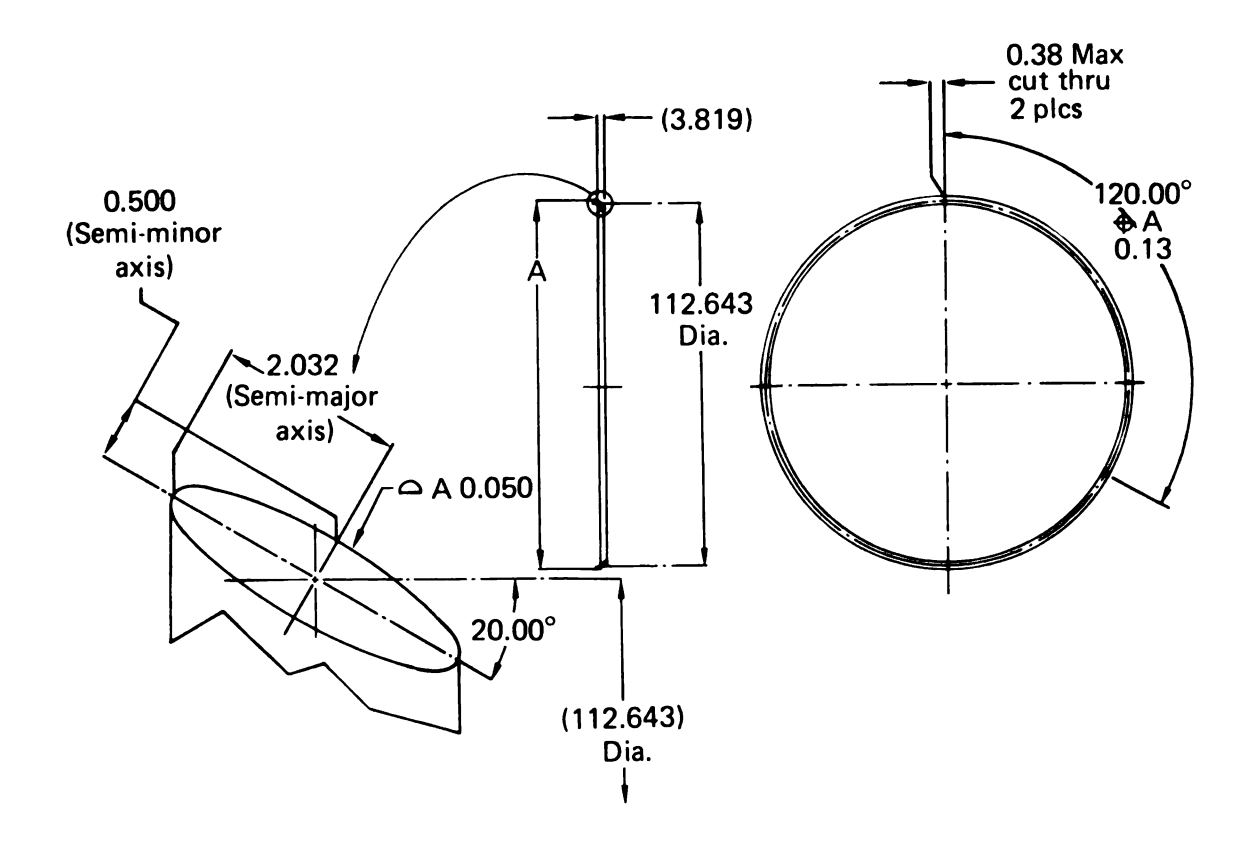


Figure 37. Engineering drawing for Test Specimen 1.

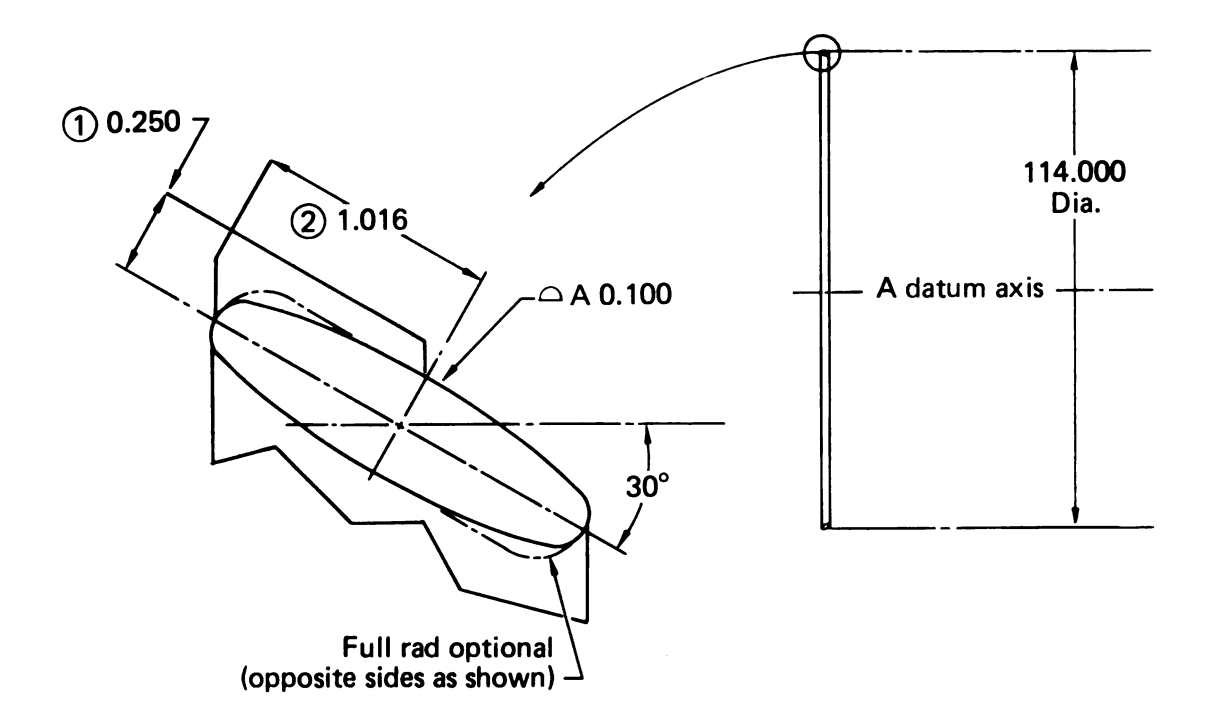


Figure 38. Engineering drawing for Test Specimen 2.

```
PARTNO ELLIPTICAL SECTION RING
UNITS/INCHES
INTOL/.0001
OUTTOL/.0001
MACHIN/GRAPHICS, XYPLAN, -. 060, .060, -. 060, .060
CUTTER/0.0
A=0.050
B=0.010
PHI=30.
R=2.25
P0=P0INT/0.,0.
P1=P0INT/R,0.
E1=ELLIPS/CENTER,P1,A,B,PHI
PENUP
GOTO/PO
GOTO/P1
INDIRV/1.,0.,0.
GO/ON,E1
PENDWN
TLON, GOLFT/E1, ON, YAXIS
GOFWD/E1,ON,XAXIS
GOFWD/E1, ON, YAXIS
GOFHD/E1,ON,XAXIS
PENUP
GOTO/PO
FINI
```

FIGURE 39. APT4 PROGRAM LISTING.

7		,									
•		ON:	INDUS		•	IC. Beach, Celifornia	92649 • Tele	phone (714) 8	98-5535		
University of California Lawrence Livermore Labs 7000 East Ave. Livermore, Calif. 94550						DATE Oct. 13, 1977 CUSTOMER ORDER NO. 8679703 S.O.NO. 11707					
DESCRIPTION OF MATERIAL	Titan:		late ASTM :	B265 Gra	ade 2	URCE: TIN	ŒŦ				
				CHEMICAL P	ROPERTIES						
HEAT NO	С.	MH.	•	5	\$1.	CR.	NI.	CU.	MO.		
P0830	.016										
HEAT NO.	N2	CB.	TA.	FE.	AL.	TI.	H <sub>2</sub>	02			
	.012			.10		Bal.	.010	.13			
				PHYSICAL P	ROPERTIES						
HEAT NO.	TEAT NO. YIELD STRENGTH		TENSILE STRENG	TH % EI	LONG.	% RED. AREA HARDNESS		REMARKS			
P0830 L	- I		66 KSI 70 "	31 28							
	Su	rface	free from	contam	inatio	h.					
	WE HE	REBY C	ERTIFY THIS I	S A TRUE	COPY OF	TEST REPOR	TS IN OUR	FILE.			
				ي		LAX)	STRIES, I	nc. Bis			
			AUTHORIZED	Dow	MAGNESIU	M DISTRIBUTOR	<b>/</b>				

Figure 40. Vendor certification of the titanium purchased for specimen fabrication.

contour gages. The closed ring eliminated optical inspection methods such as comparators. The only data which could be obtained were the inner diameter, outer diameter, and the major and minor axis.

The rings were fabricated and inspected. The inspection data and the specifications are shown in Figure 37 for the small ring and in Figure 38 for the larger specimen. The smaller ring was later cut apart and examined under the microscope. These results are discussed in Chapter VIII.

#### CHAPTER VII

## EXPERIMENTAL PROGRAM

In order to determine the feasibility of the design and to verify the accuracy of the calculational model, it was necessary to test a ring and correlate the measured data with the predicted values. The functional requirements of the design dictated that the variation of force with deflection be measured. The large deformations and the expected magnitude of the stress in the ring indicated the desirability of a strain measurement.

The testing was performed by the Materials Test Laboratory of the Materials Engineering Division at Lawrence Livermore Laboratory. This group provided the necessary facilities, personnel, and instrumentation to complete the experimental evaluation on an accelerated schedule. The test set-up was very simple: the ring was placed between parallel polished platens on a 20,000 lb Instron test machine. A load cell measured the applied force and a 1.00 inch range extensometer measured the deflection. The curve of force as a function of displacement was recorded on an x-y plotter. The system is shown schematically in Figure 41. Figures 42 and 43 are photographs of the experimental apparatus.

The determination of the stresses in the ring was a problem left unsolved in this research. Strain gages were considered and rejected because the smallest known gages (approximately 1/16 inch gage length) would have covered a substantial portion of the surface at given location.

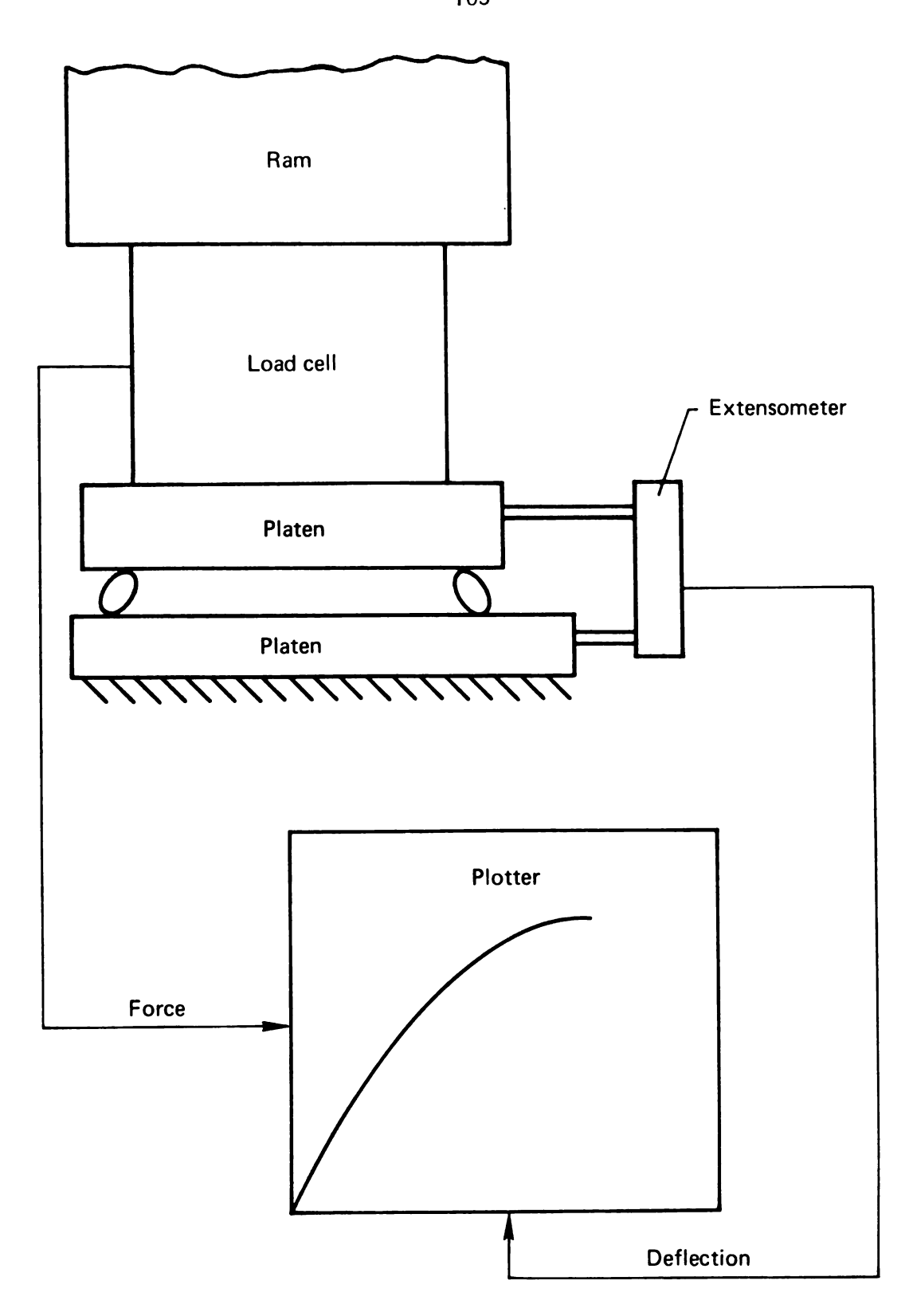


Figure 41. Instrumentation schematic for ring tests

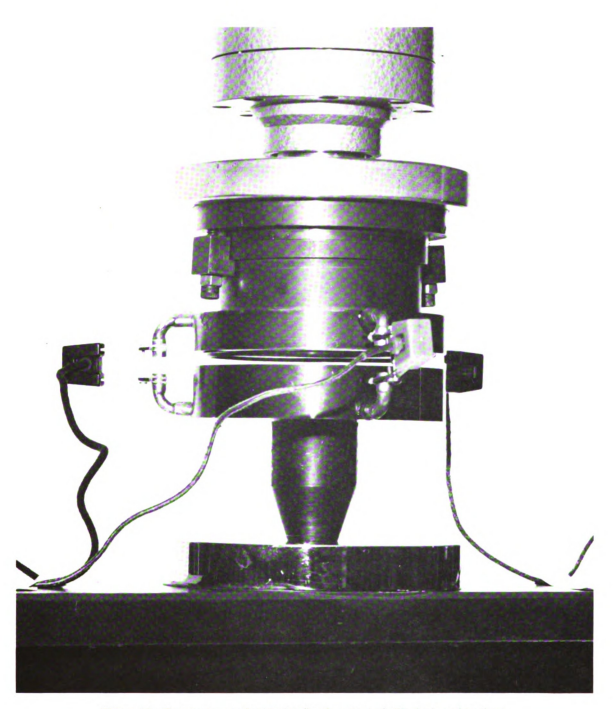


Figure 42. Test apparatus for load-deflection tests of elliptical-section rings

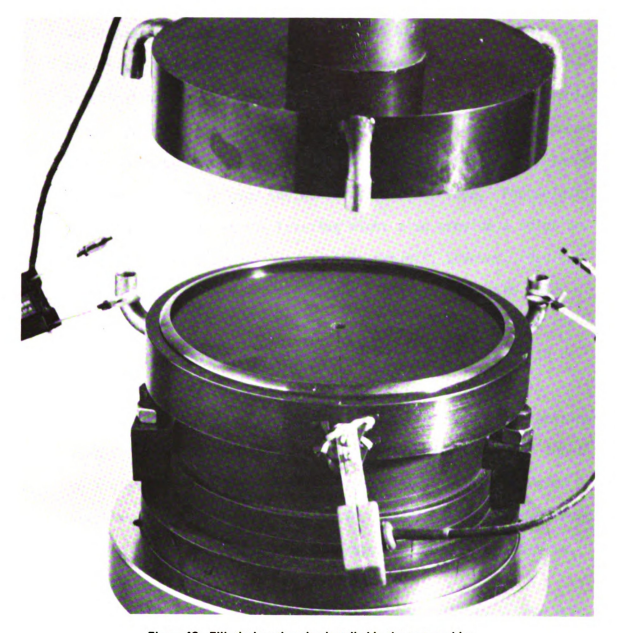


Figure 43. Elliptical-section ring installed in the test machine

Since the gage tends to indicate an average strain over the gage area, the data obtained would have been meaningless. In addition, the nature of the motion and the anticipated large deflection would have resulted in crushing the gage between the platen and the ring. Holographic and Moire' techniques were considered impractical because of the large deformations and optical difficul-Two possible solutions exist but were not considered because of schedule constraints. One possibility is to fabricate a large specimen amd strain gage the non-contacting surface. Photoelastic techniques such as stress freezing might also provide a solution. The only stress data gathered in this project, however, resulted from observation of the onset of plastic behavior in the load curve and the correlation between the calculated stress and the vendor-supplied yield point data. This will be discussed in detail in Chapter VIII.

Data plots such as those in Figures 44 and 45 were obtained directly from the test group. This data was digitized for input to a digital computer plotting routine, DPLOT, which generated graphics output such as in Figure 46. Digitization was performed using a Gerber digitizing table located at Sandia Laboratories, Livermore.

The ultimate goal of any engineering analysis is the ability to understand and predict the response of a given system to a particular input. In the case of the elliptical section ring, the predictive capability developed in Chaper V was correlated to the results of engineering tests conducted as described above. The

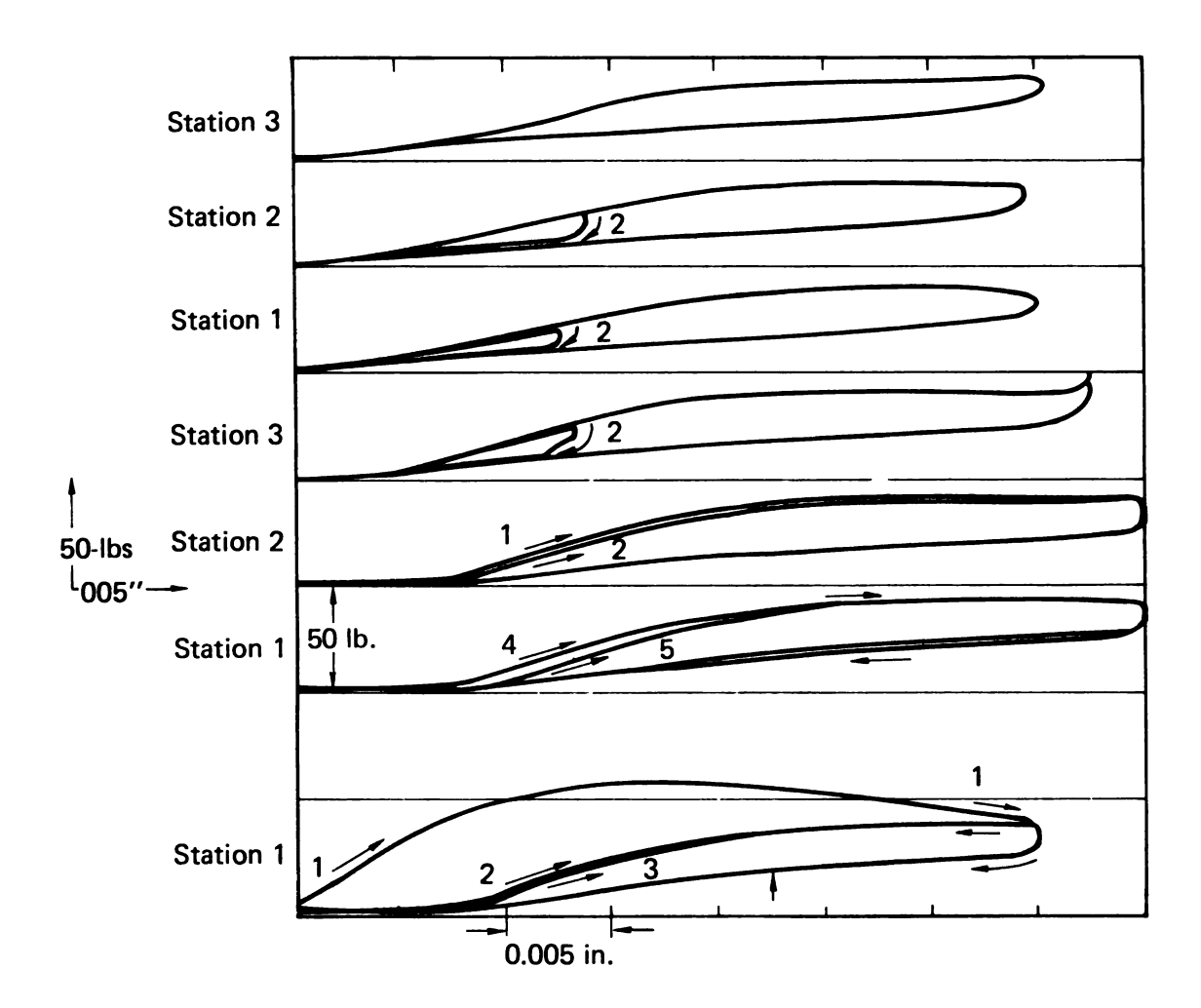


Figure 44. Test data for a titanium ring (a=0.040,b=0.010,R=2.244 inch,  $\phi_0$  = 30°).

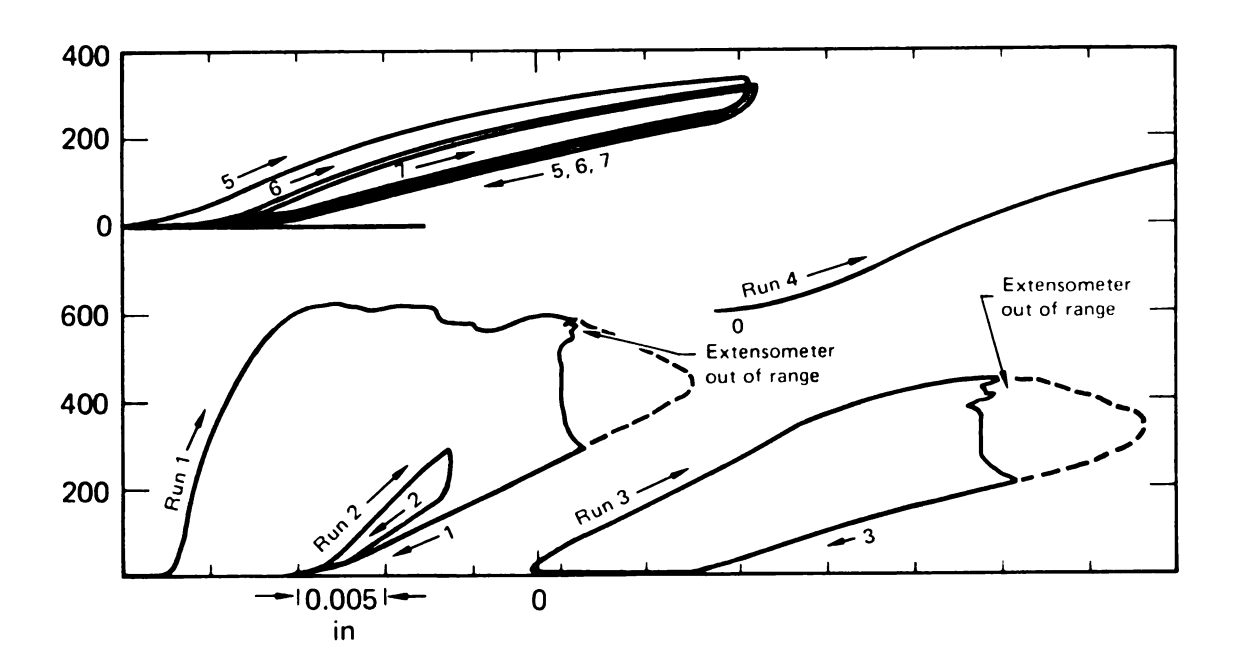
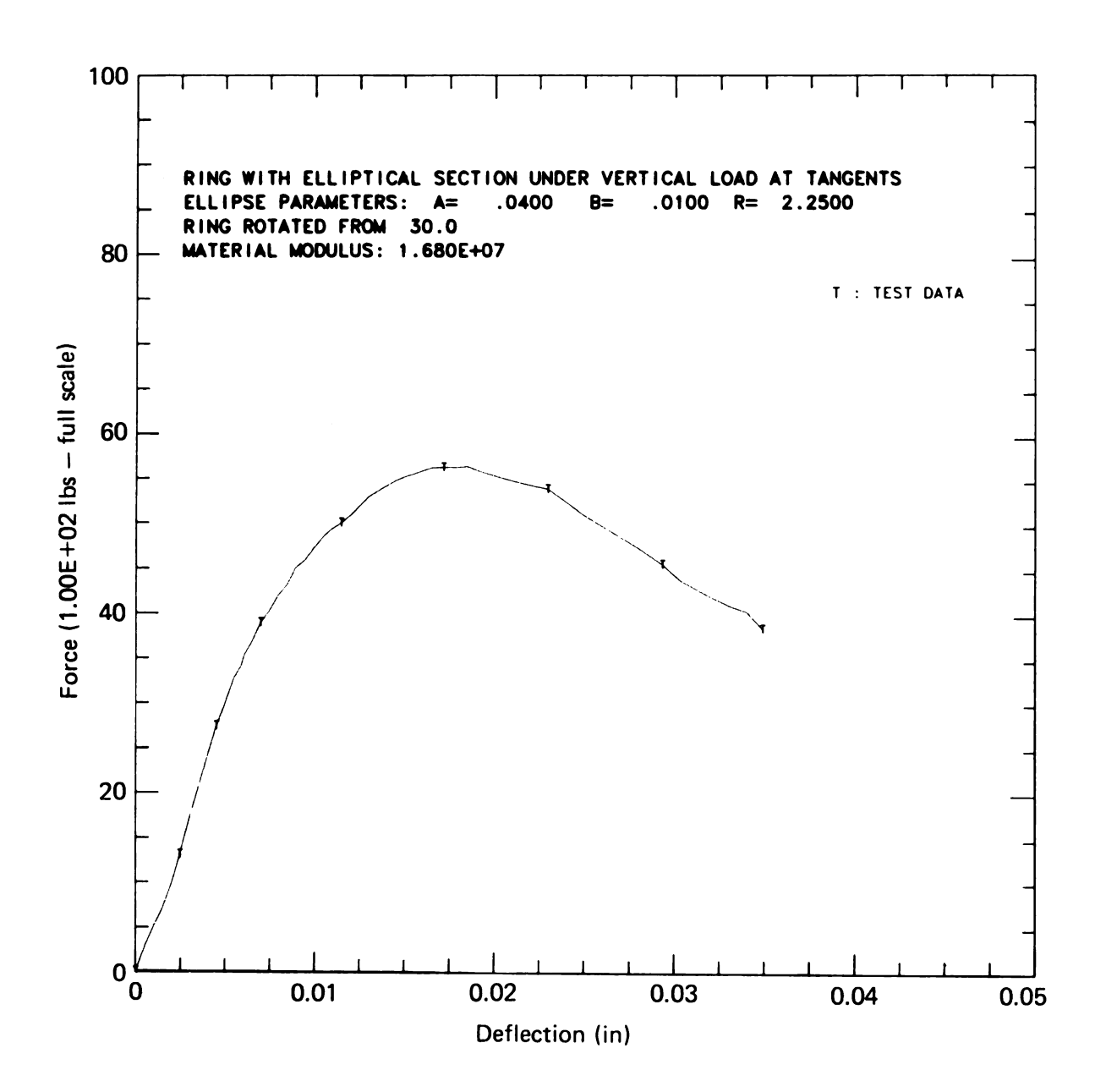


Figure 45. Test data for a titanium ring (a = 0.080, b = 0.020, R = 2.217 inch,  $\phi_0$  = 20 $^{\circ}$ ).



46. Sample of digitized test data plotted with DPLOT.

tests in this case were basically intended to assess the suitability of the ring design of a potential solution to the application described in Chaper II. Verification of the model was a secondary concern at the time.

The first specimen tested was fabricated to the specifications shown in Figure 37 and summarized below:

Semi-Major Axis: a = 1.016 mm = .040 inch

Semi-Minor Axis: b = 0.250 mm = 0.010 inch

Radius (Nominal) R = 57.000 mm = 2.244 inch

Initial Angle  $\phi_0$ : 30°

The material selected was commercially pure titanium having engineering properties as listed below:

$$E = 16.8 \times 10^6 \text{ psi}$$
  
 $v = 0.30$ 

Titanium was selected over steel on the basis of high strength and low modulus which allows larger deformations and lower force levels for the same stress in the material.

The material certification supplied by the vendor (see Figure 40) showed a yield stress of 52,000 psi which was below the range required for full deflection testing. The decision was made to test the ring using the pure titanium as received. The bases for the decision were the uncertainty in the availability of high strength alloys such as B120VCA, the lack of experience at LLL in titanium heat treatment, and the pressure of schedule constraints. It was decided that if the ring behaved as predicted up to yield,

the commitment to the design could be made at that point and better alloys could be obtained and tested.

The dimensions for the first specimen were the result of an early calculational model and a misinterpretation of the data. The force-deflection curves for the first three cycles are shown in Figure 44 and indicate large values of permanent set. Obviously, the force levels of less than 60 pounds were far below the problem requirements, and the design was considered unacceptable.

The second test specimen, was ordered immediately following the first experiment. The analysis was not corrected at that point, and the dimensions of the elliptical section were set at twice the original values. This size represented the upper bound on the envelope available and required relaxation of some constraints. The purpose of the second test was to establish the upper limit of spring response in the available space. If the test proved successful, then the final spring design could proceed based upon the analytical model without impacting on the project schedule.

The second specimen was fabricated to the specification shown in Figure 38. The parameters were:

Semi-Major Axis: a = 2.033 mm = 0.080 inch

Semi-Minor Axis: b = 0.500 mm = 0.0197 inch

Radius (Nominal): R = 112.643 mm = 2.217 inch

Initial Angle:  $\phi_0 = 20^0$ 

The actual ring is shown in Figure 47.

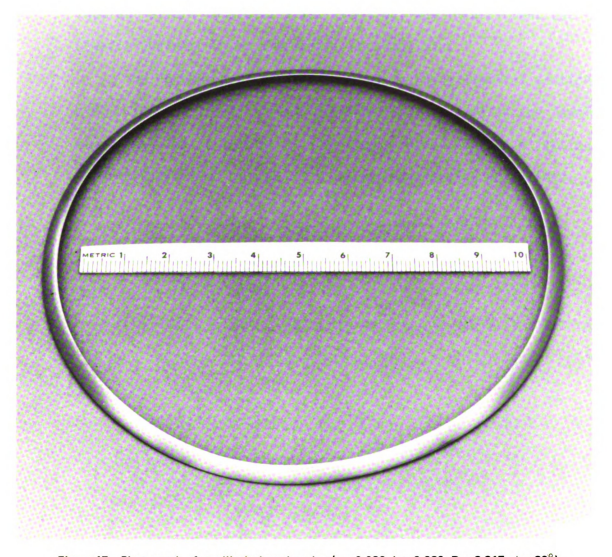


Figure 47. Photograph of an elliptical section ring (a = 0.080, b = 0.620, R = 2.217,  $\phi$  = 20°)

Figure 45 shows the results of the first three load cycles on the second test part. The first cycle test shows force values in the range required ( $\approx 600$  pounds). The deflection of 0.010 inch at failure (onset of yield behavior) was insufficient but clearly indicated that the design was feasible.

No further tests were conducted on the elliptical section ring. The analytical effort proceeded and resulted in the developments detailed in Chapter V. The test program for the elliptical ring was cancelled on the basis of non-engineering parameters.

### CHAPTER VIII

# COMPARISON OF CALCULATED AND EXPERIMENTAL VALUES

Although neither of the two tests described in Chapter VII were particularly successful from the standpoint of meeting the design objectives, both provided good data for correlation and verification of an analytical model. The equations developed in Chapter V were incorporated into a FORTRAN-language computer program which was used to generate tabular and graphics data describing the force-deflection and stress-deflection characteristics of a given ring. In writing the program, the author elected to present all of the data calculated rather than attempting to sort or optimize the calculation. The reason for this decision was the belief that the engineer can gain insight into the system by studying the data and that pre-ordained criteria may reject data which could be valuable.

The computer system at LLL is the Livermore Time-Sharing System (LTSS) presently consisting of four CDC-7600 computers and two CDC-STAR machines. These are linked by other computers to mass storage systems, output media, and a file transport system. The system is an interactive, time-share system which permits large numbers of users to run programs with fast turn-around. A variety of output media are available for text and graphics data including hard copy, 35 mm film (including color), and microfiche. A video disk system (TMDS) provides display capability on local monitors.

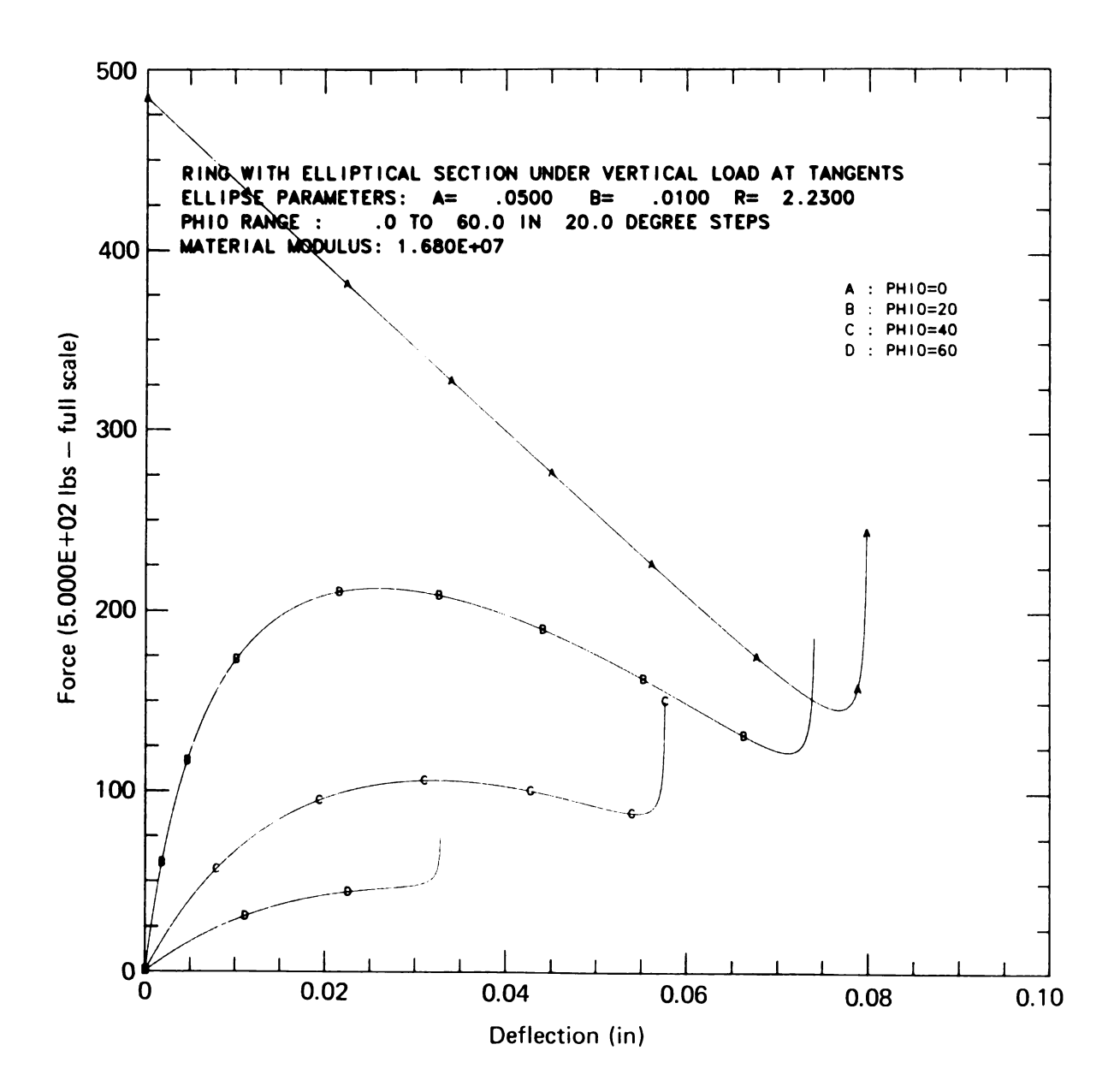
The analysis program, RING, was designed to calculate force, deflection, and stress values for a ring over a range of angle of rotation from  $\varphi_0$  to  $\varphi_{max}.$  The calculations were iterated over a range of cross-section parameters.

$$a_{\min} \leq a \leq a_{\max}$$

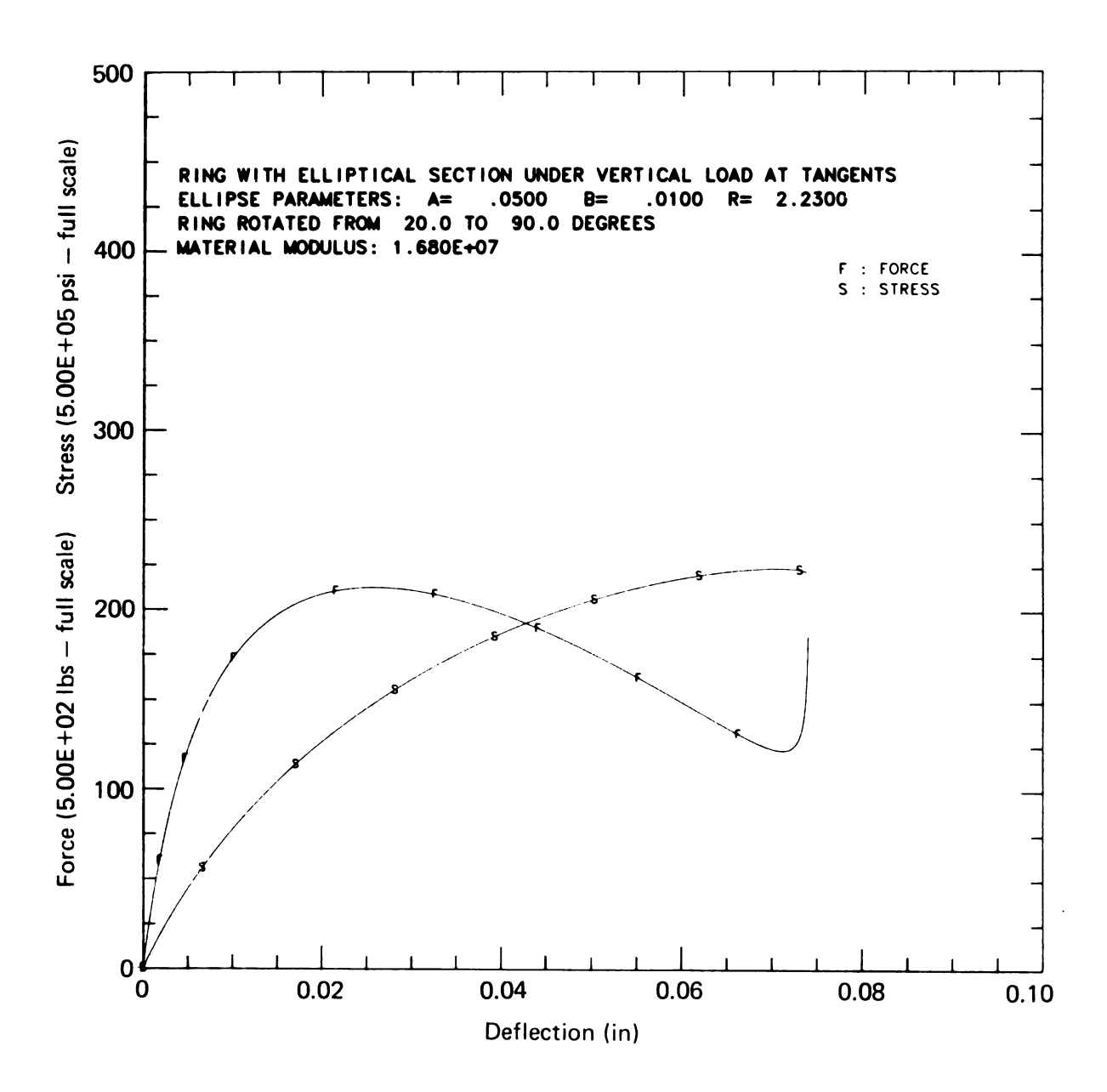
$$b_{\min} \le b \le b_{\max}$$

. Calculation of the Hertzian contact stress at the interface was performed at each increment. Recognizing that the initial orientation of the ring has a significant effect on response, the author included a feature in RING which allowed for iteration of the value of  $\phi_0$  for each cross-section. The results of these iterations were plotted as families of force-deflection curves as shown in Figure 48. The force-deflection curves were also plotted individually for each section with the stress curve scaled to fit and superposed as in Figure 49. Scaling was done with a routine written by the author which sets the full scale value of the grid to a multiple of 1.0, 2.0, or 5.0 as in standard engineering practice. Note that the stress curve is scaled to fit on the grid determined by the force data. It was decided that the forcedeflection curve required greater resolution than the stress curve. Tabular output from RING corresponding to Figures 48 and 49 is presented in Tables 3 and 4. (The number of angle increments has been reduced in the tabular output for purposes of illustration).

A second routine, DPLOT, was written to convert the digitized data from the engineering tests to computer graphics output.



48. Force-deflection curves - sample calculation.



49. Force and stress curves for  $\phi_{\rm o}$  = 20° - sample calculation.

#### TABLE 3. SAMPLE CALCULATION - OUTPUT FROM RING.

RING WITH ELLIPTICAL SECTION IN TORSION (LOAD APPLIED NORMAL TO HORIZONTAL TANGENTS)

2.230 RADIUS RING ROTATED FROM .. O DEGREES TO 90.00 DEGREES IN 5.000 DEGREE INCREMENTS ELLIPSE PARAMETER RANGE :

MAJOR AXIS : .0300 TO .0500 AT .0050 INCREMENT MINOR AXIS : .0100 TO .0200 AT .0050 INCREMENT

MATERIAL PROPERTIES :

RING MATERIAL: TITAN!UM MODULUS = 1.680E+07 NU = .300

PLATE MATERIAL: STEEL MODULUS = 2.800E+07 NU = .300 (FOR CONTACT STRESSES)

TABLE 4. SAMPLE CALCULATION - OUTPUT FROM RING.

RING WITH ELLIPTICAL SECTION UNDER VERTICAL LOAD AT TANGENTS ELLIPSE PARAMETERS: A= .0500 B= .0100 R= 2.2300

MATERIAL MODULUS: 1.680E+07

ANGLE	FORCE	DEFLECTION	STRESS S	SPEC FORCE	MOMENT ARM	STRAIN	CONTACT S
.0	. 0E+00	.0E+00	.0E+00	.0E+00	5.390E-16	. 0E+00	.0E+00
5.00	4.824E+02	-3.653E-04	3.283E+04	3.443E+01	-8.366E-03	1.954E-03	2.639E+03
10.00	4.773E+02	-1.458E-03	6.538E+04	3.407E+01	-1.666E-02	3.892E-03	3.363E+03
15.00	4.689E+02	-3.269E-03	9.739E+04	3.347E+01	-2.481E-02	5.797E-03	5.745E+05
20.00	4.573E+02	-5.782E-03	1.286E+05	3.263E+01	-3.275E-02	7.654E-03	5.745E+05
25.00	4.424E+02	-8.976E-03	1.587E+05	3.158E+01	-4.040E-02	9.448E-03	5.745E+05
30.00	4.246E+02	-1.282E-02	1.875E+05	3.030E+01	-4.768E-02	1.116E-02	5.745E+05
35.00	4.039E+02	-1.729E-02	2.148E+05	2.883E+01	-5.45 <b>3</b> E-02	1.278E-02	5.745E+05
40.00	3.806E+02	-2.232E-02	2.402E+05	2.716E+01	-6.086E-02	1.430E-02	5.745E+05
45.00	3.549E+02	-2.78 <b>9E-</b> 02	2.636E+05	2.533E+01	-6.656E-02	1.569E-02	5.745E+05
50.00	3.270E+02	-3.392E-02	2.848E+05	2.334E+01	-7.154E-02	1.695E-02	5.745E+05
55.00	2.973E+02	-4.035E-02	3.036E+05	2.122E+01	-7.561E-02	1.807E-02	5.745E+05
60.00	2.664E+02	-4.708E-02	3.197E+05	1.901E+01	-7.856E-02	1.903E-02	5.745E+05
65.00	2.348E+02	-5.402E-02	3.332E+05	1.676E+01	-7.996E-02	1.983E-02	5.745E+05
70.00	2.034E+02	-6.097E-02	3.437E+05	1.452E+01	-7.906E-02	2.046E-02	5.745E+05
75.00	1.742E+02	-6.770E-02	3.512E+05	1.244E+01	-7.431E-02	2.090E-02	5.745E+05
80.00	1.513E+02	-7.374E-02	3.555E+05	1.080E+01	-6.252E-02	2.116E-02	5.745E+05
85.00	1.494E+02	-7.825E-02	3.567E+05	1.066E+01	-3.833E-02	2.123E-02	5.74EE+05
90.00	2.115E+13	-8.000E-02	3.546E+05	1.509E+12	-8.790E-14	S.111E-05	5.265E+08

This program along with available graphics editing routines allow the superposition of test data and calculations and output via standard LLL graphics output devices. DPLOT includes the scaling from x-y data in inches (or millimeters) as generated by the Gerber digitizer to force-deflection data according to the scale factors used when the data was recorded.

The optional input of range limits for the axes allows the user to plot to the same scale as the analysis code. This combined with the capability to plot a curve without axes or labels permitted superposition of the experimental and calculated curves.

As discussed previously, the dimensions for the test specimens resulted from an early calculational model which was found to be in error. The specimens provided data to verify the calculational model which was invaluable when the experimental program was cancelled. The nominal dimensions of the first ring were:

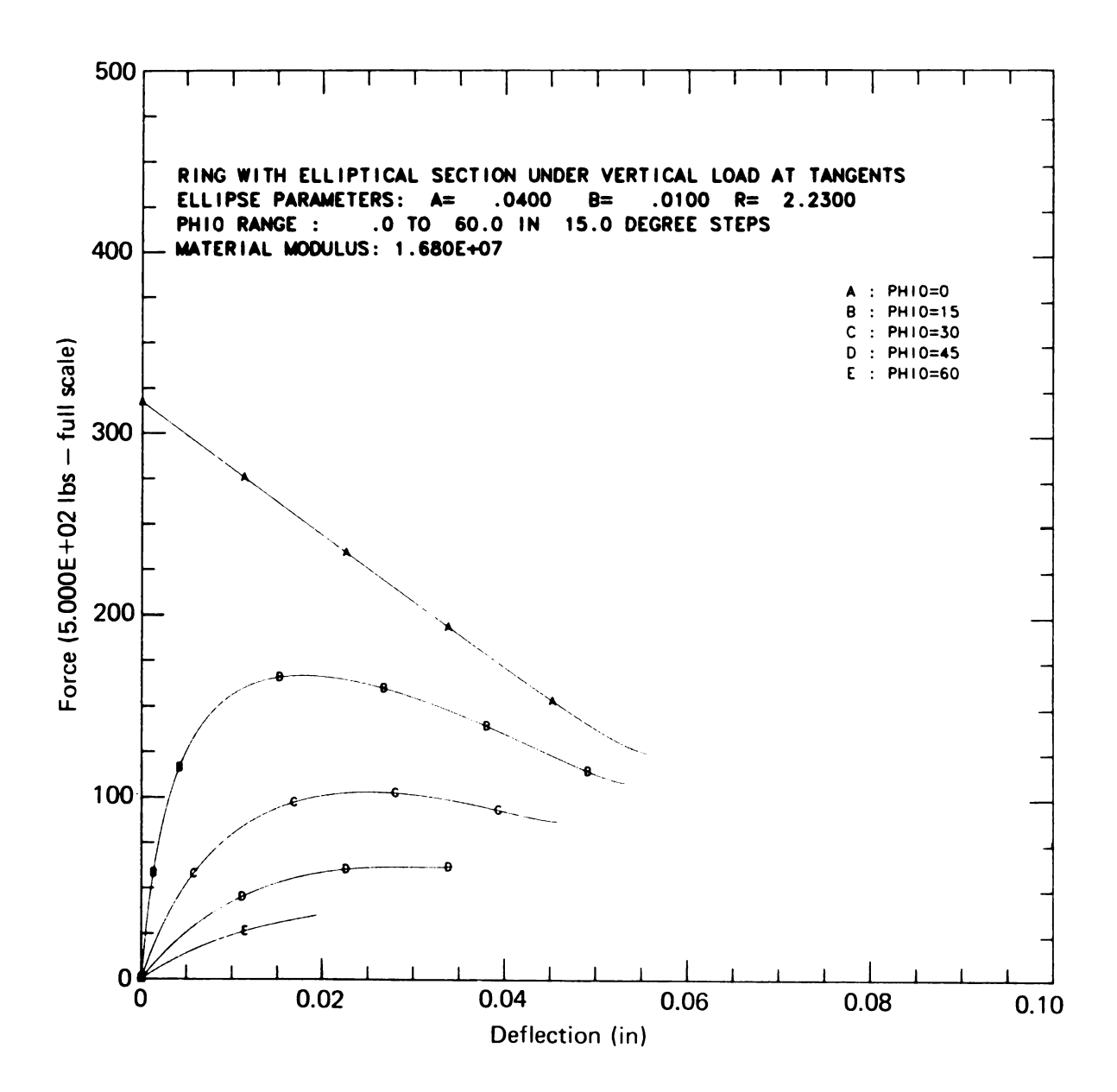
a = 0.040 inch

b = 0.010 inch

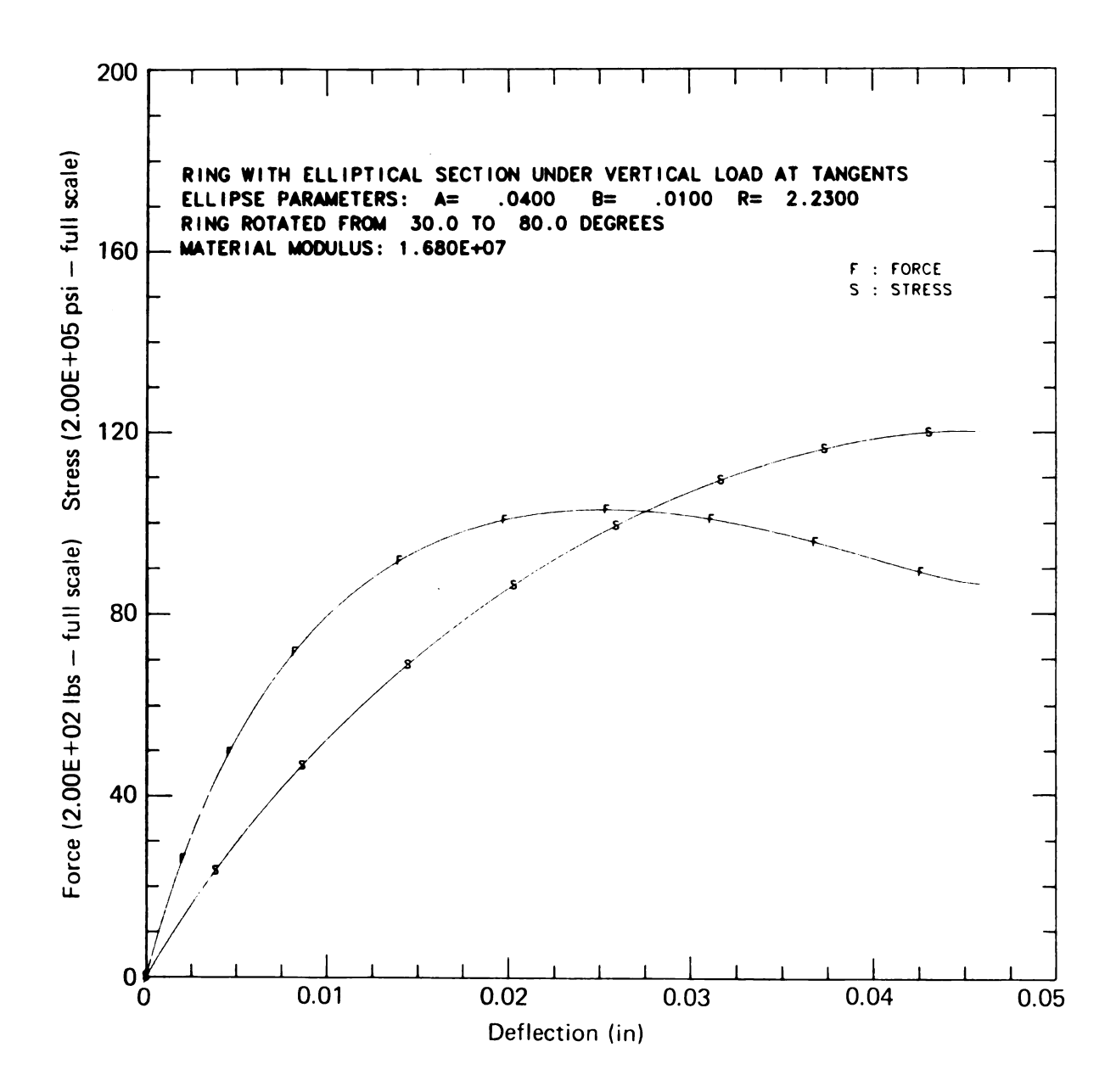
R = 2.244 inches

 $\phi_0 = 30^0$ 

Figure 50 shows the expected curve family for  $0^0 \le \phi_0 \le 60^0$  and the specified curve for  $\phi_0 = 30^0$  is shown in Figure 51. If a material yield of 50 ksi is assumed, the onset of yield will occur at approximately 0.010 inch deflection. The test data for this test specimen are shown in Figure 44 as recorded by the



50. Force curves for Test Specimen No. 1 (nominal dimensions).



51. Force and stress for Test Specimen No. 1 (nominal dimensions).

operators. The data for the first cycle were digitized and plotted with the DPLOT program (see Figure 52). The initial portion of the curve indicates a non-uniform response which was felt to be the flattening of ring warpage. A warped ring could result from residual stresses induced by machining. Figure 53 shows the test data when corrected for this effect.

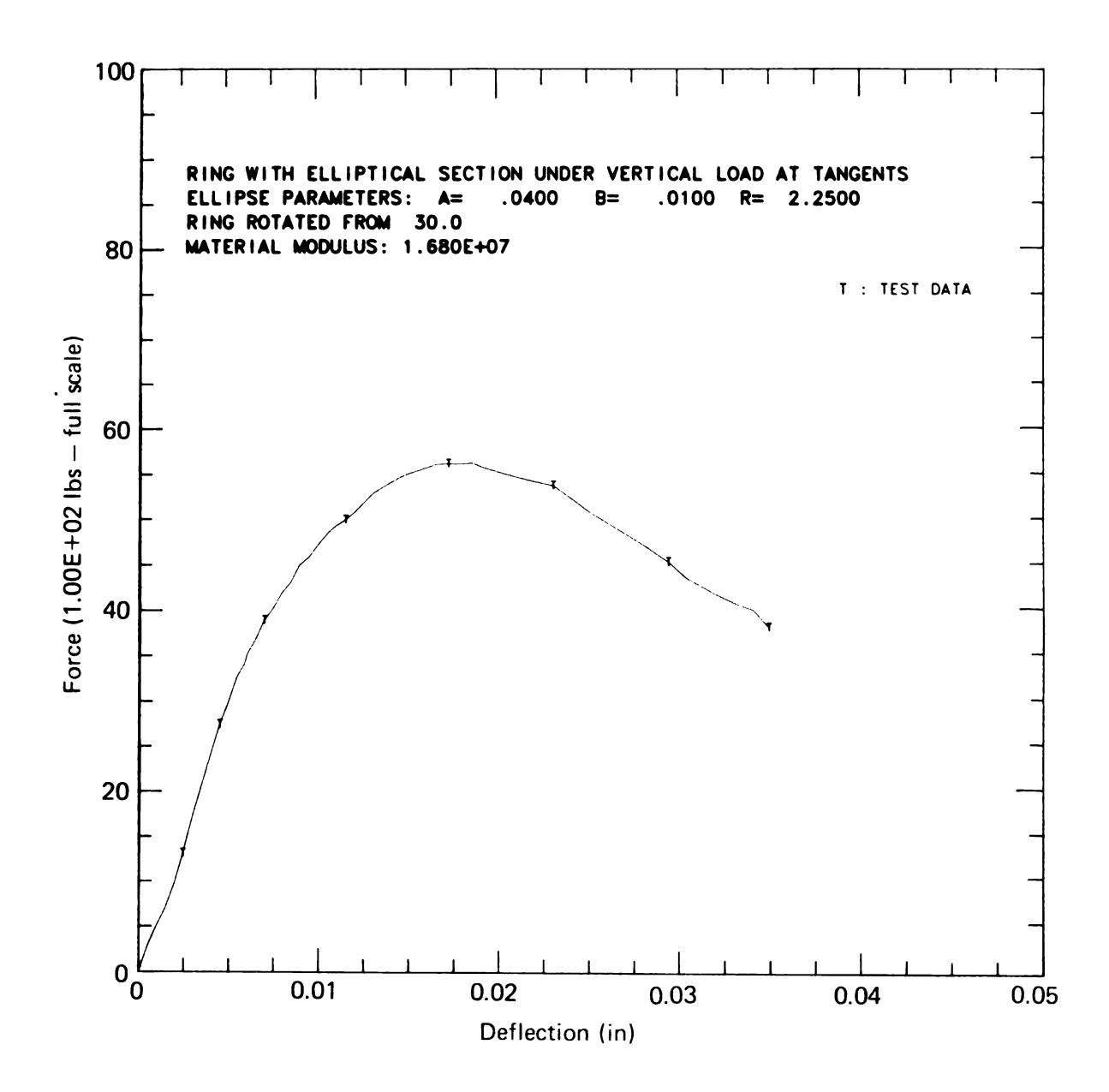
The major and minor axes of the ring were inspected prior to the test and were found to be

a = 0.0418 (0.040 nominal)

b = 0.0095 (0.010 nominal)

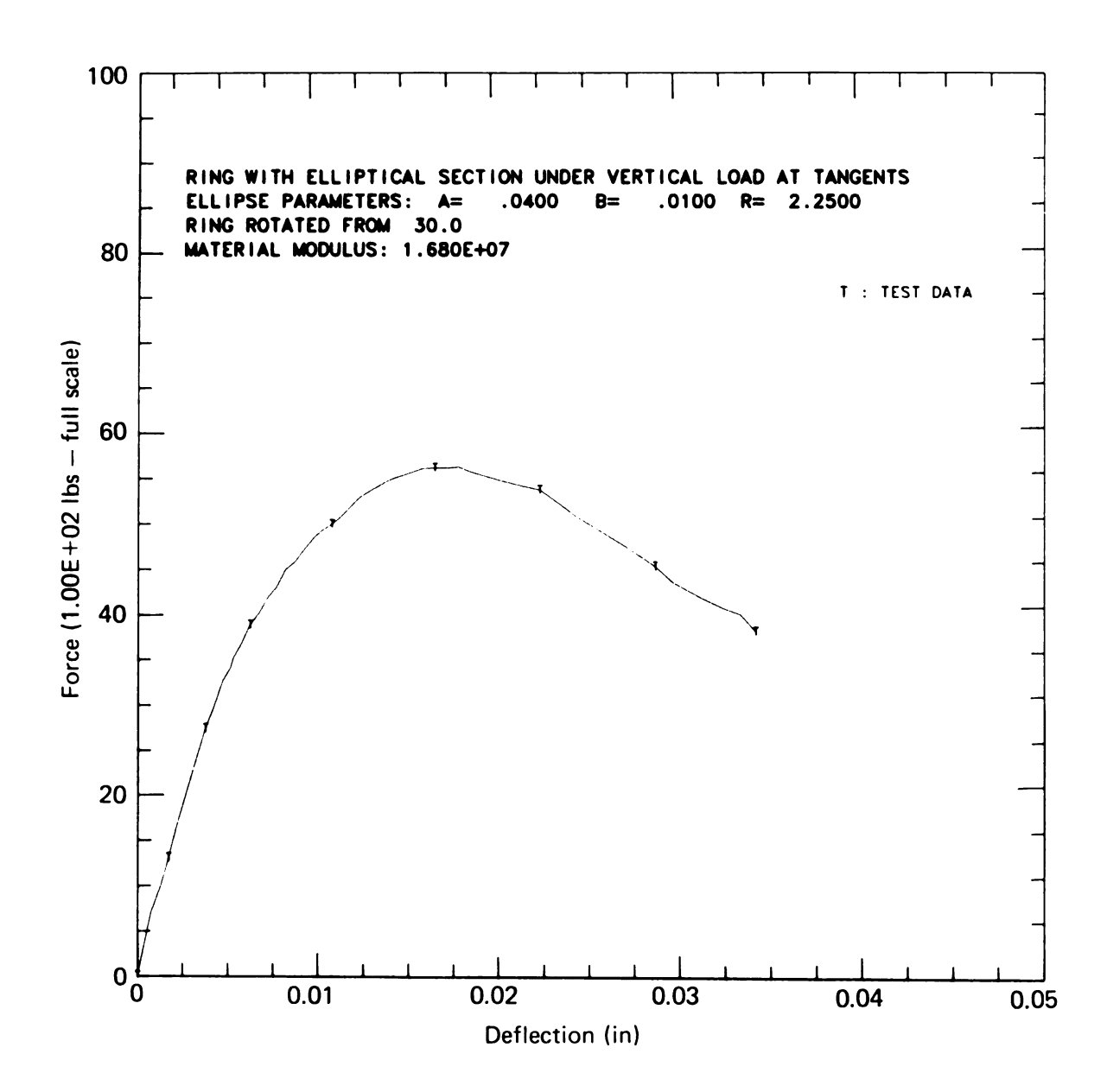
The initial angle could not be checked. Figure 54 shows the predicted curve for the actual ring cross-section with the test data superposed. The shape of the curve agrees with the expected results but the force levels are low. The calculated stress at the apparent yield ( $\delta$  = 0.015 inch) is approximately 72 ksi which exceeds the material strength by a considerable margin.

The discrepancies between the experimental and predicted responses could be the result of several factors such as a non-elliptical cross-section resulting from machining errors or a change in initial angle from the 30° specified value. After the tests, the first specimen was sectioned and examined under a microscope. Figure 55 shows a photomicrograph of the cross-section at 52.9X magnification. Figure 56 shows a similar section etched to indicate the titanium grain structure. The cross section photomicrograph was digitized and plotted to compare it with the specified ellipse (see Figure 57). The contour appears elliptical in

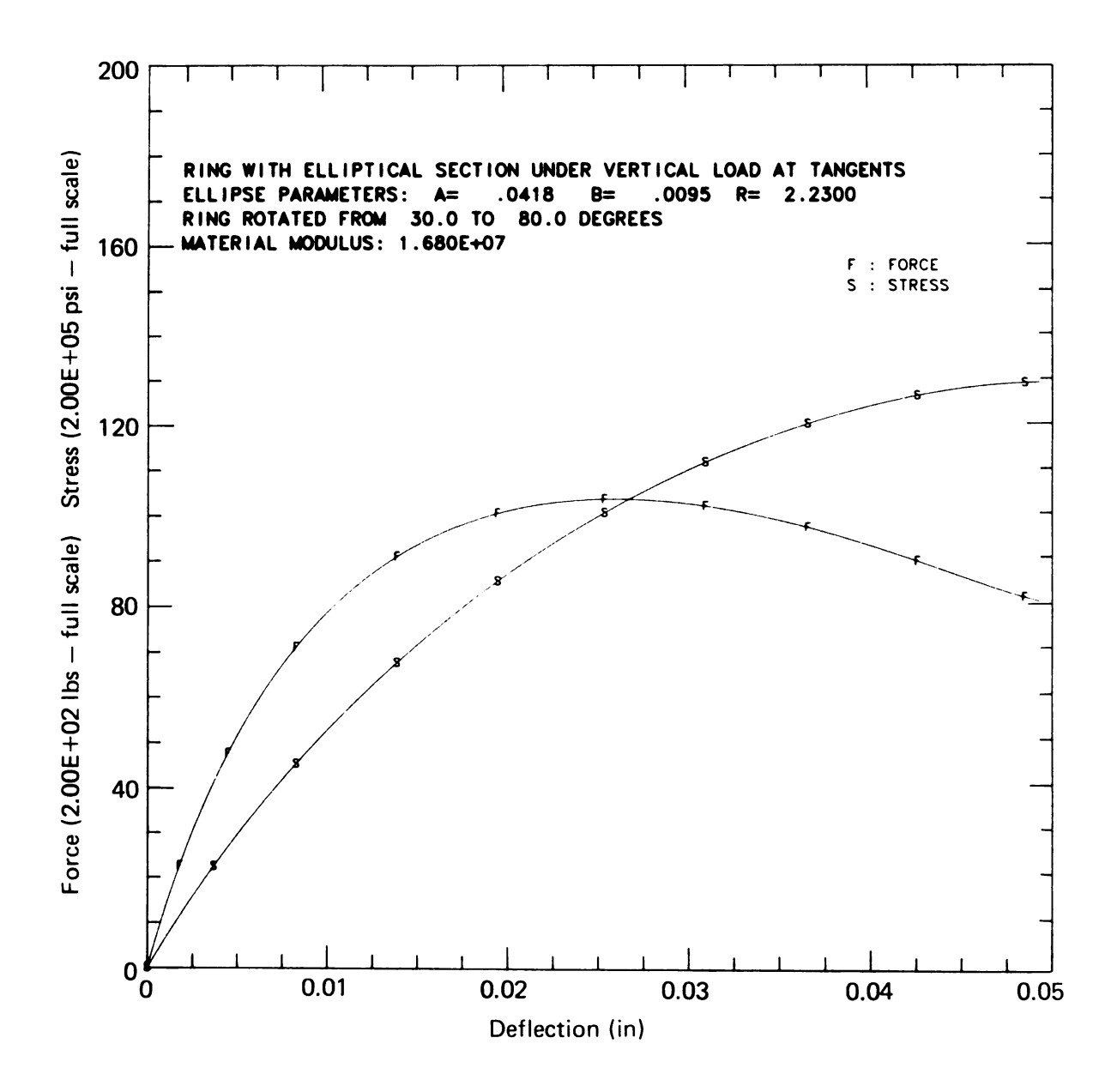


52. Test data for Specimen 1.

.



53. Specimen 1 test data corrected for zero shift.



54. Force and stress for measured cross section of Specimen 1 ( $\phi_{o}$  = 30°).



Figure 55. Photomicrograph of the cross section of Specimen No.1 (post-test).

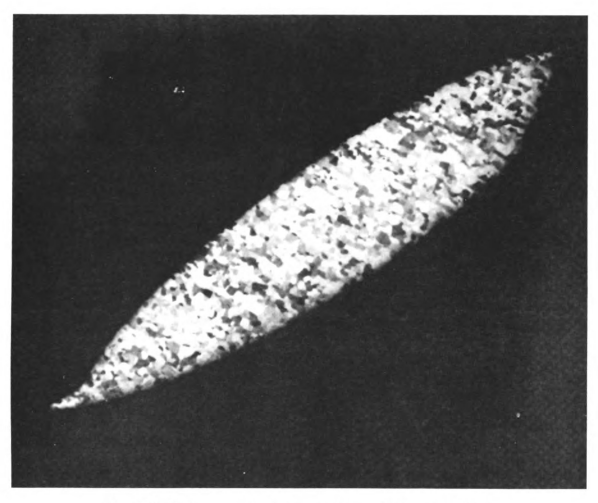


Figure 56. Photomicrograph of the cross-section of test specimen No. 1 (the section has been etched to indicate grain size)

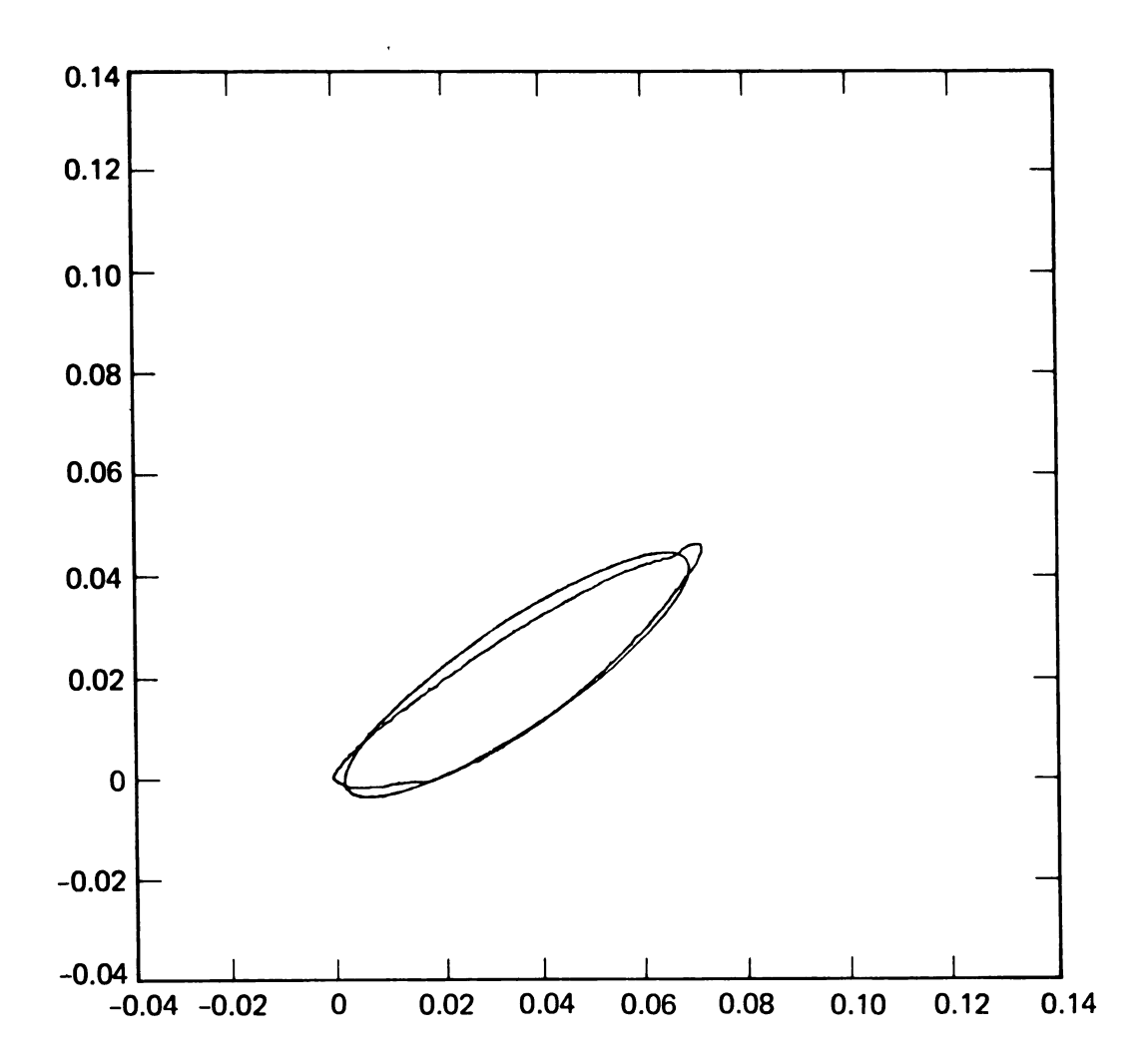


Figure 57. Plot of digitized cross section of Specimen No. 1 compared with a true ellipse.

form but could be significantly different in section properties. The initial orientation of the ellipse was lost when the section was removed from the ring.

Figure 58 shows a family of curves for the measured cross-section of the first ring over the range  $30^{\circ} \le \phi_0 \le 45^{\circ}$  with the test data superposed. It is obvious that the test data are similar to the response curve corresponding to  $\phi_0 = 40^{\circ}$ . The change in the height of the ring (between tangents) is 0.008 inch from  $30^{\circ}$  to  $40^{\circ}$  or approximately ten percent. This exceeds the tolerance band for the part but is not unlikely given the size of the part and the small cross-section. The specific curve for  $\phi_0 = 40^{\circ}$  is shown in Figure 59, again with the test data superposed. It is interesting to note that the calculated stress at apparent yield is approximately 55 ksi which agrees well with the material certification (Figure 40).

The first test specimen did not provide adequate verification of the model. Several probable sources of error could account for the discrepancies but none of these can be shown to have existed at the time of the test.

The nominal dimensions of the second test ring were:

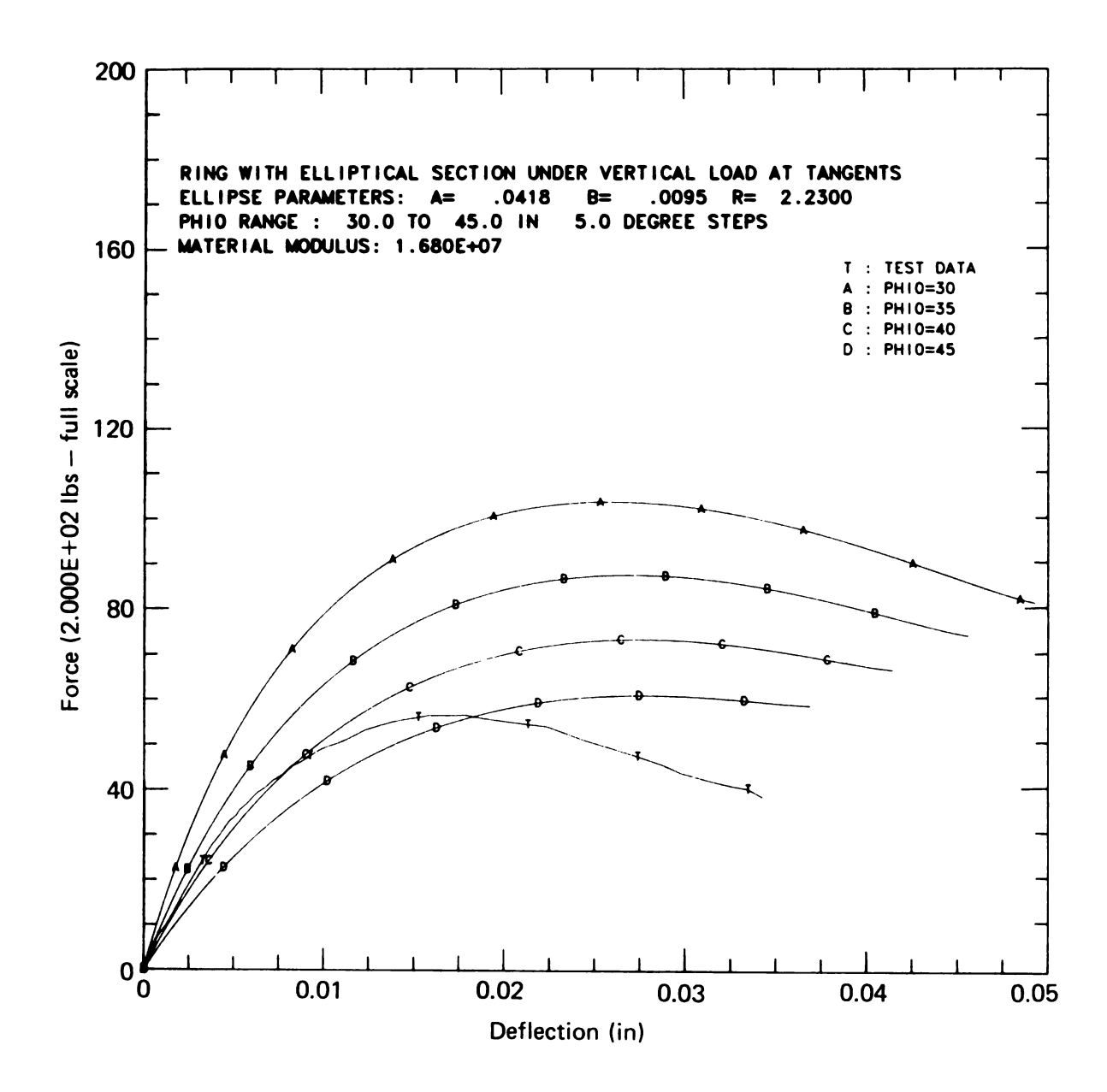
a = 0.0800 inch

b = 0.0197 inch

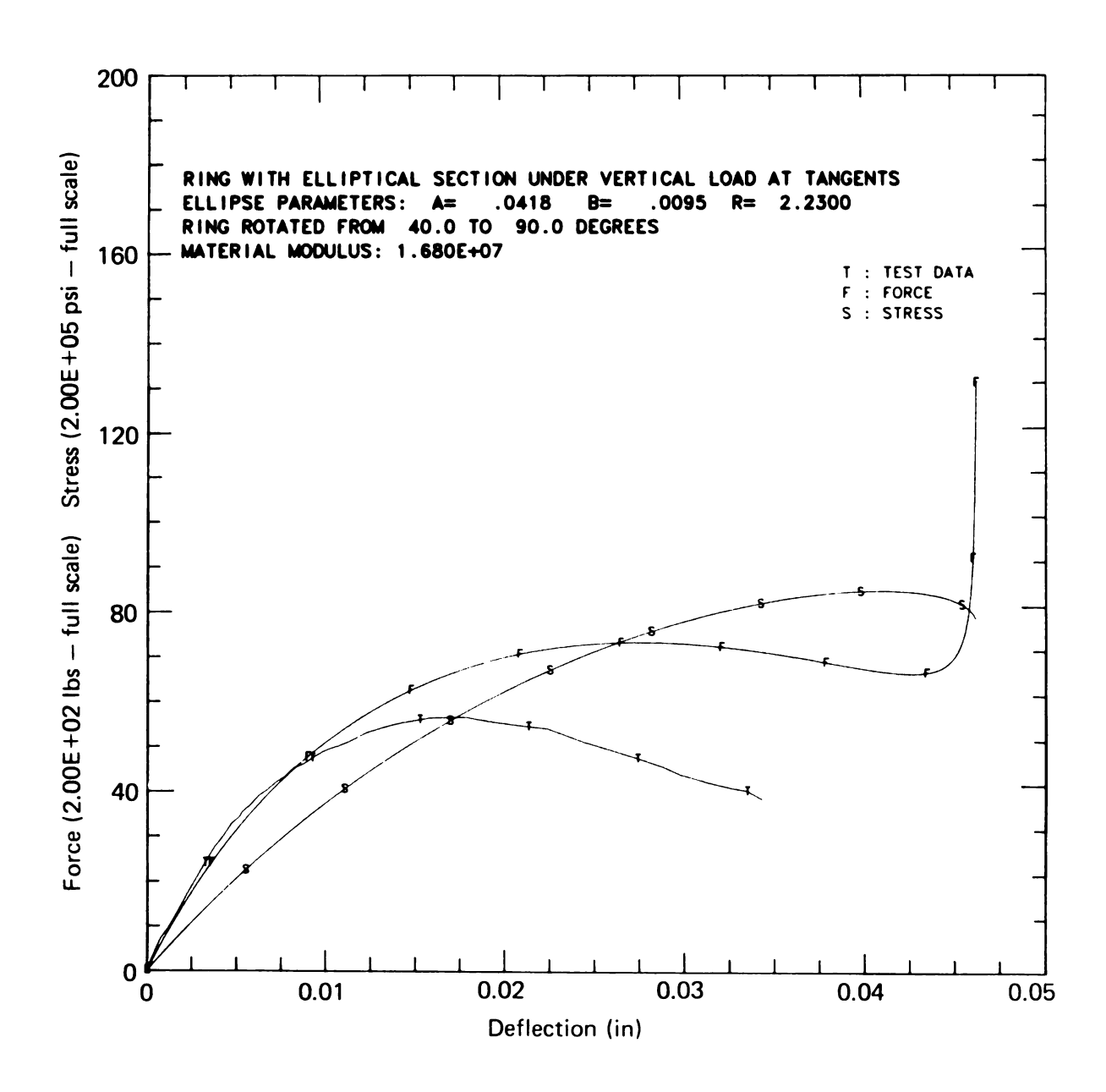
R = 2.217 inches

 $\phi_0 = 20^0$ 

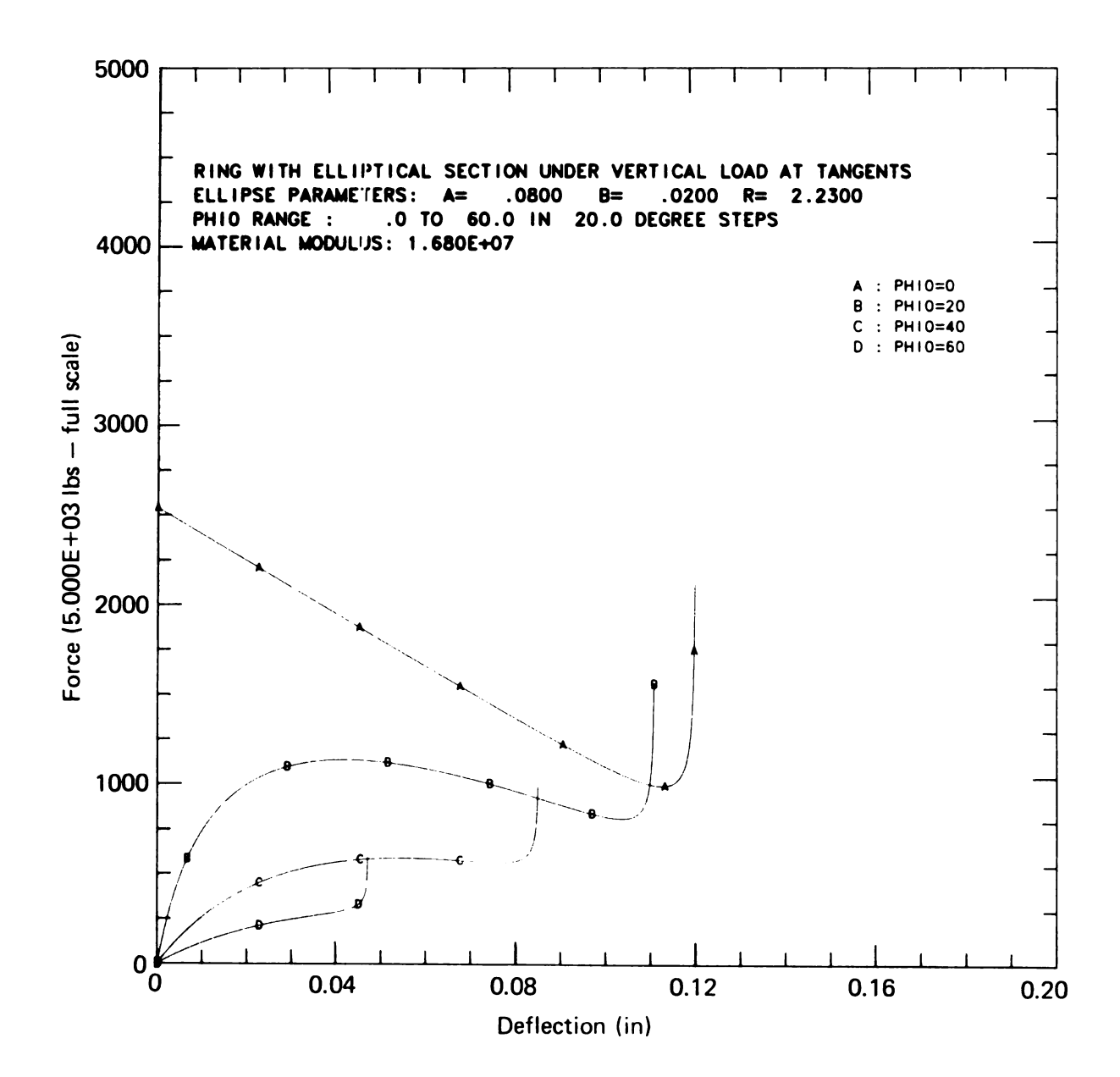
The predicted curves are shown in Figures 60 and 61. The expected force levels are higher than the first test, reaching approximately

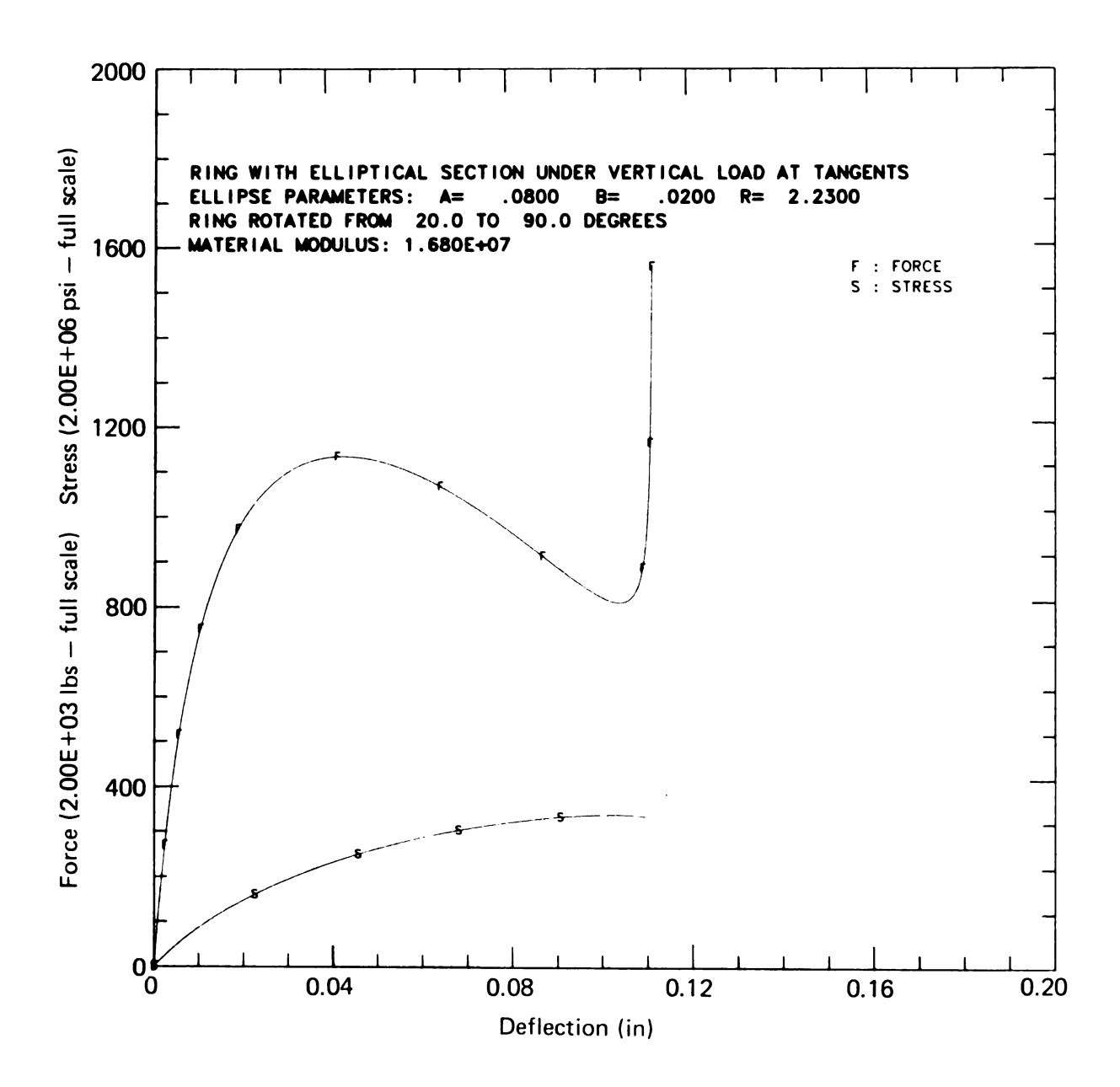


58. Force curves for measure cross section of Specimen No. 1.



59. Force and stress for measured cross section of Specimen No. 1 ( $\phi_o$  = 40°).





61. Force and stress for Test Specimen No. 2 (nominal dimensions)

500 lbs at the yield point (52 ksi). The predicted deflection at yield is 0.005 - 0.006 inch. The digitized test data for the second test specimen are plotted in Figure 62. Figure 63 shows the same data corrected for zero shift.

The actual dimensions of the second specimen were

a = 0.0815 inch

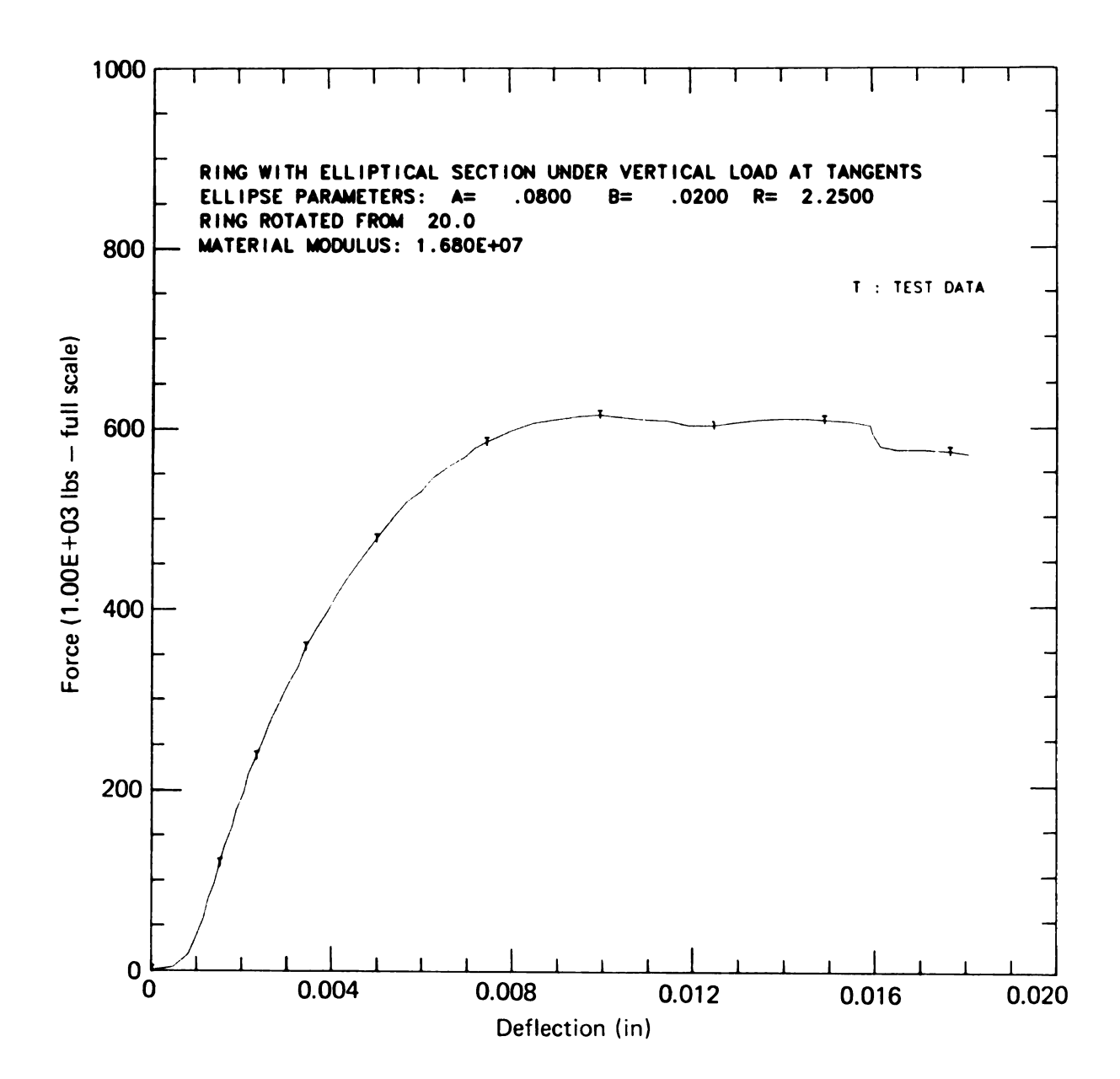
b = 0.205 inch

R = 2.2185 inches

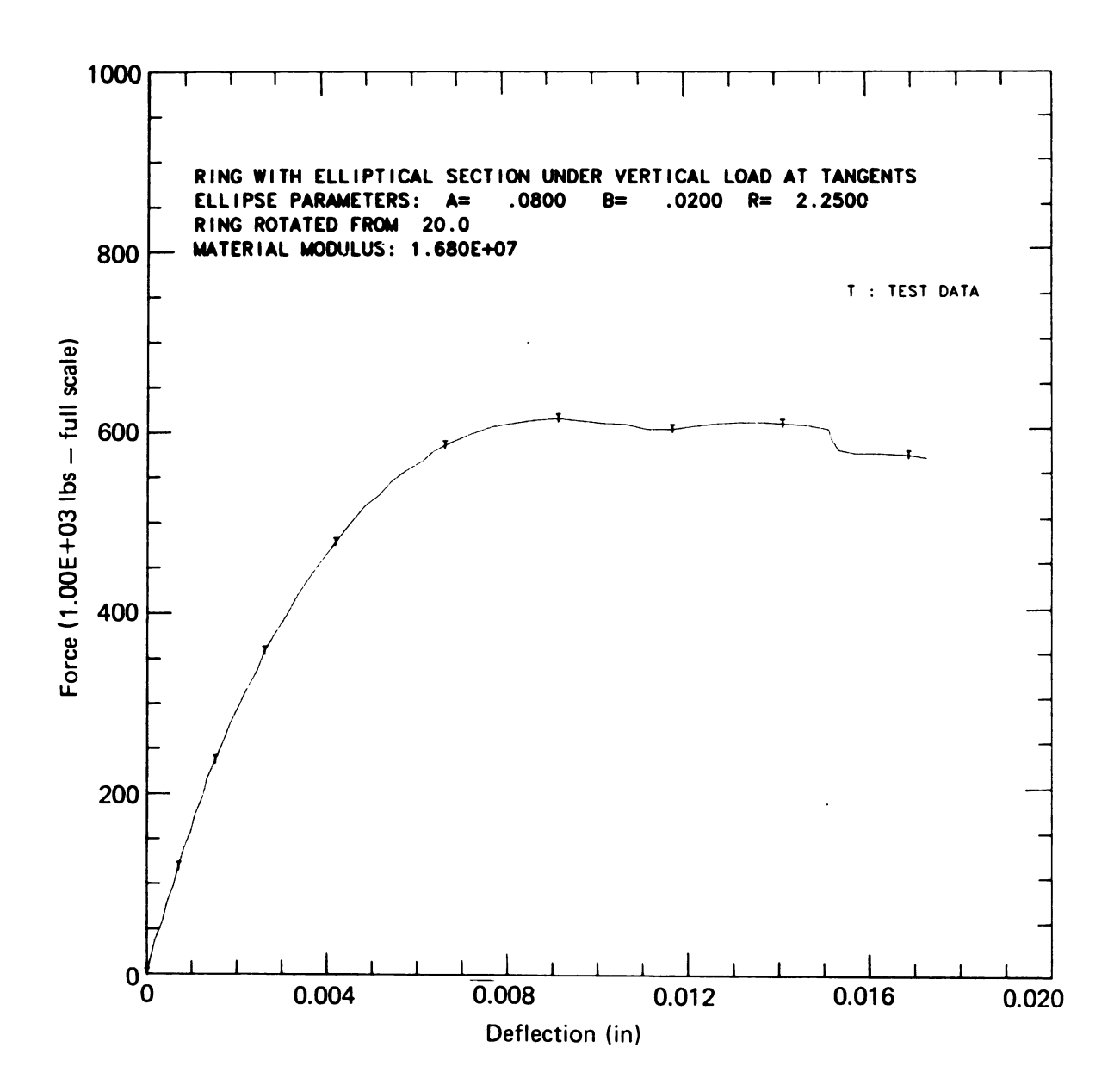
which resulted in the curves shown in Figures 64 and 65. The test data has been superposed and agrees well with the calculated response. The calculated stress at apparent yield is approximately 60 ksi. The force peaked at about 600 lbs and the deflection at the onset of yield was 0.0055 inch.

The actual force curve is higher than the predicted curve. This could be due to friction between the ring and the load platens. Rabinowicz (14) reports a coefficient of friction of 0.09 for titanium riding on a steel surface with light lubrication. This was felt to be appropriate since the platens were hardened steel and were lightly oiled. Figure 66 shows the predicted curve for  $\mu$  = 0.10 with the test data superposed. The results suggest that friction between the elements is increasing the force as expected.

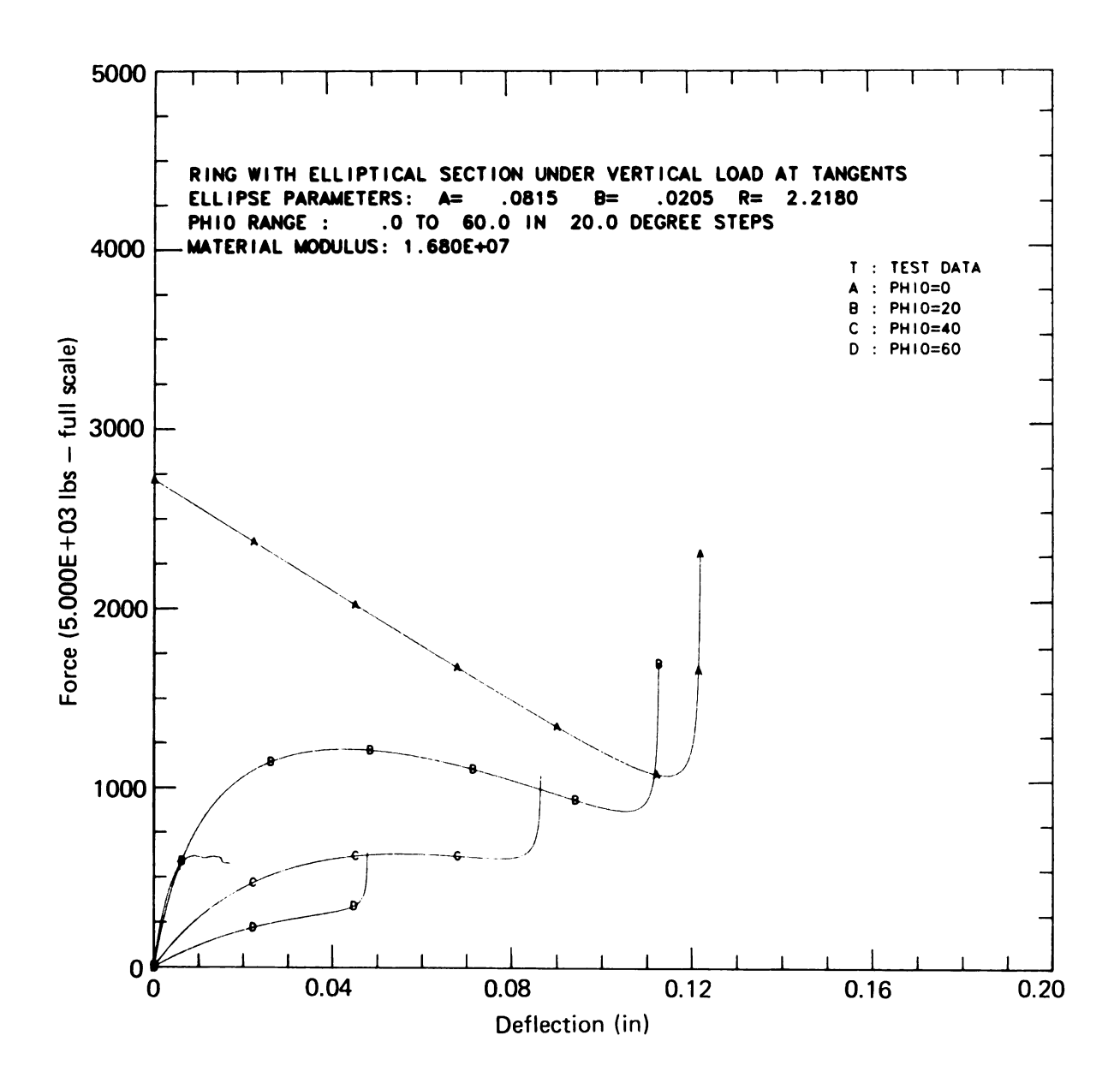
The second test correlates well with the calculated response and confirms the model. The presence of friction is suggested and can be accounted for in the calculated response. Since the ring was stressed into the plastic region and did not



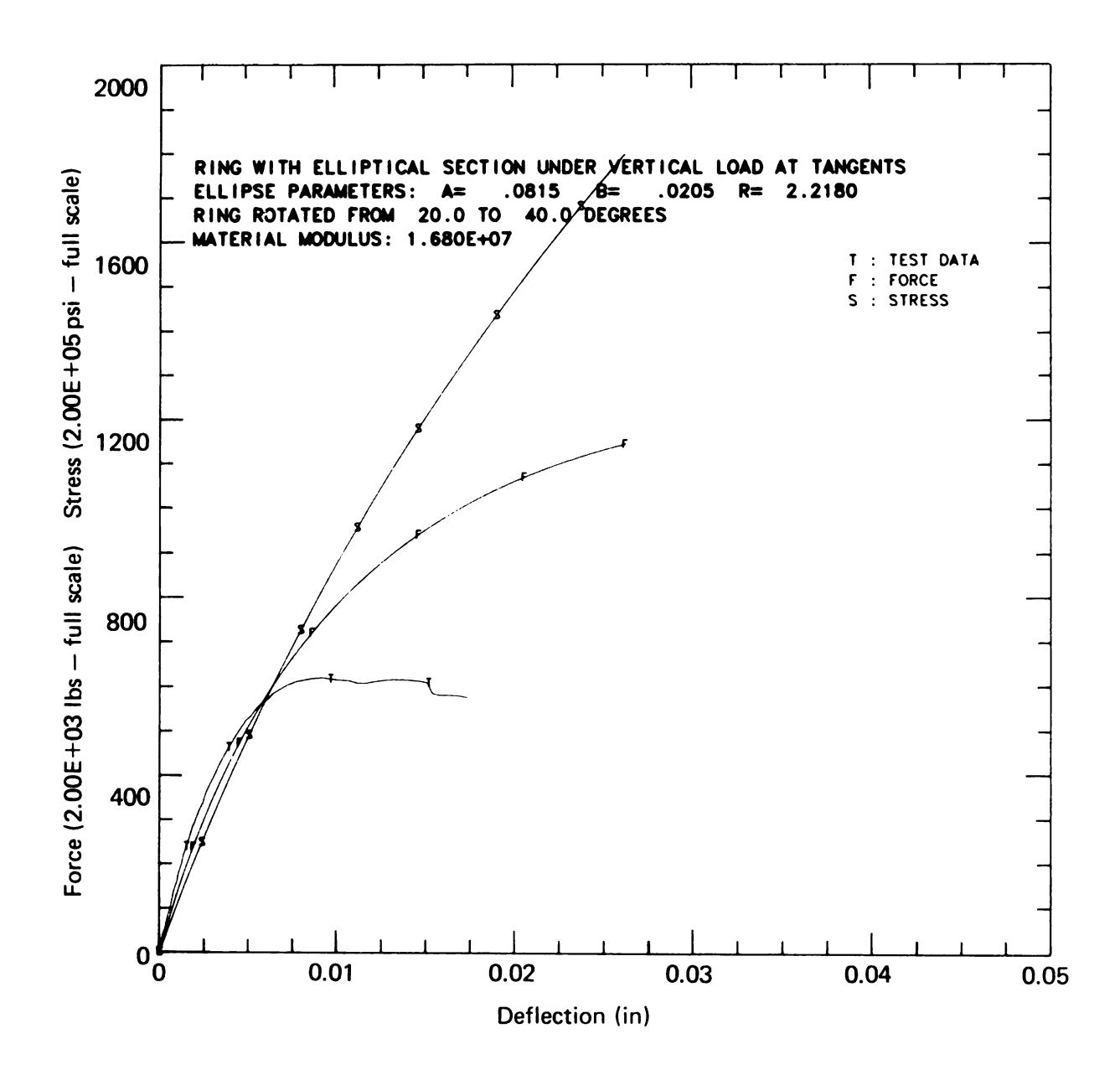
62. Test data for Specimen No. 2.



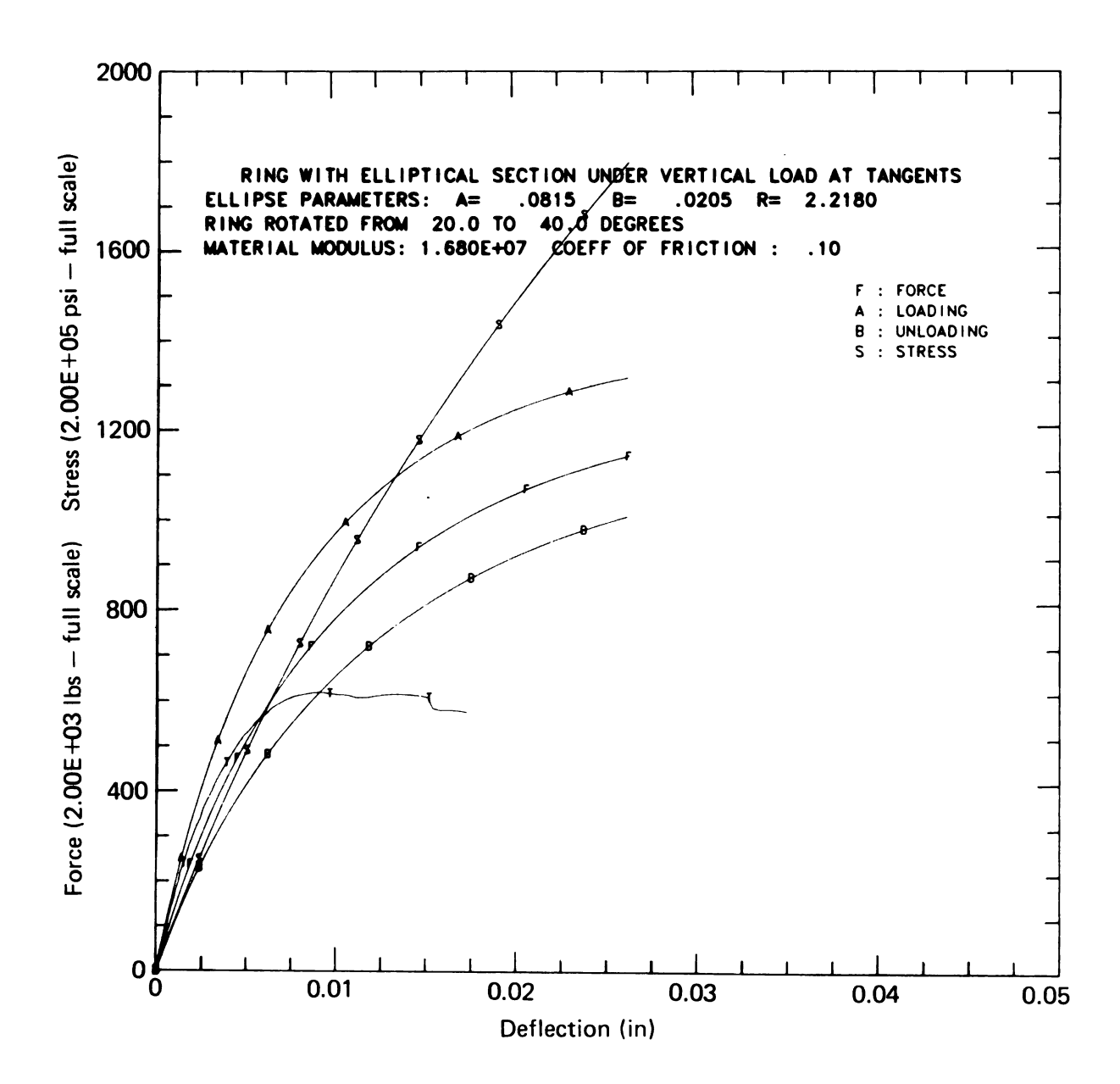
63. Specimen 2 test data corrected for zero shift.



64. Force curves for measured cross section of Specimen No. 2.



65. Force and stress for measured cross section of Specimen No. 2.



66. Effect of friction ( $\mu$  = 0.10) on the calculated response for Specimen No. 2.

return to the original value of  $\phi_0$ , it is not possible to calculate the coefficient of friction using the hysteresis loop as proposed in Chapter V. An estimate of the friction coefficient may be obtained from Run No. 2 shown in Figure 45. The permanent set from the first test is approximately 0.008 inch which corresponds to a value of  $\phi_0$  = 27.5° from Run No. 2. Table 5 shows the values for Equation (V-73) for  $\delta$  = 0.0035 inch and  $\delta$  = 0.0050 inch in Run No. 2. The values are determined for the friction constant,  $\mu$  = 0.13 and  $\mu$  = 0.15, agree well with each other and with the value expected from Run No. 1. The constants are within the range reported in (14).

TABLE 5. ESTIMATE OF THE COEFFICIENT

OF FRICTION FROM THE HYSTERESIS LOOP. (Data from Run No. 2, Figure 45.)

Defl	ecti	on
------	------	----

Parameter	$\delta = 0.0035$	$\delta = 0.0050$
<u></u> δ/ <b>a</b>	0.0429	0.0613
φ0	27.5°	27.5°
ф	30.25°	31.35°
P <sub>u</sub>	130.	190.
P <sub>L</sub>	80.	110.
	0.13	0.15
μ -		

## CHAPTER IX

## CONCLUSIONS AND RECOMMENDATIONS

The investigation of the response of an elliptical-section circular ring to a distributed axial load resulted in a mathematical model which can be used to predict the force-deflection characteristics of a given ring as well as the stress levels in the material. The effects of friction between the ring and the loading element can be predicted and the limits of operation can be specified based on the critical angles for self-locking. The project was terminated without testing a ring which satisfied the constraints of the original problem. This could be accomplished quickly should the need arise.

The following recommendations for future study are proposed:

- 1. Larger specimens of high-strength materials should be tested. Inspection prior to testing should determine the ellipse parameters (a, b,  $\phi_0$ ) and the section properties ( $I_{xx}$ ,  $I_{yy}$ ). Testing should include strain gaging to monitor the strain levels in the part.
- Hypteresis studies should be conducted to further verify the effects of friction on ring response.
- 3. Uniaxial arrays of fibrous composites such as Kevlar/ epoxy and Thormel/epoxy should be considered as ring materials. These composites have high strengths and low moduli in the fiber direction and should be well suited to this application.

## REFERENCES

- Timoshenko, S. <u>Strength of Materials</u> Vol II. Huntington,
   New York: Robert E. Krieger Publishing Co., 1976.
- Roark, Raymond J. and Warren C. Young. <u>Formulas for</u>
   <u>Stress and Strain</u>. New York: McGraw-Hill Book
   Company, 1975.
- Spotts, M. F. <u>Design of Machine Elements</u>. Englewood
   Cliffs, N.J.: Prentice-Hall, Inc., 1971.
- 4. Black, Paul H. and D. Eugene Adams Jr. <u>Machine Design</u>

  New York: McGraw-Hill Book Company, 1955.
- 5. Baumeister, Theodore, ed. Standard Handbook for

  Mechanical Engineers. New York: McGraw-Hill Book
  Company, 1969.
- 6. Nattrass, Lawrence A. "Large Deflection Buckling of Columns As An Engergy Absorption Mechanism." Unpublished Masters thesis, Case Western Reserve University, 1972.
- 7. Timoshenko, Stephen P. and James M. Gue <u>Theory of</u>
  <u>Elastic Stability</u> New York: McGraw-Hill Book
  Company, 1961.
- 8. Almen, J. O. and A. Laszlo. "The Uniform-section Disc Spring." Trans. ASME, Vol. 58, 1936
- 9. Grammel, R. Z. angew <u>Math. u. Mech.</u>, Vol. 3 and Vol. 7, 1927.

- 10. Rodriquez, D. A. "Three-Dimensional Binding of a Ring on an Elastic Foundation." <u>Journal of Applied</u>

  <u>Mechanics</u>, (Sept. 1961).
- 11. Oden, J. T. <u>Mechanics of Elastic Structures</u>. New York:

  McGraw-Hill Book Company, 1967.
- 12. Thomas, G. B. <u>Calculus and Analytic Geometry</u>.
  Reading, Massachusetts: Addison Wesley Publishing
  Company, 1965.
- 13. American Society of Metals. <u>Metals Handbook</u>, Vol. 1: Properties and Selection of Metals. Metals Park, Ohio: American Society for Metals, 1961.
- 14. Rabinowicz, E. <u>Friction and Wear of Materials.</u> New York:

  John Wiley and Sons, 1965.

MICHIGAN STATE UNIV. LIBRARIES
31293010670895